Comparative Study of Two Nozzle Assemblies For High Velocity Oxy Fuel (HVOF) Thermal Spray Coating Process

Marouf Aldosari

(B.Sc M.Sc)

A thesis submitted for the degree of
Doctor of Philosophy

School of Mechanical and Manufacturing Engineering

Dublin City University

Supervisors

Dr. Joseph Stokes

Dr. Khaled Y Benyounis

September, 2017

Declaration

I hereby certify that this material, which I now submit for assessment on the programme of study leading to the award of Doctor of Philosophy in Mechanical and Manufacturing Engineering is entirely my own work, that I have exercised reasonable care to ensure that the work is original, and does not to the best of my knowledge breach any law of copyright, and has not been taken from the work of others save and to the extent that such work has been cited and acknowledged within the text of my work.

Signed: Marouf Aldosari ID No: 12210112 September 6, 2017

Acknowledgment

I thank the almighty and absolute perfect one who enlightened me through this chance into my life, and in which I have touched many positive aspects in life. I would like to thank my family for their caring and support, especially, my mother, Amirah Eladawy, for her endless support and heavenly caring and love. My heart vibrates endless thanks to my father, Mohammad Ben Aoun Aldosari, and my brother Enad Ben Mohammad Ben Aoun Aldosari whose wisdom is still diffusing into me and helps me to see the better in life. I would like to thank my supervisor, Dr Joseph Stokes for his unlimited support and his guidance during this work and for giving me the chance to study an exiting technology such as thermal spray coating that I had not known before commencing this research with him. I admire his managerial and extraordinary communications skills. I am grateful to my co-supervisor, Dr Khaled Benyounis for his support and supervision of this work. I thank the Ministry of Higher Education of my country, Saudi Arabia, for their financial support for this study. I thank Dr Ahmad Alhamed for his advice and providing me with useful guidance. I thank Mr Naif Alharbi for his cooperation. I thank all people and colleagues in the Mechanical Engineering School of DCU and wish them all the best and success in their lives. Finally I thank every one who supported me and advised me through this PhD work.

Contents

Declaration i

Acknowledgment ii

Contents iii

List of Figures vi

List of Tables xi

Nomenclature xiii

Abstract xvii

1 Introduction 1

1.1 Motivation of the Study 1

1.2 The Aim and Contribution of This Study 2

1.3 Thesis Outline 3

2 Literature Review 5

2.1 Introduction 5

2.2 Surface Engineering 5

2.3 Thermal Spray Coating 7

2.3.1 Electric Arc Process 8

2.3.2 Plasma Spray 8

2.3.3 Flame Spray Processes 9

2.3.4 High Velocity Oxy Fuel (HVOF) 10

2.3.4.1 Experimental Approach 14
2.4 Physics and Models of HVOF 19
2.4.1 Combustion 20
2.4.2 Gas Dynamics and Turbulence 26
2.4.3 Multiphase Flow Interaction 31
2.5 HVOF Literature Modelling Results 36
2.5.1 Operating Parameters (flow rates of gases) 37
2.5.2 Particle Behaviour 39
2.5.3 Geometrical Aspects 41
2.6 Summary and Research Gaps 43

3 Research Methodolgy **44**
3.1 Introduction 44
3.2 CFD Approach 44
3.2.1 Mathematical Models 45
3.2.2 Boundary and Operating Conditions 46
3.2.3 Numerical Calculation 48
3.3 Design of Experiment Approach 49
3.3.1 Response Surface Methodology (RSM) 51
3.3.2 Box-Behnken Design (BBD) 51
3.3.2.1 Analysis of the Design 52
3.3.3 General Steps in RSM 53
3.3.4 Optimization 58
3.3.4.1 Desirability Approach 58
3.3.4.2 Optimization Approach in Design-Expert Software 60

4 Results and Discussion **61**
4.1 Introduction 61
4.2 Gas Pressure 63
4.2.1 CFD Results for Gas Pressure 65
4.2.2 DOE Results for Static pressure 68

4.3 Gas Temperature 75
4.3.1 CFD Results for Gas Temperature 75
4.3.2 DOE Results for Gas Temperature 77
4.4 Gas Velocity 88
4.4.1 CFD Results of Gas Velocity 88
4.4.2 DOE Results of Gas Velocity 89
4.5 Particle Temperature and Velocity 95
4.5.1 CFD Results 95
4.5.2 DOE Results of Particle Temperature 97
4.5.3 DOE Results of Particle Velocity 102
4.5.4 DOE Results of Particle Temperature at the Nozzle Exit 106
4.5.5 DOE Results of Particle Velocity at the Nozzle Exit 111
4.6 Validation of the Statistical Models 120
4.7 Optimization of Process Parameters 120

5 Conclusion and Recommendation for Future Work **125**

5.1 Conclusion 125
5.2 Recommendation for Future Work 126

References **129**

List of Figures

2.1 Classification of thermal spray coating techniques 6

2.2 Thermal spray coating principle [7] 7

2.3 Electric arc spray [7] 8

2.4 Plasma spray process [7] 9

2.5 Flame wire spray process [7] 10

2.6 Flame Powder spray process under which HVOF is categorized [7] 10

2.7 Process temperature and velocity range for different TS processes [8] 12

2.8 High Velocity Oxy Fuel Process [15] 12

2.9 Coating formation during High Velocity Oxy Fuel Process [22] 13

2.10 Variation of the adiabatic flame temperature with the equivalence ratio (ϕ) for different fuels combustion under the standard condition of 1 bar and 273.15 K [56] 22

2.11 Effect of initial droplet size on Kerosene combustion in HVOF [68] 25

2.12 Validation of non-premixed combustion model [78] 26

2.13 Over-expanded jet in converging-diverging nozzle [12, 21] 30

2.14 Under-expanded jet in converging barrel nozzle [12, 21] 31

2.15 Comparison between 1-D theoretical and 2-D CFD models [66] 31

2.16 Multi phase flow regime classification based on the volume fraction of the dispersed phase and the Stokes number [90]. 33

2.17 Drag coefficient (C_D) of a spherical particle as a function of Mach (M) and Reynolds number (Re) [97] 34

2.18 Multi-Physics of the HVOF process [66] 37

2.19 Velocity profile for spherical particle of different sizes along the jet centerline relative to the gas velocity [106] 39
2.20 Temperature profile for spherical particle of different sizes along the jet centerline relative to the gas velocity [106] 40

3.1 (a): Schematic diagram of the DJ1050 HVOF gun, (b): schematic diagram of the DJ2700 HVOF gun, dimensions in mm 45
3.2 Quadrilateral mesh independent cells for DJ1050 gun (a = 38258 cells, b = 40321 cells, c = 42500 cells) and DJ2700 gun (d = 72444 cells , e = 75329 cells , f = 77138 cells). 49
3.3 BBD representation of three factors [140] 52
3.4 Optimization Steps flow process [141] 60

4.1 Computed temperature profile of a 10 μm WC-12%Co particle validated by a measured temperature over the stand-off distance 62
4.2 The effect of density variation on the pressure behaviour in a DJ1050 HVOF gun for the cases considered in Table 4.3 66
4.3 Static pressure along the centerline of [a]: under-expanded jet DJ1050 and [b]: over-expanded jet DJ2700 of the contours at $\phi = 1.01$ and 175 mm spray distance 67
4.4 Normal plot of residuals DJ1050 70
4.5 Predicted Vs actual values for DJ1050 71
4.6 Perturbation plot for DJ1050 where A = equivalence ratio and B = spray distance for the pressure response 72
4.7 Interaction between the gas pressure response, equivalence ratio and spray distance DJ1050 73
4.8 Contour plot of the gas pressure response Vs the equivalence ratio and the spray distance DJ1050 73
4.9 Perturbation plot for DJ2700 where A = equivalence ratio and D = Air flow for pressure response 74
4.10 Contour plot for DJ2700 showing the relation between the gas pressure response, the equivalence ratio and spray distance. 74

4.11 Static temperature along the centreline of [a]: DJ1050 and [b]: DJ2700. The contours are for $\phi = 1.01$ and 175 mm spray distance 75
4.12 Residence time of 25μm particle in both DJ1050 and DJ2700 under the same operating conditions 76
4.13 Particle temperature profile along the centerline axis for a 25μm particle for both the DJ1050 and DJ2700 HVOF guns under the same operating conditions 77
4.14 Normal plot and predicted vs actual values for gas temperature response in the DJ1050 gun 81
4.15 Perturbation plot showing the effect of the A = equivalence ratio and B = spray distance on the maximum attainable gas temperature for the DJ1050 gun 82
4.16 Temperature contour showing the relationship between the spray distance and equivalence ratio for the DJ1050 gun 83
4.17 Interaction plot of the temperature with the spray distance and the equivalence ratio for DJ1050. (A = the equivalence ratio) 84
4.18 Perturbation plot showing the effect of A = equivalence ratio, B = spray distance and D = air flow rate on the gas temperature response for DJ2700 . 85
4.19 Contour plot of the gas temperature response vs the spray distance and the equivalence ratio for DJ2700 86
4.20 Interaction plot of the temperature with spray distance and equivalence ratio of DJ1050: A = the equivalence ratio, B = spray distance, D = air flow . . . 86
4.21 Interaction plot of temperature with spray distance and equivalence ratio for DJ2700: A = the equivalence ratio and D = air flow 87
4.22 Contour of velocity magnitude and its profile along the centerline for a): DJ1050 and b): DJ2700, the contours are for the case of $\phi = 1.01$ for both guns 88
4.23 Normal plot residuals (a) and difference between actual and predicted values (b) for the gas velocity response for DJ1050 92
4.24 Perturbation plot for velocity response for DJ1050; A = equivalence ratio and B = spray distance 93
4.25 Contour plot of the velocity response for the DJ1050 94

4.26 Perturbation plot of DJ2700; D = air flow, A = equivalence ratio, C = particle size 94
4.27 Particle temperature profile for three particle sizes along the centerline of the nozzle for DJ1050 96
4.28 Particle temperature profile for three particle sizes along the centerline of the nozzle for DJ2700 96
4.29 Particle velocity profile for three particle sizes along the centerline of the nozzle for DJ1050 97
4.30 Particle velocity profile for three particle sizes along the centerline of the nozzle for DJ2700 97
4.31 Perturbation plot for particle temperature response; C = particle size and B = spray distance for DJ1050 100
4.32 Interaction of the particle temperature response with particle size and spray distance 100
4.33 Perturbation plot for particle temperature response; C = particle size , B = spray distance, A = equivalence ratio and D = air flow rate for DJ2700 . . . 101
4.34 Perturbation plot for particle velocity response C = particle size and B = spray distance for DJ1050 104
4.35 Interaction of the particle velocity response with the particle size and spray distance for DJ1050 105
4.36 Perturbation plot for particle velocity response C = particle size and A = air flow rate for DJ2700 105
4.37 Interaction plot of particle velocity response with the equivalence ratio and particle size for DJ2700 106
4.38 Perturbation plot shows the relation between the particle temperature at the nozzle exit with the spray distance and particle size for B = spray distacne and C = particle size: DJ1050 108
4.39 Interaction of the particle velocity temperature at the nozzle exit with the particle size and spray distance for DJ1050 110

4.40 Perturbation plot for particle temperature at the nozzle exit response C = particle size and B = spray distance A = equivalence ratio and D = air flow rate for DJ2700 111
4.41 Interaction plot of particle temperature at the nozzle exit response with particle size and equivalence ratio for DJ2700 112
4.42 Perturbation plot shows the relation between the particle temperature at the nozzle exit where; B = spray distance and C = particle size and A = equivalence ratio: for DJ1050 115
4.43 Interaction plot between the spray distance, equivalence ratio and particle velocity at nozzle exit for DJ1050 115
4.44 Interaction plot between the spray distance, particle size and particle velocity at nozzle exit for DJ1050 116
4.45 Perturbation plot showing the relation between the particle temperature at the nozzle exit where; B = spray distance , C = particle size A = equivalence ratio and D = air flow: for DJ2700 117
4.46 Interaction plot between the spray distance, particle size and particle velocity at nozzle exit for DJ2700 118
4.47 Interaction plot between the spray distance, particle size and particle velocity at nozzle exit for DJ2700 119
4.48 Overlay plot for the first target for the DJ1050 gun 122
4.49 Overlay plot for the first target for the DJ1050 gun 124

List of Tables

2.1 Spary parameters for the nine operating conditions [34] 17

2.2 Particle in-flight properties measured by the DPV-2000 system [34] 17

2.3 Process parameters [30] 17

2.4 Taguchi-style, orthogonal L8 design matrix used in [30] 18

3.1 Thermophysical properties of WC-12%Co [66] 46

3.2 Operating conditions for the DJ1050 HVOF , flow units in SLPM, ϕ representing the correspondent equivalence ratio ($\phi > 1$ = rich ; $\phi < 1$ = lean) 47

3.3 Operating conditions for the DJ2700 HVOF, flow units in in SLPM, ϕ representing the correspondent equivalence ratio ($\phi > 1$ = rich ; $\phi < 1$ = lean) 48

3.4 Process variables and experimental design used 54

3.5 DOE operating conditions for DJ1050, where ϕ represents the correspondent equivalence ratio 55

3.6 DOE operating conditions for DJ2700, where ϕ represents the correspondent equivalence ratio 56

3.7 ANOVA table for full model 57

4.1 Calculated responses for DJ1050 63

4.2 Calculated responses for DJ2700. 64

4.3 Calculated responses for DJ2700. 65

4.4 ANOVA analysis for Static pressure model for DJ1050. 69

4.5 ANOVA analysis for Static pressure model for DJ2700. 69

4.6 ANOVA analysis for Static temperature model for the DJ1050 gun. 78
4.7 ANOVA analysis for Static temperature model for the DJ2700 gun. 78
4.8 ANOVA analysis for gas velocity response model for the DJ1050 gun. 90
4.9 ANOVA analysis for gas velocity response model for the DJ2700 gun. 90
4.10 ANOVA analysis for particle temperature model for DJ1050. 98
4.11 ANOVA analysis for particle temperature model for DJ2700. 98
4.12 ANOVA analysis for particle velocity response model for DJ1050. 103
4.13 ANOVA analysis for particle velocity response model for DJ2700. 104
4.14 ANOVA analysis for the particle temperature response at the nozzle exit response model for DJ1050. 107
4.15 ANOVA analysis for particle temperature at the nozzle exit response model for DJ2700. 107
4.16 ANOVA analysis for particle velocity at the nozzle exit response model for DJ1050. 112
4.17 ANOVA analysis for particle velocity at the nozzle exit(response model for DJ2700). 113
4.18 Optimization criterion (i.e. Quality) low to medium gas / particle temperature and high velocity of gas /particle as the targets for the DJ1050 gun 121
4.19 Solution of the operating parameters for the DJ1050 gun 121
4.20 optimization criterion (i.e. quality) low to medium gas / particle temperature and high velocity of gas /particle as the targets for the DJ2700 gun 123
4.21 Solution of the optimized operating parameters for the DJ2700 gun 123

Nomenclature

Abbreviations

DOE	Design of experiment
g/h	Gram per hour
g/m	Gram per minute
L/m	Litre per minute
$SCFH$	Standard cubic feet per hour
SOD	Stand off distance
APS	Atmospheric Plasma APS
CFD	Computational Fluid Dynamics
CGS	Cold Gas Spray
DG	Detonation Gun
EDM	Eddy Dissipation Model
FR	Feed Rate
FRED	Finite Rate Eddy Dissipation
HVAF	High Velocity Air Fuel
HVOF	High Velocity Oxy Fuel
LFR	laminar Finite Rate
LPPS	Low Pressure Plasma Spray

SEM	Scanning Electron Microscopy
SOD	Stand off distance
VPS	Vacuum Plasma Spray
XRD	X Ray Diffraction

Symbols

$\dot{\omega_k}$	Rate of reaction of species k
$\eta_{j,i}^{'}$	Reaction rate exponent of species j in reaction r
Γ	Stoichiometric coefficient of reactant k in reaction r
∇	Gradient operator
ϕ	equivalence ratio
ρ	Density
t	Time in *second*
$v_{j,i}^{''}$	Product rate exponent of species j in reaction r
$\bar{\rho}\tilde{u}'\tilde{e}'$	Energy Reynolds flux component
$\bar{\rho}\tilde{u}'\tilde{u}'$	Reynolds stress component
$\bar{\tau}$	Shear stress tensor
$\delta_{i,j}$	Kronecker delta
ϵ	Turbulence dissipation rate
λ_t	Prandtle number for turbulent energy
μ_t	The eddy viscosity
ρ_g	Gas density
A_p	Surface area of the particle
C_D	Drag coefficient

C_{D0}	Drag coefficient of a particle in an incompressible fluid, where $M \simeq 0$
$C_{j,r}$	Molar concentration of species j in reaction r in $Kmol/m^3$
e	The total energy per unit mass $e = \sum_{k=1}^{N} h_k Y_k - P/\rho$
f_k	Body force of k species
h_k	Enthalpy of species k
k	Turbulent kinetic energy
k_n	Knudsen number is the ratio of the molecules free path to the particle diameter $= \lambda/d_p$
$k_{b,r}$	Backward rate constant for reaction r
$k_{f,r}$	Forward rate constant for reaction r
M	Mach number
m_p	Mass of the particle
m_{fuel}	mass fraction of a Fuel
$m_{oxidizer}$	mass fraction of an oxidizer
$M_{w,k}$	Molecular weight of species k
n_{fuel}	mole fraction of a fuel
$n_{oxidizer}$	mole fraction of an oxidizer
P	Pressure in Pascal
q	Heat flux
$R_{k,r}$	Rate of destruction/creation of species k in every reaction r in which it participates
Re	Reynold's number
S_{ij}	The mean strain rate tensor

T	Temperature in Kelvin or degree Celsius
T_c	Temperature of the continuum
T_d	Particle temperature
u	Velocity component
v_g	Gas velocity
V_k	Diffusivity of species k
v_p	Particle velocity
$v''_{k,r}$	Stoichiometric coefficient of product k in reaction r
W	Total molecular weight of the species
Y_k	Mass fraction of k species in the transport equation
Y_P	mass fraction of product species
Y_R	mass fraction of reactant species

Abstract

The aim of this study is to provide the thermal spray coating community with a parametric study and optimized quantifiable variables for two gun nozzle geometries (Oerlikon Metco DJ1050 and DJ2700) used in High Velocity Oxy Fuel thermal spray coating. The study applied a statistical Design of Experiment technique to the results obtained by Computational Fluid Dynamics models performed using the ANSYS FLUENT programme. The study parametrize and optimize the particle velocity and temperature, so as to achieve low to medium particle temperature and the maximum particle velocity, as this is the criterion to gain low porous, more dense coating and higher coating bond strength. The first stage of the research was to study effect of the density variation with the pressure and temperature at the inlet boundary condition. This type of investigation was never conducted before and thus is, to be the best of the author's knowledge, a novel approach. The computational modelling was then validated against an experimentally measured particle temperature. Equivalence ratio, spray distance, particle size and the air flow rate were found to be the process parameters required to optimize for the required targets. The results of this study also gives description and explanation on the behaviour and interaction between the process variables under investigation via the statistical and mathematical relations developed in the study. Finally, the results of this study were intended to be a guide in the design of the High Velocity Oxy Fuel by referring to the parametric relations and optimized parameters developed in this study by applying a Design of Experiment technique on a reliable set of Computational Fluid Dynamics results, which is considered the novelty of the study. For both the DJ1050 and DJ2700, the equivalence ratio was found to be the most influential parameter followed by the particle size to achieve the criteria of low to medium gas temperature, maximum gas velocity and maximum particle temperature. The

less effective parameter was found to be the spray distance. However, a set of optimum operating parameters considered in this study were obtained for each gun, which shows that for the DJ1050 gun a range of the equivalence ratio between 0.87 ($fuel - lean$) and 1.44 (fuel-rich) can be applied with an average spray distance of 190 mm and an average particle size of 30 μm are the optimum values to be applied to reach the favourable target in HVOF process. While for the DJ2700, the optimized set of the equivalence ratio was biased toward fuel rich mixture ($\phi > 1$) with constant spray distance of 150 mm and particle size of 5 μm to achieve the desired target of HVOF process.

Chapter 1

Introduction

1.1 Motivation of the Study

The motivation of this study was based on the growing demand and application of the growing ubiquitous technology of High Velocity Oxy Fuel (HVOF) Thermal spray process. The process has been expanding rapidly since its advent in the 1980's into many different industries along with other thermal spray techniques. The High Velocity Oxy Fuel coating process is mainly used to conduct treatment/enhance surfaces of engineering components that are usually subjected to harsh and hostile environments. In general, thermal spray coating techniques are used to provide such affected surfaces of the engineering materials with a protective coating. Depending on the application, the purpose of the coating could be a protection from some physical/chemical deterioration processes , and/or an improvement in the surface material quality.

To give some examples, turbines blades in any thermal power plants are normally exposed to very high temperatures and as a result high thermal stresses are developed in the surface of the material within such turbines blades. High Velocity Oxy Fuel process has been successfully used to overcome such problems and has increased the life expectancy of the blade material. Another example is the pipelines used in the Oil and Gas industry. The interior surface of the pipes degrade due to wear and corrosion, which is a typical and inevitable problem in such industries. The High Velocity Oxy Fuel has again been proven to

be a good solution to such a problem. High Velocity Oxy Fuel process is based on injecting powdered materials into an accelerated combustible jet in order to be heated to a molten and semi-molten state, and then accelerated this impinging particles into the surface to be coated. The process typically involves: combustion, supersonic jet, and particle flow.

1.2 The Aim and Contribution of This Study

The main aim of this study was to apply both Computational Fluid Dynamics and Design of Experiment approaches to the HVOF so as to conduct a parametric study for the multiphase flow of such coating process. The combined approach was never adopted to parametrize some of the main process parameters to achieve higher particle velocity and low to medium temperature at the point of impact, which is a target in this industry. Higher particle velocity and low to medium temperature at the point of impact is known to be the main reason of producing high dense or low porous coating with greater bond strength, regardless of the application or the coating material used.

Firstly, Computational Fluid Dynamic modelling was conducted to simulate the multi phase flow within two nozzle geometries (Oerlikon Metco DJ1050 and DJ2700 HVOF guns). ANSYS FLUENT code was applied to simulate the process. An investigation on the effect of the density variation on the mass flow rate at the boundary condition on the flow was conducted. The model was then validated against an experimental measurement. The Computational Fluid Dynamics models was expanded to cover a range of operating conditions used in High Velocity Oxy Fuel of WC-12%Co, the most popular powder sprayed using this technique. The parametric study was then conducted by applying Design of Experiment techniques on two different nozzle geometries and a comparative study between their performance was analysed.

Having parametrized the process parameters of interest, an optimization technique was conducted to optimize the process parameters. The target of the optimization was to achieve medium to high particle temperature and high particle velocity. The process parameters considered in this study were:

1. Equivalence ratio
2. Spray distance
3. Particle size
4. Air flow rate (just for DJ2700)

The process parameters effect on some of the process variables were studied and quantitative relations/models between them were developed. The process variables that were considered in this study were:

1. Maximum gas static pressure
2. Maximum gas static temperature
3. Maximum gas velocity magnitude
4. Particle temperature at the maximum spray distance (substrate location)
5. Particle velocity at the maximum spray distance (substrate location)
6. Particle temperature at the exit of nozzle
7. Particle velocity at the exit of nozzle

The statistical models and optimized parameters could be used to serve as a guidance in the design of the High Velocity Oxy Fuel gun for optimizing coating performance. The advantage of the approach adopted in this study was that some variables of the High Velocity Oxy Fuel are difficult to be measured, such as the temperature and the pressure inside the nozzle. It is in this context that Computational Fluid Dynamics modelling was applied along with the Design of Experiment in order to provide thermal spray coating community with more adequately quantitative relations between some of the most important process parameters/variables, which is truly novel within the thermal spray literature.

1.3 Thesis Outline

The thesis introduction offers an overview of the motivation of this study followed by the main aim and contribution of this study to the thermal spray coating community. The

second chapter of this thesis includes some of the key publication of the experimental work conducted on the High Velocity Oxy Fuel thermal spray process. The literature review on the experimental literature is a focus on some of the experimental parametric work, in order to highlight some of the most important process parameters influencing the High Velocity Oxy Fuel thermal spray process. The literature review chapter concentrates on all the previous modelling work conducted on the High Velocity Oxy Fuel process to date and the chapter ends by highlighting the contribution of work to the thermal spray coating community. Chapter three provides the details of the research methodology applied in this study. The results are presented and discussed within the fourth chapter of this thesis. The final chapter is intended to provide a conclusion of the study and recommendations for future work.

Chapter 2

Literature Review

2.1 Introduction

The literature review provides a detailed introduction to surface engineering and the physical and chemical phenomena that occurs at the surface of many engineering components within different applications. An explanation of thermal spray coating technologies is also provided. The literature is then concentrated on the High Velocity Oxy Fuel (HVOF) which was the process of investigation in this study.

The fundamental concepts of the physics of the HVOF process are provided in this chapter. Since this research is based on computational modelling approach, a literature review of previous, related experimental and modelling work published is summarized. The operating parameters of the HVOF process are discussed and their relative importance are given. Finally, the contribution of this work to thermal spray coating community is provided in this chapter.

2.2 Surface Engineering

Engineering components service life is severely affected by degradation due to wear, corrosion, thermal stresses and other surface phenomena. The cost of degradation of materials within engineering components is estimated to be of an order of billions of dollars in the United

States of America alone, which is approximately 3 to 5% of its GDP [1, 2]. The durability and reliability of an engineering component is strongly dependent on the characteristics of its surface.

Surface engineering science was established to tackle these problems for many different applications and industries. Surface engineering can be defined as "the branch of science that deals with methods for achieving the desired surface requirements and their behaviour in service for engineering components" [3]. Many techniques have been developed to enhance engineering components surfaces, and these techniques are collectively described as coating techniques.

In any coating process, a material is deposited onto the surface of another material in order to improve some properties of the coated material's (bulk material) surface. The available coating techniques are classified into two main groups; metallic and non-metallic [4]. However, the classification of thermal spray coating techniques is illustrated in Figure 2.1.

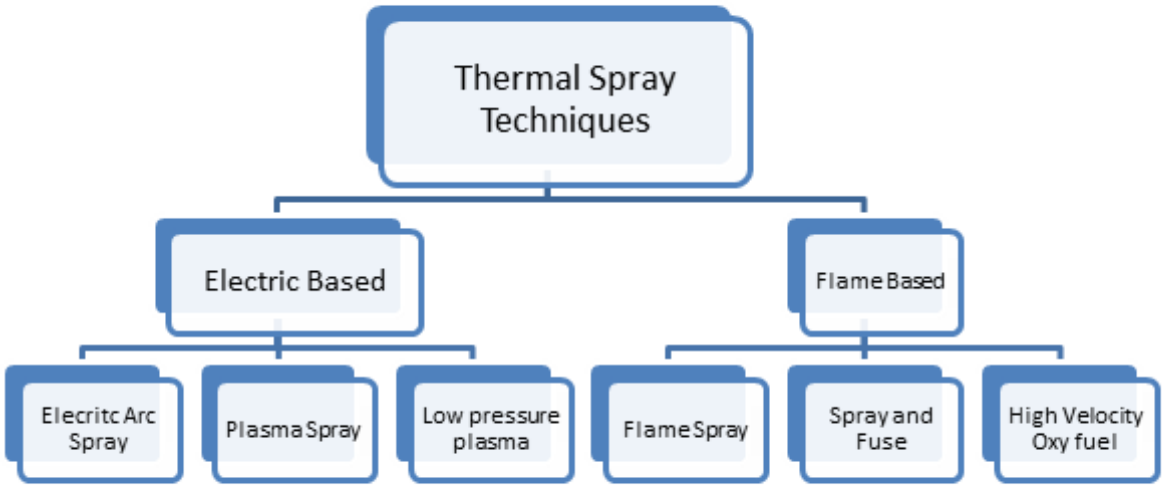

Figure 2.1: Classification of thermal spray coating techniques

Amongst those techniques developed so far, thermal spray coating techniques are considered as one of the most effective and economical method for many industrial applications [5]

2.3 Thermal Spray Coating

Thermal spray deposition was discovered by Dr. Max Schoop over a century (1912) ago when he extracted the idea from a canon toy of his child. In 1933, the process was adopted by the group Metco incorporated, which continued to develop and expand the process for purposes of machine element repair work and anti-corrosion by depositing resistant zinc coatings. The technology of thermal spraying continued to expand in industry and many different techniques were developed in the last century. Nowadays, thermal spray processes are one of the most rapidly growing surface engineering and modification technologies [5–7]. A general illustration of thermal spray process is given in Figure 2.2.

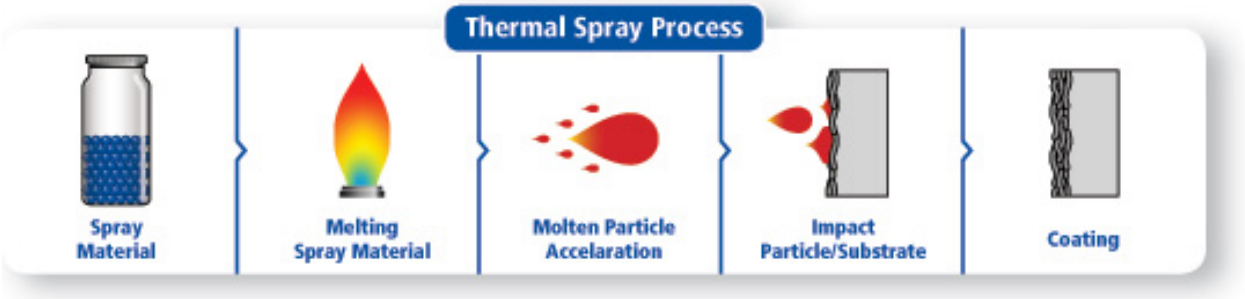

Figure 2.2: Thermal spray coating principle [7]

The working principle of any thermal spray coating process is based on heating and accelerating a feedstock (powders/particles) by transferring sufficient amount of kinetic and thermal energy via a confined working fluid to them and then propelling them towards the surface to be coated [6, 8]. Usually, the source of energy used in thermal spray processes is either electrical or combustion.

Based on the source of energy, thermal spray processes are classified into electrical based; plasma spray method (atmospheric plasma APS, vacuum plasma spray VPS, and low pressure plasma LPPS), electric arc wire, combustion based; flame spray, high

velocity oxy/air-fuel (HVOF/HVAF), detonation gun (DG), and, the most recent developed technology, cold spray (CGS) [8].

2.3.1 Electric Arc Process

In the electric arc spray, two electrically conductive consumable rods or wires are used to form an electric arc of a direct current. As a result of the Ohmic heat generated by the current arc, the rods or wires materials melt and the tips of them are atomized and propelled toward the substrate to be coated Figure 2.3. It is worth mentioning that this technique was the one developed by Dr.Schoop in 1910. However, the main constraint of electric arc spray process is that only materials in the form of wire or rods can be sprayed [7, 9].

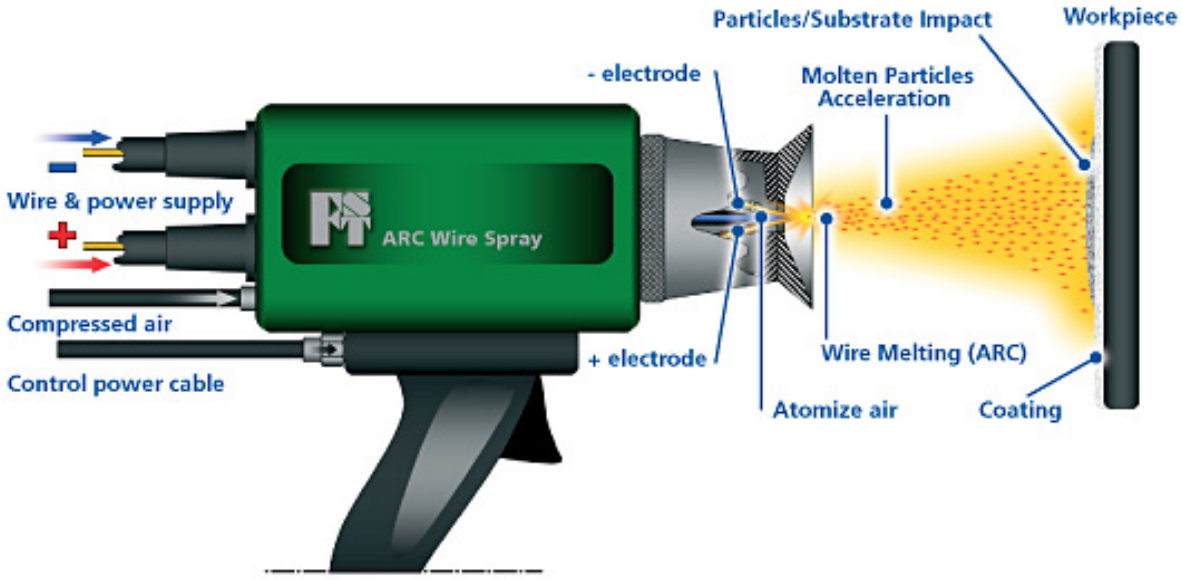

Figure 2.3: Electric arc spray [7]

2.3.2 Plasma Spray

In plasma spray, the working fluid (electrically conductive gas) flows around the cathode and through a confining tube or nozzle (anode), Figure 2.4. The working gas is ionized by a current (arc) created by a high-voltage pulse between the cathode and anode parts of the assembly [7, 10, 11]. The temperature output produced by ionizing the gas is significantly high (e.g., $> 10,000$ K), which makes the process suitable only for materials with high

melting point. The plasma is confined by the cold nonconductive gas around the surface of the water-cooled nozzle or confining tube. Most of the available commercial plasma spray torches operate at atmospheric pressure with electric power levels ranging between 10 and 100 kW, arc currents between 250 and 1000 A, arc voltages between 30 and 100 V, and flow rates between 20 and 150 SLPM (standard liters per minute) [7]. Common gases used in thermal plasma processing are Ar, He, N_2, O_2, and mixtures of these .

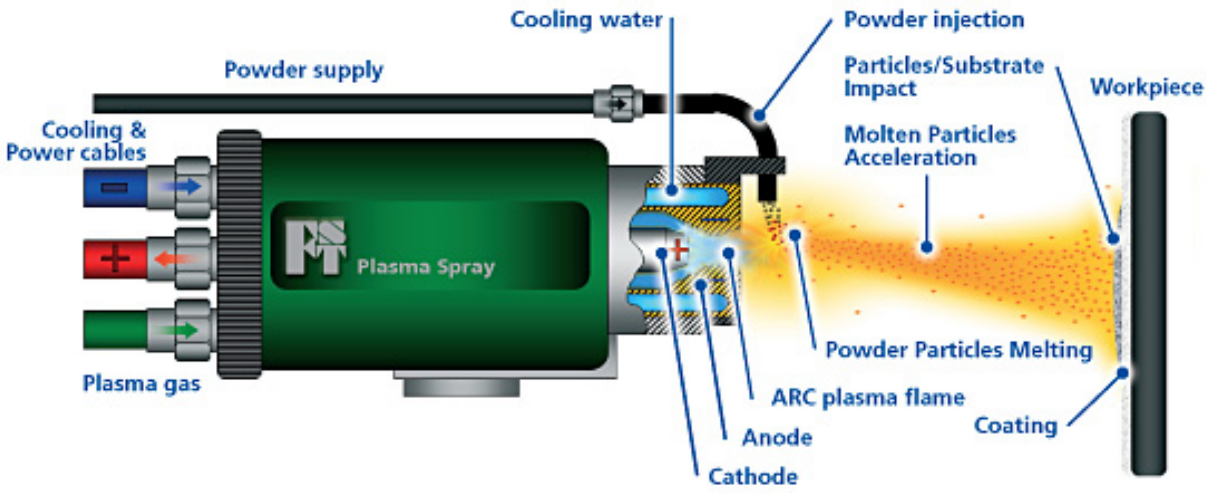

Figure 2.4: Plasma spray process [7]

2.3.3 Flame Spray Processes

This branch of thermal spray processes, in which HVOF process is included, is based on combustion energy rather than electrical energy source and the coating material can be of either wire or powder form. The wire materials are usually inexpensive, contain high level of porosity and oxides and a rough surface could be obtained if desired [7]. An illustration of wire spray process is shown in Figure 2.5. On the other hand, a wide range of materials in the form of powder can be coated and a dense or low porosity coating can be obtained. HVOF is classified as one of this processes Figure 2.6.

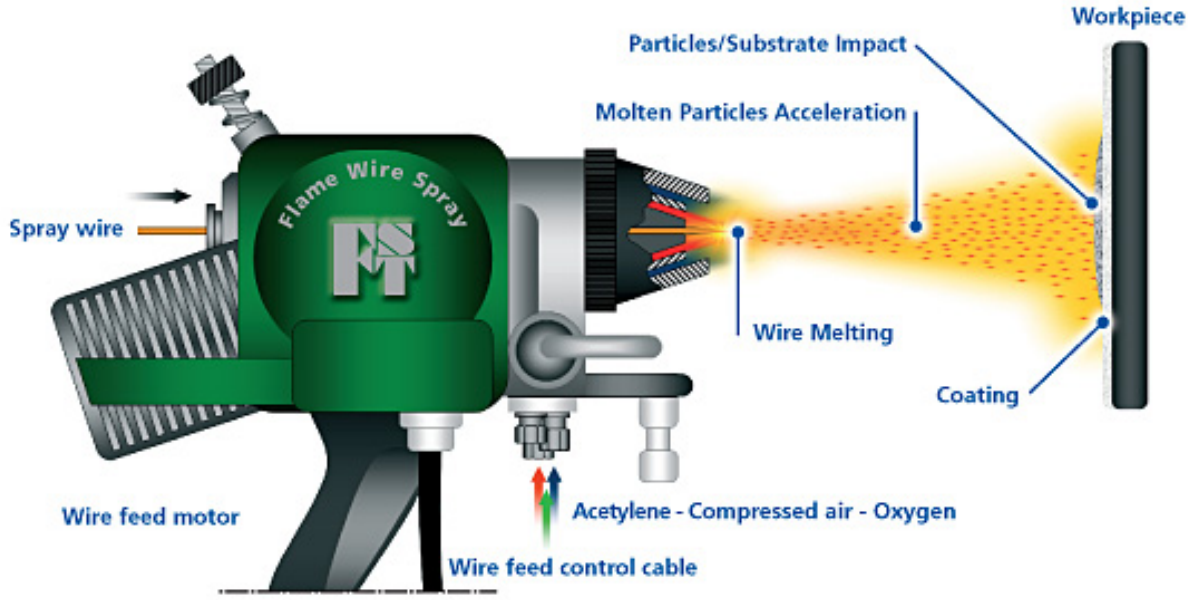

Figure 2.5: Flame wire spray process [7]

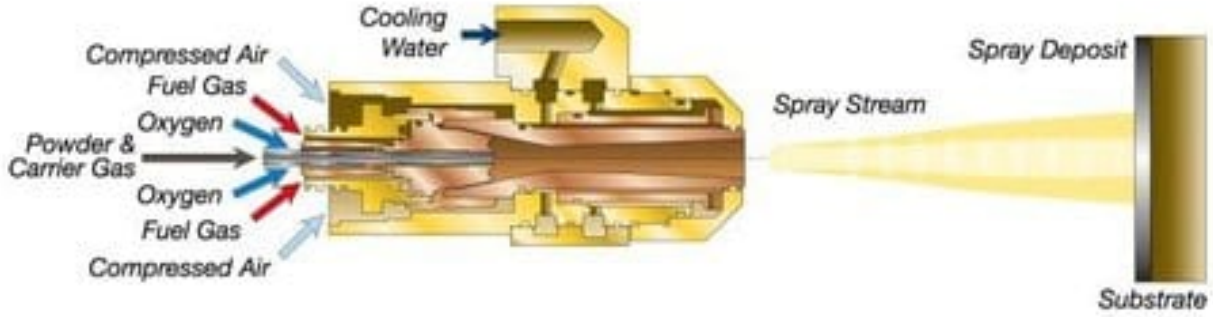

Figure 2.6: Flame Powder spray process under which HVOF is categorized [7]

2.3.4 High Velocity Oxy Fuel (HVOF)

The chemical and physical state of the particle at the point of impact play a crucial role in the quality and characteristics of the coating. Temperature and velocity of the coating particles are taken as parameters which contribute to the particle state upon impact and relate to the quality and characteristics of coating [8, 12]. In general, the development trend of thermal spray processes is towards achieving higher velocities and lower temperatures.

During the 1980's, a new combustion-based thermal spray technique, HVOF, was developed to achieve relatively high velocities and low to medium temperatures. This desirable combination of velocity and temperature within the HVOF process is the main advantage the process has over other thermal spray techniques.

In addition, the wide range of materials that can be coated by HVOF is another key advantage. In contrast to plasma spray, where materials with low melting points can not be coated due the tremendous amount of heat produced by the plasma, or cold spray by which material with high volume deformation rate can only be used [12–14]. The HVOF does not pose such issues. A representation of the thermal spray development and where HVOF fits relative to other processes is shown in Figure 2.7.

Generally, any material that can melt and deform can be used as a coating material and the majority of the known materials satisfy these characteristics. Materials such as cermets, ceramics, metals, polymers, and composites of them can be used in HVOF thermal spray coating [15]. However, cermet or carbides, such as tungsten carbide WC and chromium carbide Cr_3C_2 are the dominant hard-phase materials used as compositions for thermally sprayed coating . Cobalt Co and Nickel Ni are the most commonly used metals (binders) and can be blended with the carbide powder to form feed-stock powders typically in the range of (5-45) μm [16].

The combination of low to medium temperatures and high velocity of HVOF is thought to be the main reason for producing dense or low porous coating, which is a common target in many industrial applications [8]. Recently, HVOF has been considered as a good alternative to hard chromium electroplating (a highly costly technique). Nevertheless, further developments can still be achieved for HVOF thermal spray process through alternative or new feedstock material manufacturing [17]. HVOF has attracted many researchers of many different fields due to its outstanding performance and wide range of applicability [15]. Despite its simple operation depicted in Figure 2.8, one of the main disadvantages of HVOF or combustion based processes is its complexity in terms of its underlying multi physics and multi scale interaction of the process variables making it difficult to handle and control the operating parameters [18–20].

As mentioned, HVOF is a combustion based process in which a mixture of hydrocarbons fuel (C_nH_n) and oxidant, normally air or oxygen, under pressure ($4 \longrightarrow 10$ bar) flow towards a chamber to generate combustion and subsequently accelerate through varying area nozzles [12]. The jet of the combustion flow then expands supersonically through expansion and compression waves (Prandtle-Meyer fans) [21] to the atmosphere, while the coating material

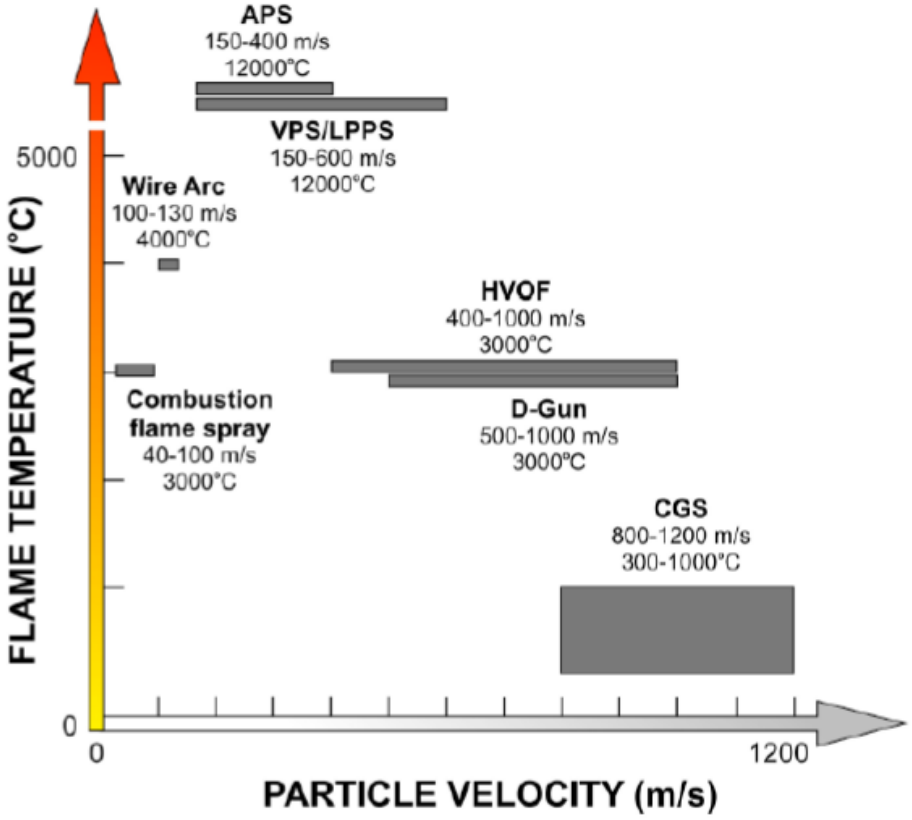

Figure 2.7: Process temperature and velocity range for different TS processes [8]

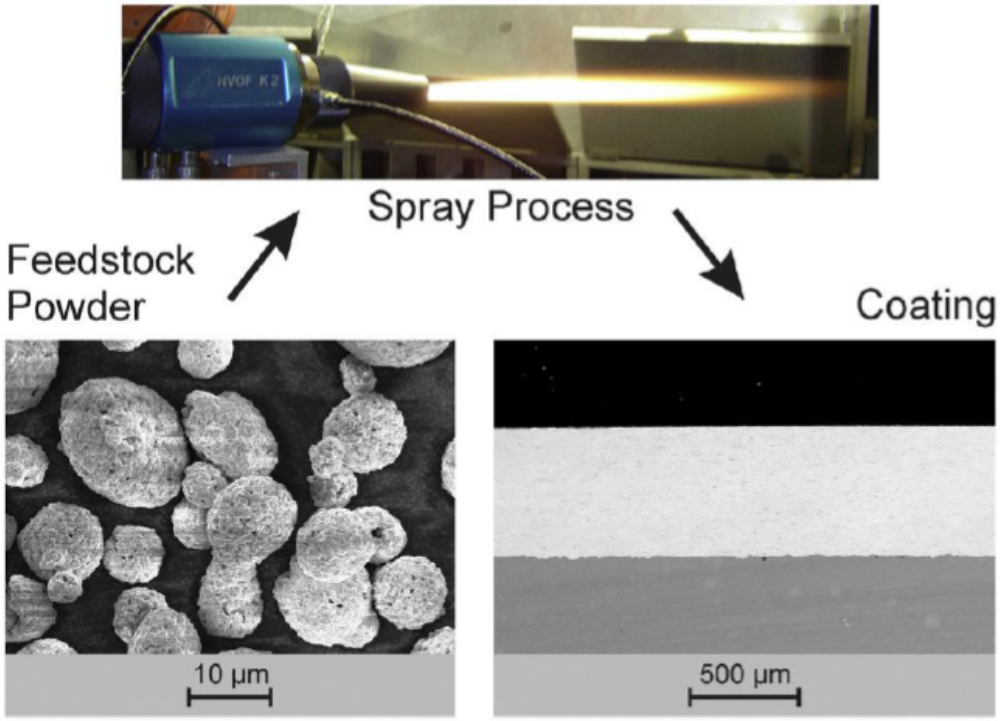

Figure 2.8: High Velocity Oxy Fuel Process [15]

in the form of powders of different sizes are injected either radially or axially into the flow to be heated and accelerated towards a substrate (receiving surface).

The particles are heated to a molten or semi-molten state and accelerated by the flame temperature (3000 $\longrightarrow$ 3500 K) and velocity (1000$\longrightarrow$2100 m/s), before impinge, solidify and adhere to the substrate to be coated [8, 12, 13]. The process is repeated to produce a pancake-like lamellar structured coating of a desired thickness and physical/metallurgical properties [22] as illustrated in Figure 2.9.

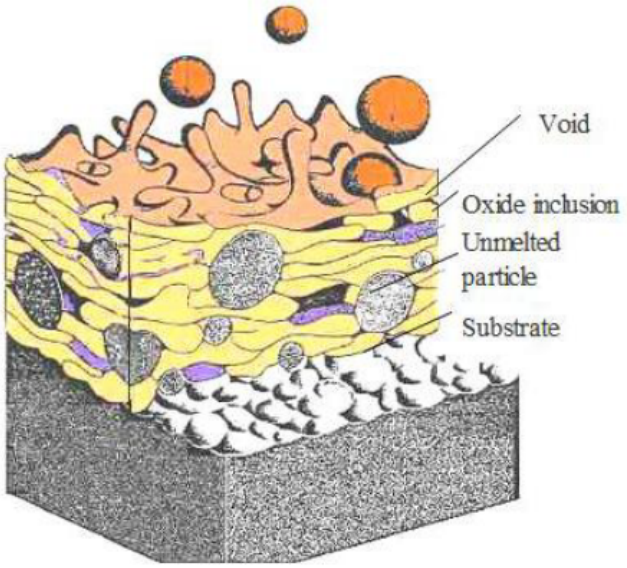

Figure 2.9: Coating formation during High Velocity Oxy Fuel Process [22]

Regardless of the kind of feedstock material used during any thermal spray coating process, a complex chemical and physical interaction occurs between the working fluid (the flame) and coating particles. Metallurgical and physical transformations are usually developed due to this interaction [23]. Some of these transformations are beneficial while others are detrimental [24–26]. It was found that under an optimum fuel-to-oxygen ratio a photocatyltic TiO_2 surfaces with a high anatase ratio can be obtained by HVOF process to increase the photocatalytic activity of solar panels [24]. On the other hand, an oxidation of the particle in flight is a main reason for the oxide content in the coating which decrease the density and quailty of the coating [27, 28].

A considerable portion of the literature on HVOF thermal spray coating was found to be focused on achieving an optimum combination of temperature and velocity of the particle to enhance the coating properties for a specific application [24–38]. The applications that benefit from HVOF thermal spray technology are numerous, ranging from biomedical, electronic, oil and gas, automation, aviation and even renewable energy sector, such as in

fuel cell manufacturing, and improving the photocatalytic activity of solar panels, through a favourable phase transformation [12, 24, 26, 39, 40]. Some of the relevant experimental work in the literature is briefly discussed in the following section.

2.3.4.1 Experimental Approach

As the ultimate aim of any thermal spray process is to enhance some tribological and chemical properties of the surface, generally, against wear and corrosion. The majority of experimental procedures in the literature aim to correlate the effect of process parameters against coating performance and microstructure (process optimization /deposition control) [8, 19]. The state of the art instruments for diagnosing and measuring the process parameters are well established, however, measuring some properties like the suspension of nano particles in a liquid prove difficult to determine using current instruments [12].

Generally, both the morphology (microstructure) and phase composition of either, the coating material and as-sprayed coating are diagnosed by optical techniques of SEM (Scanning Electron Microscopy) and XRD (X Ray Diffraction) [41]. In addition, many instruments are used to measure the other variables such as reaction enthalpy, particle temperature, particle velocity and particle size and flux. An enthalpy probe system was used to measure the plasma plume temperature distribution under the effect of using anodes with different inner diameters by Steffen et al. [42] , where steady state conditions were reached for the measurement.

Accuraspray-G3, a commercially available measuring system, is able to measure and characterize the spray plume and average particle temperature and velocity. It was used to study the effect of different gas flow rates (fuel, oxidant, total and equivalence ratio) on the particles temperature and velocity by Picas et al. [29]. The device is based on cross-correlation of signals, dual fibre optic, recorded at two closely spaced locations in the spray stream and the temperature is determined via two-colour pyrometry [43].

Another device based on an optical principle, is the DVP2000 diagnostic system. This system operates via two spectral IR wavelength ranges of 18 $\rightarrow$ 790 nm and 18 $\rightarrow$ 990 nm [44]. The signal of the heat emitted by particle can be analysed in terms of particle

volume, velocity and temperature while it passes through a measurement volume. The advantage of two-color pyrometry is that it eliminates the effect of particle size, emissivity and non-ideal focusing and so can be used with all materials without material-specified calibration.

However, an assumption of grey body emitters is a disadvantage of such measurement principle and can lead to inaccurate measurements of 273 K . The velocity of the particle can be generally measured by Laser Doppler Anemometer. PIV (Particle Image velocimetry) can be used and the theory of working principle can be found in [44,45]. Many experimental studies were conducted to correlate the process parameters with the quality of the coating for a specific application. Hong et al. [38] optimized the spray distance and the flow rate of oxygen and kerosene for a corrosion resistance application, the values obtained for the parameters were 300 mm for spray distance, 1900 $SCFH$ (Standard Cubic Feet per Hour) for the oxygen flow as an optimized set of parameters for the application of interest.

Watanabe et al. [33] investigated the nitrogen flow rate influence on the microstructural and mechanical properties of metallic coatings in a warm spray process, during which nitrogen is used to decrease the flame temperature. It was found that nitrogen flow rate had a significant effect on the mechanical properties of the coating.

Picas et al. [29] studied the effect of the flow rate of hydrogen and kerosene fuel on the particle velocity and temperature. It was concluded that higher flow of kerosene fuel resulted in higher particle velocity and lower temperature than hydrogen fuel, the oxygen flow rate affect the combustion reaction and an excess of oxygen decreased the flame temperature. Additionally, it was found that increasing the total gas flow rate increased the particle velocity and consequently decreased the particle dwell time and temperature. The density of the coating increased with increasing particle velocity and temperature as the phase transformation of a WC−CoCr to W_2C in the coating material increased for both fuels.

It is worth mentioning that within this study [29] two different spray guns were used, namely Wokajet-400 and DJ-2600, however both yielded different wear resistance performance of the coating. In a similar study to Picas et al. [29], Gaona et al. [32] deposited nanostructured titanium oxide TiO_2 powders onto Ti-6Al-4V substrates to correlate the

particle temperature and velocity to coating properties and a linear relation between particle temperature, velocity and residual stress, anatase phase transformation, microhardness and bond strength was obtained.

The microstructure and mechanical performance (abrasive and sliding wear) of WC-12%Co coating was related to the variation of propylene flow rate according to Wang et al. [37]. The decarburization of WC and the density of the coating increased linearly with increasing propylene flow rate. The hardness and fracture initially increased and then decreased with an increase of the propylene flow rate. Particles of different sizes experienced different degrees of melting and as a result different degrees of decarburiztion and their microstructure within the coating, affects the wear performance of the coating. Similar results of Wang et al. [37] work were found by Zhang et al. [34, 46], the only difference was the coating material.

In Zhang et al. work [34], the particle in-flight properties was diagnosed by a Particle Diagnostic System (DPV-2000) for nine set of operating conditions, in which the parameters of oxygen flow rate, fuel flow rate, carrier gas, powder feed rate, and spray distance, or stand off distance (SOD) were considered as shown Table 2.1 and Table 2.2.

A 10% variation in the particle temperature was observed for the nine operating conditions, and the second operating condition yielded the highest particle temperature and the third gave the lowest one. The second operating parameter gave the highest particle velocity while the ninth yielded the lowest one. It was noted that all the parameters under investigation had a significant effect on the particle temperature and velocity, but the velocity changes more rapidly than temperature [34].

A Design of Experiment (DOE) approach was applied by Saaedi et al. [30]. In this work, a Taguchi style was applied on Ni−Cr HVOF coating process to set eight combinations of five process parameters of: oxygen flow rate, fuel flow rate, air flow rate, spraying distance (SOD), and feed rate(FR). Each parameter was varied between two values, designated maximum and minimum as shown in Table 2.3 and Table 2.4, and evaluation of the results showed that the most influential parameters affecting the in-flight particle temperature and velocity were fuel flow, spray distance, oxygen flow. The Fuel-to-oxygen ratio had a pronounced effect on

Table 2.1: Spary parameters for the nine operating conditions [34]

Coating	$O_2(L/m)$	$H_2(L/m)$	(N_2) (L/m)	FR (g/m)	SOD (mm)
1	231	609	20	40	290
2	231	609	20	40	250
3	175	545	20	40	290
4	228	652	20	65	270
5	202	578	20	65	270
6	202	578	20	100	270
7	202	578	20	30	270
8	204	636	20	80	250
9	176	504	20	65	270

Table 2.2: Particle in-flight properties measured by the DPV-2000 system [34]

Coating	Temp.(C)	Velocity (m/s))
1	2121	512
2	2145	521
3	1956	465
4	2116	496
5	2031	471
6	2003	451
7	2061	499
8	2016	474
9	1976	436

the coating quality, especially oxide content and density, while the stand off distance (SOD)

Table 2.3: Process parameters [30]

Parameter	O_2 (L/m)	Fuel (L/m)	Air (L/m)	SOD (mm)	FR (g/m)
Minimum	300	60	355	200	23
Maximum	350	85	405	300	34

had a marginal effect in the process under investigation. In another experimental parametric study, Selvadurai et al. [31] investigated the influence of substrate temperature, number of runs, SOD, track pitch, and gun velocity on the residual stress and hardness of WC-12%Co coating on C45 steel substrate of a complex geometry. A set of operating parameters was first determined based on a DOE run for the standard deposition rate, porosity, and standard

Table 2.4: Taguchi-style, orthogonal L8 design matrix used in [30]

Run no.	O_2	Fuel	Air	SOF	FR
1	-	-	-	-	-
2	-	-	-	+	+
3	-	+	+	-	-
4	-	+	+	+	+
5	+	-	+	-	+
6	+	-	+	+	+
7	+	+	-	-	+
8	+	+	-	+	-

hardness values. The outcome parameters values were identified to be: SOD of 170 mm, gun velocity of 300 mm/min and track pitch of 4 mm. The variation of the kerosene fuel and air flow from the standard values resulted in increasing the compressive residual stresses of the coating. It was also noticed that the substrate temperature was influenced by varying the operating parameters under investigation which affected the residual stresses.

It was concluded that the Oxygen-to-Fuel ratio, flow rate, stand-off distance, particle velocity, and particle temperature were the common parameters to be considered in the experimental approach in the literature [12,47]. Optimizing a set of parameters for a thermal spray process is totally dependent on the desired quality and characteristics of the coating for a specific application. Generally, dense or low porous and low oxide content coating is desirable for many engineering applications.

During the development of thermal spray techniques, it was inferred that this is achievable through increasing the velocity of the particle and reducing its temperature. However, the current instruments used for diagnosing the process parameters have some limitations, especially when the size of coating particles is reduced and that was in agreement with the results founded by Jadidi et al. [12] and Sova et al. [47].

The modelling approach is often thought to be a complement to the experimental work to address the limitations imposed upon the current measuring capabilities. The main advantage of applying modelling and computational techniques is the ability to shed a light on different aspect of the multi-physics in HVOF or any thermal spray process that would

otherwise be difficult to gain through the experimental instruments.

As an example, the combustion process involved in the HVOF process and the subsequent flow inside the nozzle can not be adequately measured by most of the current instruments. Combustion modelling can inform this knowledge. In the next section an introductory to the physics involved followed by a thorough survey of modelling and simulation work conducted so far for HVOF process will be given.

In summary, it can be concluded that some of the process parameters were commonly taken into account in the experimental work as discussed in this section. The discussion in this section was not an inclusive survey of the experimental work for HVOF, rather it was just to highlight some of these parameters.

2.4 Physics and Models of HVOF

The physico-chemical process of HVOF is a multidisciplinary process during which, based on modelling perspective, four physico-chemical processes are involved [18–20,48]. They can be ordered as follows:

1. Combustion
2. Compressible turbulent flow (subsonic/supersonic transition)
3. Multiphase flow interaction
4. Particle deformation and solidification (not included in this study)

Each of the aforementioned characterstics has its own quantitative and mathematical modelling representations. The intrinsic multi-physics and multi scale characteristic of the HVOF process makes it difficult to develop a theoretical or analytical model to describe the process. However, due to the advancement in numerical/computational methods and computing capability, many codes and simulation programs are constantly developed to simulate such complex multi-physics/disciplines, adding scientific value to a process like HVOF.

These codes are generally classified as either an open source code, solver such as

OpenFOAM [49] and SU2 [50], or commercial codes like ANSYS [51]. The obvious advantage of Open Sources codes over the commercial ones are their free availability and a manipulation of the code. However, the learning curve can be very steep due the lack of a graphical user interface and a solid background in C and C++ (the typical programming language by which the codes are generally written) is required. Commercial programs, on the other hand, are provided with a flexible graphical user interface, but with limited manipulation allowed.

Regardless of the code design and the algorithm applied, there are some established mathematical models for some of the physics involved in the process. These models have become standardized and applied in the majority of the simulation work produced so far. Models that can be considered to have matured are for; combustion, turbulence and flow dynamics. In the subsequent sections, each of the physical characteristics involved in the HVOF process will be described and their mathematical models are provided.

2.4.1 Combustion

The combustion of hydrocarbon fuels is generally the most common energy source for HVOF, hydrogen is much less used as a fuel. Hydrocarbon combustion can be described by the following chemical equation [52–56]:

$$C_xH_y + zO_2 + 3.71\,zN_2 \longrightarrow xCO_2 + y/_4H_2O + 3.71\,zN_2 \tag{2.1}$$

if the air, as an oxidant in the above equation, is considered to be composed of $79\%N_2$ and $21\%O_2$. Usually, Nitrogen is considered inert in the above combustion equation and does not participate in the reaction. If the oxidant is Oxygen, the Nitrogen compound in Equation 2.1 is eliminated, then the equation takes the form:

$$C_xH_y + zO_2 \longrightarrow xCO_2 + y/_4H_2O \tag{2.2}$$

the mole fraction for each compound in Equation 2.1 and Equation 2.2 represents the stoichiometric mole fraction for the both chemical reactions. The stoichiometric reaction is identified by the amount of oxidant and fuel needed to balance the above equations

of combustion. Once the stoichiometric reaction is determined, an important parameter which is the equivalence ratio (ϕ) can be obtained, which can be algebracilly described by Equation 2.3 [52–56]:

$$\phi = \frac{(m_{fuel}/m_{oxidizer})_{actual}}{(m_{fuel}/m_{oxidizer})_{stiochiometric}} = \frac{(n_{fuel}/n_{oxidizer})_{actual}}{(n_{fuel}/n_{oxidizer})_{stiochiometric}} \tag{2.3}$$

where the ratio of the actual mass or mole fraction of the fuel to oxidizer, $(m_{fuel}/m_{oxidizer})_{actual}$, is stoichiometrically balanced, where m and n stand for the mass and the number of moles, respectively. For fuel-rich mixtures ($\phi > 1$), generally less efficient but can produce more power and burn cooler, whereas fuel-lean mixtures ($\phi < 1.0$) are more efficient, but can produce higher amount of Nitrogen Oxides thus ($\phi = 1$) is defined as the stoichiometric condition, where enough oxygen exists to burn up all of the fuel.

The effect of ϕ on the behaviour of the jet is significant, especially with respect to temperature, which can be quantitatively indicated for different fuel combustion under the standard condition of 1 bar and 273.15 K (Figure 2.10). Most of adiabatic temperatures for the combustion of hydrocarbon fuels have a similar relationship with the equivalence ratio. The adiabatic temperature is one that satisfies a balanced change of enthalpy for the combustion reaction [57].

Generally, it has been deduced that the adiabatic combustion temperature peaks around an equivalence ratio of 1 towards the fuel-rich side ($\phi \simeq 1$). Usually, the combustion pressure in a HVOF process is in the range of $3 \rightarrow 10$ bar [12], despite the first review article on modelling of HVOF claiming that combustion pressure ranged from $5 \rightarrow 20$ bar [2]. Increasing the combustion pressure results in an increase in the adiabatic flame temperature.

Furthermore, higher combustion pressure affects the structure, turbulence length, and velocity time scales of a premixed flame, concluded by various studies by Kobayashi et al. [58–61]. As the mixture of a fuel and oxidant is introduced into the combustor part of the nozzle assembly, the combustion process can be categorized as a premixed combustion [52].

Mathematically, the combustion can be modelled as a general transport or convection-diffusion partial differential equation for the species involved in the reaction plus a source term represents the rate of reaction for each species. A general transport equation

can take the following form of Equation 2.4 [62]:

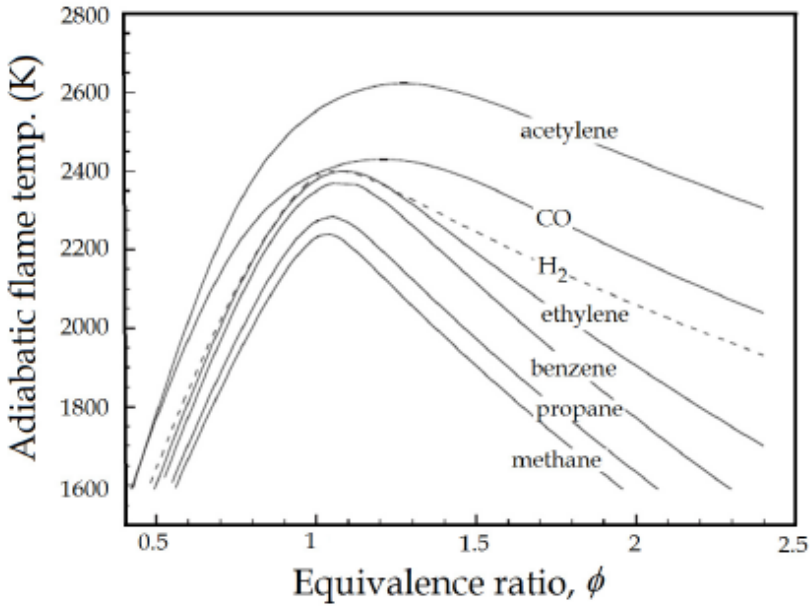

Figure 2.10: Variation of the adiabatic flame temperature with the equivalence ratio (ϕ) for different fuels combustion under the standard condition of 1 bar and 273.15 K [56]

.

$$\rho\frac{\partial Y_k}{\partial t} + \rho u \cdot \bigtriangledown Y_k = \bigtriangledown \cdot (-\rho V_k Y_k) + \dot{\omega_k} \qquad \forall \quad k = (1, \cdots, N) \tag{2.4}$$

where ρ, Y_k, u, V_k, $\dot{\omega_k}$, and N are the density, mass fraction, velocity, diffusivity, reaction rate of species k, and the total number of species, respectively. The combustion reactions represented by Equation 2.1 and Equation 2.2 can be considered as the simplified and ideal form of the hydrocarbon reactions. Combustion can contain a series of intermediate reactions that can be summed up to around 50 reactions as in the combustion of CH_4 (Methane) with oxygen [63, 64]. If every reaction step is to be taken into account, the computational cost time would increase dramatically.

To simplify the combustion process, a multi step combustion can be represented as one step global reaction [65–69]. If a multi-step reaction is applied, the kinetic rate of reaction (Arrhenius expressions) is the source of a computational load for such cases. The summation of the detailed Arrhenius rates for each species is equal to the rate of creation/destruction, given as [63]:

$$\dot{\omega_k} = M_{w,k} \sum_{r=1}^{N} R_{k,r} \tag{2.5}$$

$$R_{k,r} = \Gamma(v_{k_r}^{''} - v_{k,r}^{'}) \left(k_{f,r} \prod_{j=1}^{N} [C_{j,r}]^{\eta_{j,i}^{'}} - k_{b,r} \prod_{j=1}^{N} [C_{j,r}]^{v_{j,i}^{''}} \right) \tag{2.6}$$

which is also valid for both reversible and irreversible reaction, where the parameters in Equation 2.5 represent:

1. $M_{w,k}$ molecular weight of species k
2. Γ the net effect of a third body on the reaction rate, where $\Gamma = \sum_{j}^{N} \gamma_{j,r} C_j$
3. $v_{k,r}^{''}$ stoichiometric coefficient of reactant k in reaction r
4. $v_{k,r}^{'}$ stoichiometric coefficient of product k in reaction r
5. $k_{f,r}$ forward rate constant for reaction r
6. $k_{b,r}$ backward rate constant for reaction r
7. $C_{j,r}$ molar concentration of species j in reaction r in $kmol/m^3$
8. $\eta_{j,i}^{'}$ reaction rate exponent of species j in reaction r
9. $v_{j,i}^{''}$ product rate exponent of species j in reaction r

The backward rate constant for an irreversible reaction $k_{b,r}$ is zero, therefore the fourth term in the Arrhenius expression equation would be eliminated.

A combustion model was developed by Magnussen and Hjertager [70], to correlate the rate of the reaction to the time scale of turbulent eddies. The model greatly reduces the computation time for Arrhenius rates. The model is based on the fact that most fuels are fast burning and are mixed or convected by turbulence into the combustion zone, so thus are said to be mixing-limited, and chemical kinetics or Arrhenius rates can be ignored. The reaction rate is limited by the time scale of the large eddy of turbulence, k/ϵ, where k and ϵ are the turbulence kinetic energy and rate of dissipation or destruction of the large eddy. The two turbulent quantities are related to two expressions for the rate of reaction in the form [67]:

$$\dot{\omega_k} = v_{k,r}^{'} M_{w,k} A n \rho \frac{\epsilon}{k} min_R \left[\frac{Y_R}{V_{R,r}^{r} M_{w,R}} \right] \tag{2.7}$$

$$\dot{\omega_k} = v'_{k,r} M_{w,k} AB\rho \frac{\epsilon}{k} \left[\frac{\sum_P Y_P}{\sum_j^N V''^r_{j,} M_{w,j}} \right] \tag{2.8}$$

Where A, B are empirical constants equal to 4 and 0.5, respectively. Y_P and Y_R are mass fraction of any product species P and reactant R, respectively. The smallest value resulting from Equation 2.7 and Equation 2.8 is taken as the rate of combustion reaction in eddy dissipation modelling. In general, eddy dissipation model (EDM) is usually used in combustion simulation for gaseous and liquid fuels [57, 66–69, 71–77], therefore good experimentally validated results were obtained.

In addition of the EDM, finite rate eddy dissipation modeling (FRED) and laminar finite rate (LFR) was applied by Kamnis and Gu [67], to compare each model. It was concluded that EDM and FRED can capture the conical flame structure correctly in contrary to the LFR model, which was unable to correctly represent the flame structure. Since the LFR model does not take the turbulent calculation into account, the temperature is therefore over-predicted, and the gas species concentrate around the center line.

The combustion of liquid kerosene was investigated by Kamnis and Gu [68] and Tabbara and Gu [69], in which the kerosene was injected into the combustion chamber as droplets, which broke up and evaporated due to combustion. It was concluded that the combustion and the consequent flame structure is dependent on the initial droplet size (atomization) and the location of the injection ports. It was also shown that the droplet size had a marginal effect on the gas velocity, but had a considerable effect on the temperature, especially in the combustion chamber Figure 2.11. It should be noted that droplet break-up, can be modelled by a separate model, which was not considered in the previous mentioned work.

Recently, the combustion process was simulated as a non-premixed reaction by Wang et al. [78], based on the argument that every gas enters the combustion chamber through separate streams/channels. That was the case of the nozzle design considered in this study [78], (Praxair-TAFA, US). The pre-mixed model adopted in this study provided good agreement with those of the experimental results as shown in Figure 2.12. The main advantage of the model was in reducing the convection-diffusion transport equation for the species to a single conservation equation for a single conserved scalar, which was the mixture

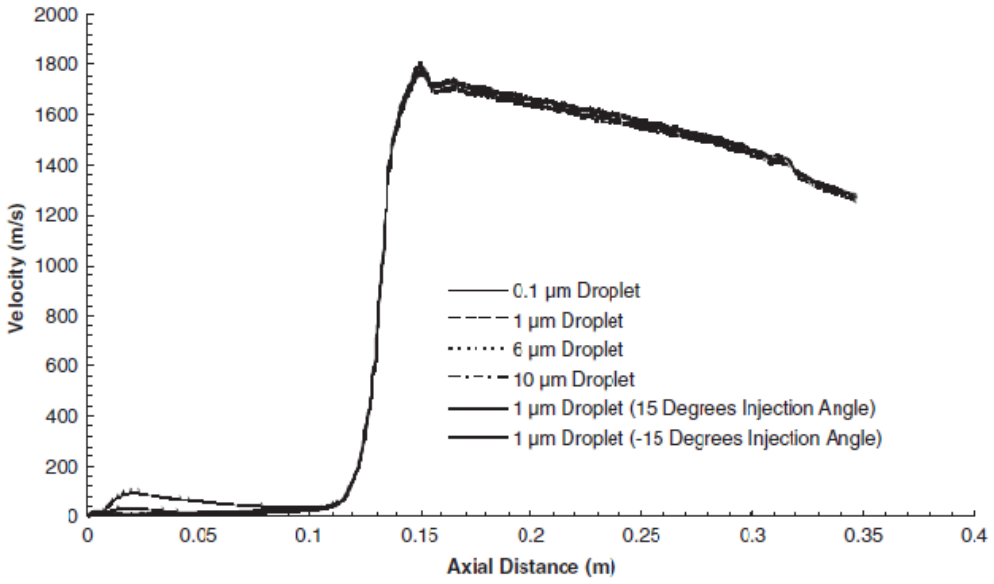

Gas velocity profiles along the centreline.

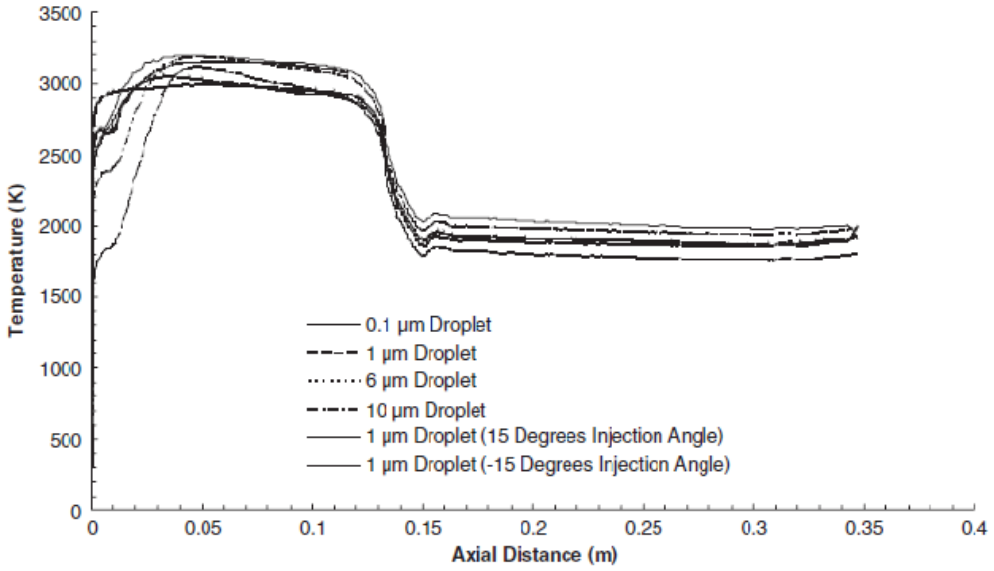

Gas temperature profiles along the centreline.

Figure 2.11: Effect of initial droplet size on Kerosene combustion in HVOF [68]

fraction. A detailed discussion on the model can be found in Sivathanu et al. [79].

The applicability of the model depends on the design of the nozzle assembly such that, whether the fuel and oxidant are premixed or not.

It can be concluded from the combustion modelling survey that either FREDM or EDM were proved to be a good models for simulating HVOF process for both gaseous and liquid fuels. LFR was not suitable for modelling HVOF process since the process is intrinsically

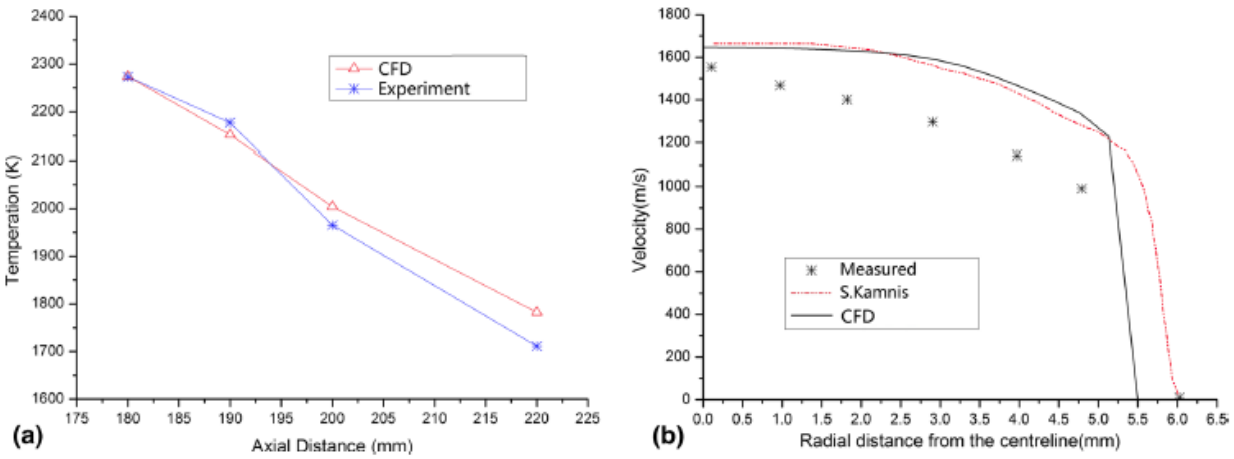

Figure 2.12: Validation of non-premixed combustion model [78]

turbulent.

Arrhenius rates of reaction can be safely ignored in the simulation of HVOF since most of the fuel used in HVOF process are fast burning ones. Results obtained by applying single step reaction were comparable and in a good agreement with that of multi step reaction calculation and that was concluded in the work of Oberkampf and Talpallikar [72].

2.4.2 Gas Dynamics and Turbulence

The target of a nozzle design for HVOF process is to produce a supersonic combustible jet. As discussed earlier, the reason for this is to create a suitable thermal and velocity fields for heating and accelerating powdered material to form a coating [6]. The nozzle design plays an important role on the performance of the process, since the flow characteristics and behaviour, is to a great extent, dependent on this factor.

The importance of the nozzle design is even reflected on the classification of the three generations of HVOF processes developed so far. The first and second generation are distinguished by the nozzle design [8]. The design of the second generation was a convergent-divergent nozzle (de Laval) or a convergent part followed by a straight barrel, and then a divergent part, while the first generation was that of a convergent part followed by a straight barrel. The geometrical design of the third generation was similar to that of the second with higher combustion pressure input.

There are two modelling approaches to simulate the HVOF dynamics. The first is the classical quasi one-dimensional isentropic relations that were applied by some authors. The detailed derivation of these relations can be found in White [80]. These relations can be useful in the design process, but not adequate for capturing the details of the flow behaviour, especially the compressibility effects due to the quasi 1-D approximation assumption. The second approach is applying Copmutaional Fluid Dynamics (CFD) techniques on the fundamental governing equations of the mass continuity, momentum, and energy equation coupled with an equation of state to account for the compressibility effect or the density variation. The fundamental governing equations can take the form of [81];

Continuity:

$$\frac{\partial \rho}{\partial t} + \nabla \cdot \rho u = 0 \tag{2.9}$$

Momentum (Navier-Stokes):

$$\rho \frac{\partial u}{\partial t} + \rho u \cdot \nabla u = -\nabla p + \nabla \cdot \tau + \rho \sum_{k=1}^{N} Y_k f_k \tag{2.10}$$

Energy:

$$\rho \frac{\partial e}{\partial t} + \rho u \cdot \nabla e = -\nabla \cdot q - p \nabla \cdot u + \tau \cdot \nabla u + \rho \sum_{K=1}^{N} Y_k f_k \cdot V_k \tag{2.11}$$

Equation of state:

$$P = \rho R T = \rho R_u T \sum_{k=1}^{N} (Y_k / W) \tag{2.12}$$

where ρ, p, q u, and τ, are the gas density, pressure, heat flux, velocity vector, and viscous shear stress, respectively. While e stands for the mixture total energy ($e = \sum_{k=1}^{N} h_k Y_k - P/\rho$, where h_k is the enthalpy of k_{th} species), f_k and V_k stands for the body force and diffusivity related to the $k_t h$ species, respectively. Note, the above equations can be represented in different forms by some authors, using different mathematical symbolic conventions. A detailed derivation and discussion for the above equations can be found in Anderson and Wendt [81].

The above equations can be applied for the majority of fluid flow problems, such as steady or unsteady, compressible or incompressible [82]. Once they are transformed to a system of linear algebraic equations (discretization), a suitable numerical algorithm can

be used to solve the system of linear algebraic equations. A discussion about numerical algorithms will be given in the next chapter.

The velocity in m/s of the gas in HVOF is typically high, around two orders of magnitude, which implies that the flow is fully turbulent, the Reynold's number becomes the criterion to determine the flow regime, which is defined as the ratio of the inertia force to viscous force. The higher the velocity, the higher the Reynolds's number since the inertia force becomes dominant in a great portion of the flow domain except near the walls, or what is so called the boundary layer [80].

The turbulent flow is characterized by the randomness in the flow field variables. Nevertheless, the concept of turbulence modelling is to average the fluctuating flow field variables and decompose them into mean and fluctuating quantity [83]. To computationally capture the fluctuating quantities of turbulence, an extensive amount of computational cells must cover the flow domain. Direct Numerical simulation (DNS) methods are available to simulate the turbulence fluctuating quantities, but the procedure is indeed computationally exhaustive.

Some other models are based on averaging techniques to resolve the turbulence quantities over an acceptable time and length scales. Reynolds-averaged and Favre-averaged Navier-Stokes are the most common two models used for turbulence simulation. The difference between the two models is the quantity on which the averaging of the flow variables is taken, for time in the former and density in the latter.

Applying averaging on the conservation equations (Equation 2.9, Equation 2.10, and Equation 2.11), they can be expressed as follows:
Continuity:

$$\frac{\partial \bar{\rho}}{\partial t} + \nabla \cdot \bar{\rho}\tilde{u} = 0 \tag{2.13}$$

Momentum:

$$\bar{\rho}\frac{\partial \tilde{u}}{\partial t} + \bar{\rho}\tilde{u}\nabla \cdot \tilde{u} = -\nabla \bar{p}\nabla \cdot \bar{\tau} + \bar{\rho}\sum_{k=1}^{N}\widetilde{Y_k f_k} + \nabla \cdot (\bar{\rho}\widetilde{u'u'}) \tag{2.14}$$

Energy:

$$\bar{\rho}\frac{\partial \tilde{e}}{\partial t} + \bar{\rho}\tilde{u}\cdot\nabla\tilde{e} = -\nabla\cdot\tilde{q} - \overline{p\nabla\cdot u} + \overline{\tau\cdot\nabla u} + \bar{\rho}\sum_{K=1}^{N}\tilde{Y_k}\tilde{f_k}\cdot\tilde{V_k} - \nabla\cdot(\bar{\rho}\tilde{u}'\tilde{e}') \tag{2.15}$$

where $\bar{\rho}\tilde{u}'\tilde{u}'$ and $\bar{\rho}\tilde{u}'\tilde{e}'$ are the Reynolds stress and energy flux respectively, and $\tilde{u}'$ and $\tilde{e}'$ are the fluctuating components for the velocity and energy, respectively. One of the most popular empirical models that is used to close the the Reynolds stresses and fluxes in turbulence modelling is based on the Boussinesq assumption, which relates the Reynolds stress term to the mean velocity component. Mathematically it is represented as [83]:

$$-\rho\overline{u_i\prime u_j\prime} = 2\mu_t S_{ij} - \frac{2}{3}\rho k\delta_{i,j} \tag{2.16}$$

where $S_{i,j} = \frac{1}{2}\left(\frac{\partial u_i}{\partial x_j} + \frac{\partial u_j}{\partial x_i}\right)$ is the mean strain rate tensor, μ_t is the eddy viscosity, and k is the turbulent kinetic energy. The Reynolds flux component for the energy fluctuation can be represented as:

$$-\rho\overline{u_i\prime T\prime} = \rho\lambda_t\frac{\partial T}{\partial x_i} \tag{2.17}$$

where $\lambda_t = \frac{c_p\mu_t}{pr_t}$ is the Prandtle number for turbulent energy. Amongst several turbulence models developed so far, $k-\epsilon$ model is the most widely applied one to simulate the HVOF process, generally for many turbulent flow simulation. Details about turbulence modelling and simulation can be found in many references devoted to the topic such as the introductory chapter in Versteeg [83]. Nevertheless, the previously mentioned model have been extensively validated in the literature against experimental data and good agreement was found.

The supersonic jet developed in such a flow can be characterized by three cases, depending on the flow pressure at the nozzle exit. The first case can be an under-expanded jet if the $p_e/p_a > 1$ or over-expanded, if $p_e/p_a < 1$ and ideal if fully expanded, $p_e/p_a = 1$, where p_e was the gas pressure at the nozzle exit and p_a was the ambient pressure, usually the atmospheric pressure of 1 bar. In the case of an over-expanded or under-expanded jet, it develops expansion and compression pressure waves (Prandtle-Mayer fans) between two slip lines (jet boundaries) before the flow matches the ambient pressure [2, 6, 12, 18, 21, 66, 81, 84].

The compression and expansion waves are created by the shock incident in such a way

that when an expansion wave is reflected by the slip as a compression wave, and such a behaviour is repeated as long as the flow exceeds its sonic speed. A normal shock wave known as Mach disk can be developed when $p_e/p_a < 1$ or $p_e/p_a > 1$, which is a very strong shock and characterized by a triple point. Normally, the waves developed by the shock incident reflect obliquely in the flow stream. Both flow behaviours of over-expanded and under- expanded jets can be seen in Figure 2.13 and Figure 2.14

It was noticed that the supersonic flow in a convering-diverging nozzle develops an over expanded-jet, while that of convergent barrel develops an under-expanded jet. It should be mentioned that the nozzle geometry can alter the previous description of the flow regime. For example, it was observed that if the throat of the converging-diverging nozzle is sharply angled (hourglass shaped) and not smoothly curved and relatively long, shock waves and Mach disks can develop inside the nozzle regardless of the condition at the outside of the nozzle [85–87], which consequently changes the outside jet regime.

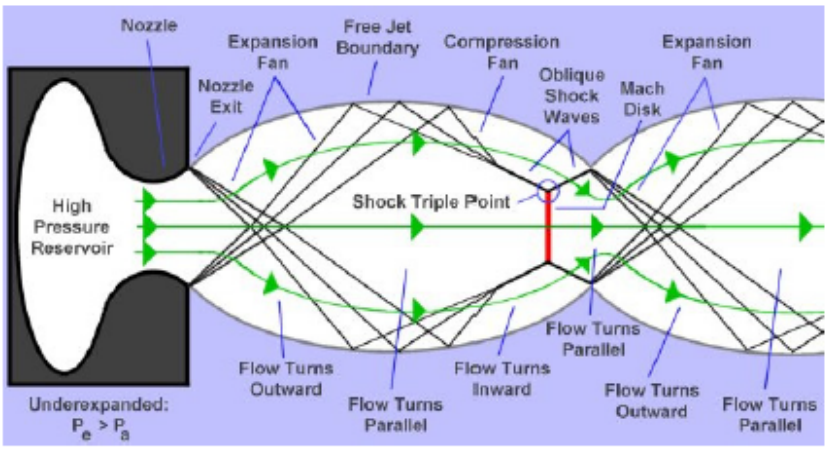

Figure 2.13: Over-expanded jet in converging-diverging nozzle [12, 21]

Some early gas dynamic modelling work have applied the classical theoretical isentropic relations of compressible flow [80]. One such example is within the work of Li et al. [19, 20], where the aforementioned theoretical relations were applied to develop a mathematical based feed control system for the process. But it was deduced by the same author that the analytical model of gas dynamics was unable to capture the compressibility behaviour or the shock waves of the supersonic jet as can be seen in Figure 2.15 [66]

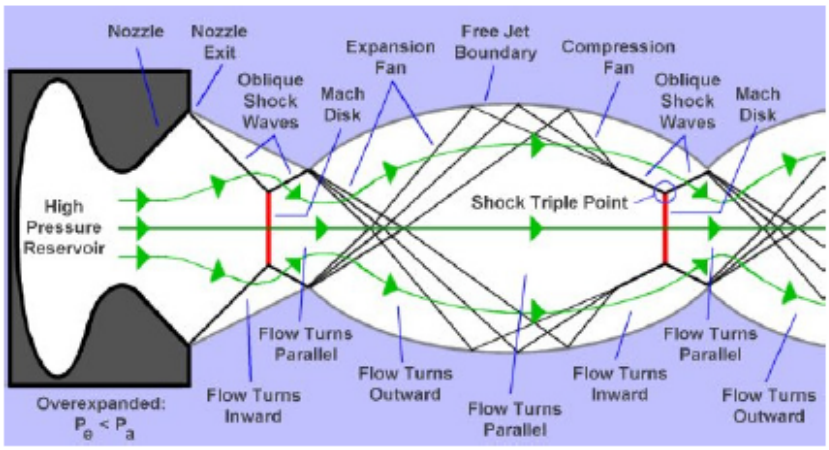

Figure 2.14: Under-expanded jet in converging barrel nozzle [12, 21]

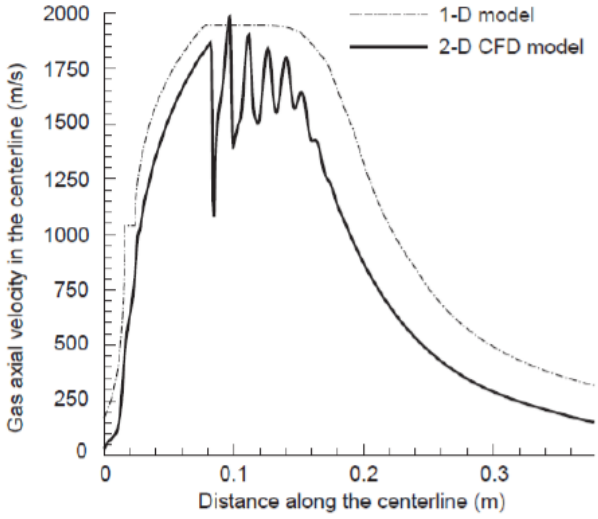

Figure 2.15: Comparison between 1-D theoretical and 2-D CFD models [66]

2.4.3 Multiphase Flow Interaction

Multiphase interaction can be applied in a wide area of engineering and science and can be even found in many natural phenomena. Many computational studies have been conducted to investigate different multiphase flow phenomena and applications. In general, thress computational methods have been developed and were applied to the majority of the mutliphase flow interactions, including thermal spray processes [2, 12, 18]. These models can be characterized as follow:

1. Eulerian-Lagrangian (Lagrangian trajectory) (mostly for fluid-particle/droplet interaction)

2. Eulerian-Eulerian (continuum-continuum / two fluid interaction model)

3. Kinetic theory (molecular dynamics)

In the Eulerian-Lagrangian method, the fluid is considered as a continuum while the particle/droplet is tracked and followed in the continuum domain by solving the governing equation of motion and heat transfer in each computational cell in the continuum domain. The mathematical coupling between the equations that represent each phase is classified as either a one way or two way (coupled).

In a one way coupled procedure, the effect of the particle/droplet on the continuum is considered to be negligible and the model can be said to be deterministic. On the other hand, if the the interaction between the two phases in such a flow, is to be taken into account, the two way coupling is then chosen as the applicable approach, so that the effect of the particle physics is added as a source term within the transport equations of the continuum. In turn, the effect of continuum of the particle momentum and trajectory calculation is quantitatively considered. The Eulerian-Lagrangian model is said to be stochastic in the case of turbulent flow since the turbulence effect on the particle is taken into account. The Eulerian-Lagrangian method can also be applicable to dilute flow [88–90].

All of the phases are considered to be continuum, in the Eulerian-Eulerian method and fully coupled, and is applicable when the mass fraction of each phase is comparable to that of the others, in what is so called "DensFlow" [91, 92]. When the momentum transfer arising from the molecular collisions is considered, the kinetic theory can be applied. Nonetheless, only the Eulerian-Lagrangian and Eulerian-Eulerian methods have been used in thermal spray process simulations. The criterion by which the model is used for simulating a multiphase flow is by determining the effect of phases on each other through the volume fraction of the disperesed or the diffused phase [93].

That can be quantitatively represented as follows. If $V_i < 10^{-6}$, then the Eulerein-Lagrangian, is a one way couple, if $10^{-3} < V_i < 10^{-6}$, then the Eulerein-Lagragian, is a two way couple and if $V_i > 10^{-3}$, then the Eulerian-Eulerian must be the model of choice.

The multi phase regime can be related to the volume fraction and the Stokes number as

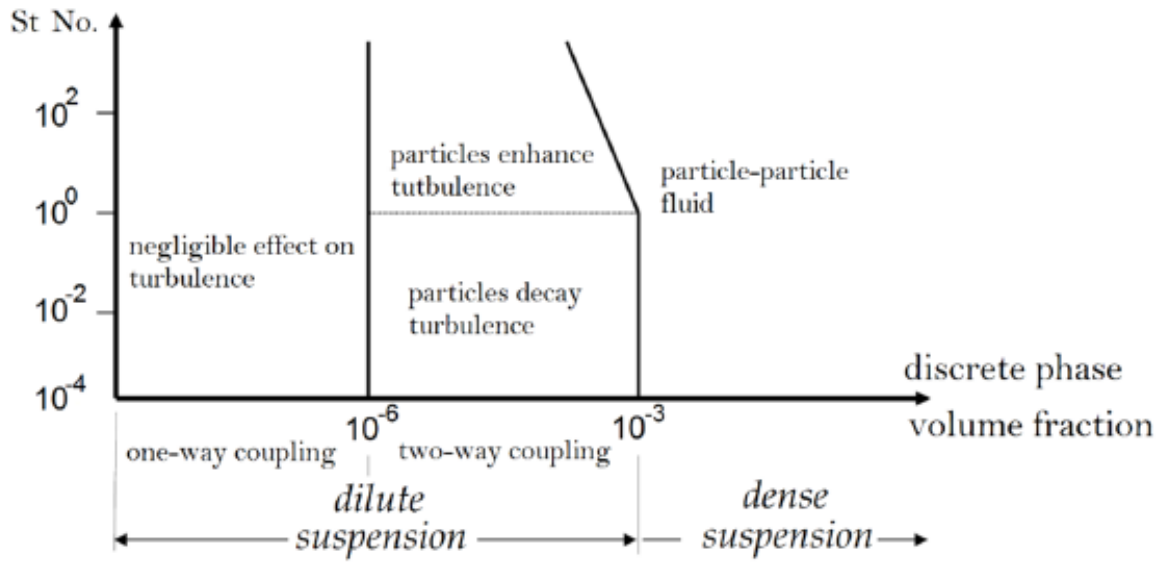

Figure 2.16: Multi phase flow regime classification based on the volume fraction of the dispersed phase and the Stokes number [90].

in Figure 2.16. The Stokes number gives a physical indication to how the particle dynamically responds to the flow such that, the higher the Stokes number the slower the particle moves with the flow. Upon determining the multiphase flow regime, the forces that act on the particle have to be determined. The forces that act on the particle can be categorized into three general forces:

1. Fluid-particle
2. Particle-particle interaction (mostly negligible Van der Waals)
3. External fields' forces (mostly negligible electrical, magnetic and gravitational)

Amongst the particle-fluid forces, drag and thermophoresis forces can be considered as the dominant ones and Basset, carried mass (virtual mass), buoyancy, staffman, and Magnus can be negligible in the most of the cases in the simulation of a HVOF process [12,89,94,95] Balancing the linear momentum of the particle with that of the drag force, results in two mathematical formulae derived as follows:

$$m_p \frac{dv_p}{dt} = 0.5 C_D \rho_g A_p (v_g - v_p)|v_g - v_p| \tag{2.18}$$

$$\frac{dx_p}{dt} = v_p \tag{2.19}$$

where x_p, v_p, v_g, ρ_p, A_p, C_D, are the particle's position, the particle velocity, gas velocity, particle density, particle surface area, and drag coefficient, respectively. The drag coefficient C_D calculation has been always derived empirically and taken many different forms and is still a controversial matter in the research around particle-fluid flow [2]. Some research has been totally devoted to the drag coefficient calculation [96]. However, the drag coefficient was always related, as a function, to the Mach (M) and Reynolds number (Re) [2,12,18,87]. As can be deduced from the surface graph in Figure 2.17.

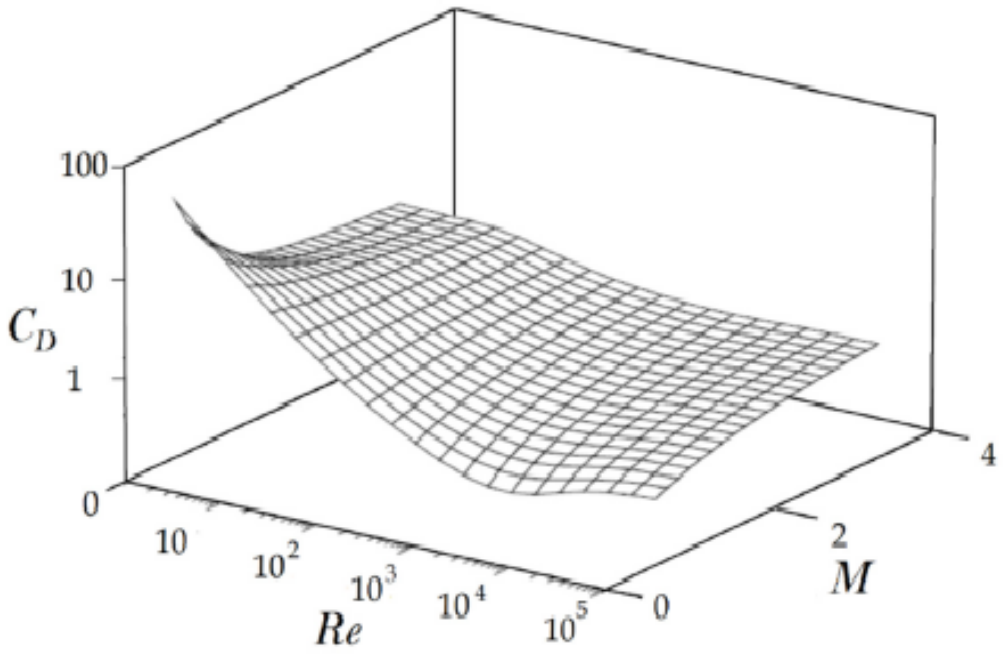

Figure 2.17: Drag coefficient (C_D) of a spherical particle as a function of Mach (M) and Reynolds number (Re) [97]

At high Reynolds number, the drag coefficient has a proportional relationship with the Mach number, while at low Reynolds number the relationship is sharply, inversely proportional up to below 2 Mach number and then becomes almost constant. The most general drag coefficient formula that takes into account different Reynolds and Mach number regime was developed by Crow [97, 98]. The model took into account the Knudsen number as a function of Mach and Rynolds number to determine whether the continuum assumption was applicable or not. Knudsen number is the ratio of the molecules mean free path, λ , the distance a molecule should lapse before colliding with another one [53], to the diameter of the particle, such that $k_n = \lambda/d_p$. If k_n was high, (> 0.25), then the mean free path was

comparable to the diameter of the particle and molecular kinetic theory had to be taken into account. If k_n was small ($k_n < 10^{-3}$) the continuum assumption would be valid. Finally, when $10^{-3} < k_n < 0.25$, then the boundary layer of temperature and velocity gradient develops on the particle surface [98]. The model presented by Crow is represented as follows:

$$C_D = 2 + (C_{D0} - 2)^{-3.07\sqrt{\gamma}g(Re)M/Re} + \frac{h(M)}{\sqrt{\gamma}M}e^{-Re/(2M)} \tag{2.20}$$

where γ is the specific heat ratio and C_{D_0} is the drag for an incompressible flow ($M \approx 0$) [99], $g(Re)$ and $h(M)$ are as follows:

$$g(Re) = \frac{1 + Re(12.278 + 0.548Re)}{1 + 11.278Re} \tag{2.21}$$

$$h(M) = \frac{5.6}{1 + M} + 1.7\sqrt{\frac{T_d}{T_c}} \tag{2.22}$$

where T_d and T_c is the temperature of particle and gas, respectively. At critical Reynolds number the above formulation is not applicable, but this is not the case for thermal spray processes [86].

The second force, thermophoresis, can have an effect on the momentum of the particle. The force is created by the temperature gradient in the continuum field and as a result molecules in the higher temperature side become more active and transfer momentum to the other on the lower temperature side, which can cause the particle to move in a direction opposite to the gradient [98]. One empirical formula has been extensively used to model the thermophoretic force, is given as follows [12]:

$$F_T = \frac{-6\pi\mu_c^2 dC_s}{\rho_c m_d}\frac{1}{1 + 6C_m k_n}\frac{k_c/k_d + 2C_t k_n}{1 + 2k_c/k_d + 4C_t k_n}\frac{\nabla T}{T} \tag{2.23}$$

where k_c and k_d are the gas and particle thermal conductivities, respectively, m_d is the particle mass, d is the particle diameter, T is the gas temperature, ρ_c is the gas density, and μ_c is the gas viscosity. C_s, C_m and C_t are 1.17, 1.14, and 2.18, respectively [97]. A wide range of Knudsen and thermal conductivities are suitable for the thermophorosis formula. Lumped capacity model can be applied when the Biot number is less than $\frac{1}{10}$. The Biot number indicates the ratio of the thermal resistance at the surface of the particle to that

inside it, $Bi = \frac{hd}{k_d}$. The lumped capacity model is of the form [12, 18, 66]:

$$m_d C \frac{dT_d}{dt} = hA(T_c - T_d) \tag{2.24}$$

where C is the particle material specific heat, h is the heat transfer coefficient, A is the particle surface area, and $(T_c - T_d)$ is the temperature difference between the particle and the continuum phase. The Nusselt number (Nu), estimated by Ranz-Marshal equation, can be used to calculate the heat transfer coefficient:

$$Nu = \frac{hd}{K_c} = 2 + 0.6 Re_p^{1/2} Pr_r^{1/3} \tag{2.25}$$

where p_r is the Prandtle number of the continuum phase. The radiation heat transfer can be taken into account in the heat transfer calculation, but for HVOF this can be ignored, however if the radiation is to be considered radiation heat transfer term is therefore added to Equation 2.24 to give:

$$m_d C \frac{dT_d}{dt} = hA(T_c - T_d) + A\alpha\sigma_b(T_\infty^4 - T_d^4) \tag{2.26}$$

where the Stefan-Boltzmann constant $\sigma_b = 5.6704 * 10^{-8} W/(m^2.K^4)$, and T_∞ is the ambient temperature. Radiation can be safely neglected since the convective heat transfer is the dominant mode, normally 100 times larger than the radiative one [18].

2.5 HVOF Literature Modelling Results

In the previous section, the models outlined can be applied to simulate the physics involved in the HVOF process, as illustrated in Figure 2.18 [66]. In the next section, a summary of the simulation work resulting from research into the HVOF process. The results are presented according to aspects such as; operating parameters, particle behaviour, nozzle design and stand-off distance.

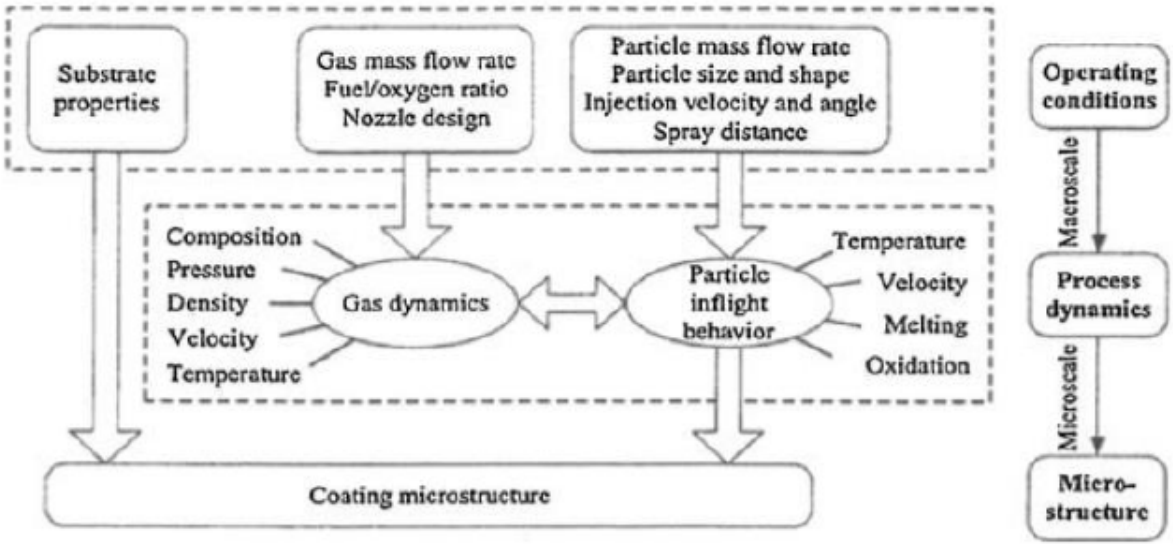

Figure 2.18: Multi-Physics of the HVOF process [66]

2.5.1 Operating Parameters (flow rates of gases)

Since HVOF is a combustion based process, combustion plays an important role, especially in the gas dynamic behaviour. The supersonic combustible jet behaviour and characteristics, such as velocity and temperature are totally dependent on the combustion process. The effect of combustion can be quantitatively related to the gas behaviour through the flow rate of the reacting gases.

Therefore, the gas flow rate of the fuel, oxidant and other gases involved in the process are important parameters to be controlled and understood [20]. The effect of the flow rate of the gases, and the equivalence ratio, (Equation 2.3), on the gas and particle behaviour have been extensively studied and reviewed in the literature [18, 20, 57, 66, 73, 74, 100]. Two key studies were conducted by Cheng et al. [101] and Li et al. [66], regarding the effect of flow rate parameters.

In the former study, the effect of the total flow rate of gases and the oxy-fuel flow rate on the behvaiour of the gas dynamic was investigated. The ratio of the different gases was kept constant. It was concluded that if the total flow rate was increased, the velocity and temperature of the gas and the mass flow rate at the nozzle exit increased. Increasing the total flow rate of gases increased the spaces between the shock waves as well. Increasing the oxy-fuel flow rate had a significant effect on the temperature and velocity of the gas in the

outside jet while a marginal effect on the same parameters inside the nozzle, especially in the convergent section of the gun. Similar results was found in the latter study involving Li et al. [73, 74, 102].

In a similar investigation by Gu et al. [102], the propylene flow rate was correlated to the equivalence ratio. It was found that for a fuel- rich mixture, increasing the propylene flow rate would only slightly increase the flow temperature and velocity of the gas, while for a fuel-lean mixture increasing the fuel flow rate increased the same parameters. It was found in the same study that the cooling air had a marginal influence on the temperature inside the nozzle and a slight decrease on the outside jet, and no effect on the outside flow. Increasing the nitrogen flow rate can have a dramatic decrease in the flow temperature and velocity, since it is inert, does not participate in the combustion reaction, so nitrogen can extract sufficient amount of heat, that was also concluded by Li et al. [48], hence the recommendation is for keeping it at minimum flow rate.

A specific range of equivalence ratio was investigated by Li et al, [18–20, 66], for a slightly higher than stoichiometric ratio the highest equilibrium temperature was obtained. Increasing the equivalence ratio from 0.6 to 1.6 resulted in a decrease in the total mass flow rate, density at the nozzle throat, velocity, and sonic speed at the throat increased. Increasing the combustion pressure from 5 to 15 bar, increased the gas density, mass flow rate, velocity, and temperature at the throat. Also air as an oxidant was taken into account by the same group, Nitrogen and Argon were added as constituents of air such as [66]:

$$\phi C_3H_6 + 4.5\,O_2 + x(N_2 + \frac{1}{79}\,Ar) \longrightarrow xCO_2 + y/_4H_2O \tag{2.27}$$

where x varied between 0 to 16.7, such that pure oxygen corresponded to x=0, and x=16.7 in the case of pure air. No difference was observed between the combustion with air and oxygen when x was held constant in the gas properties. If the total flow rate was held constant, it was found that the combustion pressure and temperature decreased with increasing x. The equivalence ratio, corresponding to the peak equilibrium temperature decreased from 1.23 to 1.05 with increasing the fraction of Nitrogen and Argon in Equation 2.27. It was also deduced that the combustion chamber pressure was influenced solely by the oxy/fuel

ratio, and as the chamber pressure increased, the particle velocity and temperature increased dramatically and marginally, respectively. With a fuel-rich mixture of 1.2 equivalence ratio, the particle temperature was less than that corresponding to 0.8 equivalence ratio, but with no effect on the particle velocity. Finally a direct proportionality was found between particle velocity, temperature, and melting ratio with the total mass flow rate.

2.5.2 Particle Behaviour

Generally, the particle size is the most dominant factor regarding particle behaviour. As the particle size increases, the particle dynamic and thermal response becomes slower [103]. Particle morphology was investigated by Cheng et al. [104], Ganser's drag coefficient [105], which correlates the drag coefficient to the particle sphericity, was applied. It was shown that as particle sphericity increased, the drag reduced. As for the velocity, as the particle size decreased it gains higher momentum and velocity as shown in Figure 2.19. The same behaviour of the particle temperature was obtained for studied range of particle size as shown in Figure 2.20. The thermal behaviour of a small particle can be rapid, while it is slow for larger ones.

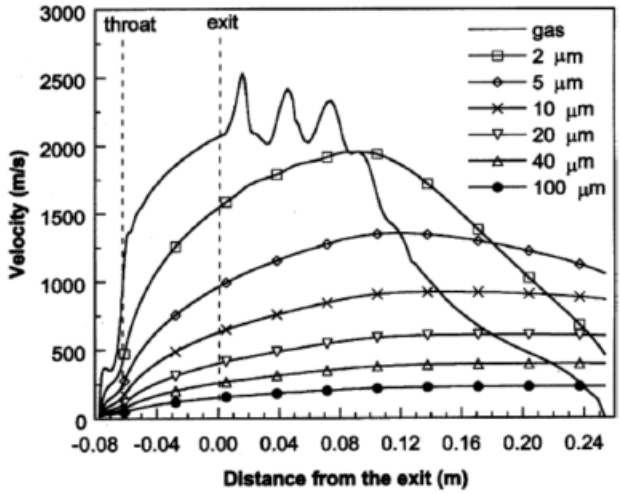

Figure 2.19: Velocity profile for spherical particle of different sizes along the jet centerline relative to the gas velocity [106]

Similar results, regarding the particle morphology (sphericity), was found by Kamnis and Gu [106, 107]. The same drag coefficient of Ganser's was applied for WC−Co powder injected into a kerosene fueled HVOF gun. Both the radial and axial injection of the particle

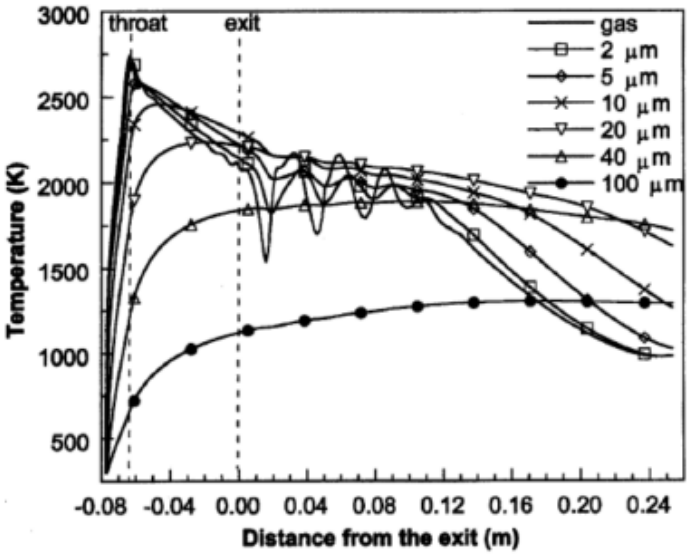

Figure 2.20: Temperature profile for spherical particle of different sizes along the jet centerline relative to the gas velocity [106]

was investigated. It was found that non-spherical particles had higher axial velocity than the spherical ones and their trajectories were more aligned to the centerline of the gun. However, the sphericity effect on the particle behaviour was marginal when the particle size decreased.

Knudsen number influence on the particle behaviour was investigated by Joshi et al. [108,109]. The Knudsen number became more effective as the particle size reduced [110–112]. On the other hand, the thermophoresis force had an affect only on the small particles as was concluded by Ait-Messaoudene [113].

In a study by Zeoli et al. [114], the oxidation process of the particle in-flight in a kerosen fuelled gun was modelled by adopting the oxidation theory of metals by Cabrera [115]. The theory correlates the oxidation process to the ion transfer through the oxidation layer. It was concluded that as the particle size decreased the oxidation layer grew, since the ratio of the surface area of the particle to its volume increases as the particle size decreases. The maximum oxygen concentration and the temperature of the gas corresponded to the fastest oxidation growth. The effect of injection port on the oxidation growth was also taken into account. It was revealed that the further the injection port is located away from the combustion chamber, the less the oxidation growth.

2.5.3 Geometrical Aspects

Kamnis et al. [116] investigated the powder injection position on the spherical particles in a liquid kerosene fueled gun. The particles were radially injected into the gun through two angled holes. The study also considered the initial velocity of the particle at the injection port and under the range of initial velocities considered it was found that for an initial velocity of 10 m/s particles could travel across the centerline of the flow without colliding with the nozzle walls. It was also found that the injection port has an effect on the particle temperature such that the closer the port to the throat of the nozzle the higher the temperature gain for the particle.

Different powder injection positions were examined by Hackett and Settles [117], Li and Christofides et al. [20]. and Lopez et al. [118]. It was concluded that the injection position had an effect only on the particle temperature. Gu et al. [119] investigated the effect of particles initial velocity and injection port on the its subsequent behaviour in the flow. It was revealed that increasing the particle initial velocity at the injection port had a marginal effect on its temperature along the flow, but the injection position had an effect on the trajectories of the particles.

An investigation on the effect of surface roughness of the nozzle and the cooling rate of the gas and particle behaviour was done by Katanoda et al. [120, 121]. It was revealed that the velocity of both the particle and gas decreased with increasing the roughness while the temperature of both increased. Increasing the cooling rate increased the velocity of particle/gas, and decreased their temperature. The ratio of the length of the diverging part to that of the barrel part was also investigated in these studies. It was shown that if the ratio is one, the highest particle velocity at the nozzle exit could be obtained.

A particle could gain higher velocity in the supersonic nozzle than in the subsonic nozzle but less temperature could be obtained due to the shorter dwell time in the supersonic nozzle as was documented by Kadyrov et al. [122]. Regardless of the flow type, increasing the barrel length enhances the particle velocity at the gun exit [101, 103]. While increasing the combustion length would increase the residence time of the particle in the combustion zone which as a result increased the particle temperature and oxidation growth. [119].

The flow behaviour inside a curved air cap was studied by Hassan et al. [123] and Lopez et al. [118]. The flow was revealed to be non-uniform near the cap exit in the subsonic region due the air entrainment and separation points developed at the corners of the cap and as a result the spray angle was different to that of the curved cap.

An external shroud was added to the DJ2700 Sulzer Metco gun (Now Oerlikon Metco gun), experimental and numerical investigation were conducted by Dolatabadi et al. [124, 125]. The aim of this procedure was to reduce the air entrainment into the outside jet and hence reduce the oxidation growth on the particles, and that aim was indeed achieved in this study, as one of the main reason of oxidation is due to the high concentration of the oxygen and temperature the in-flight particle experiences [114]. However, experimental results of this study revealed that the shroud reduced the particle velocity due to the recirculation at the shroud edges which enhanced the coating porosity, but the amount of oxygen reduction was still achieved which enhanced the coating quality [126, 127].

Any thermal spray process can be evaluated through the deposition efficiency, which is defined as the ratio of the amount of the coating injected to the spray nozzle to that deposited on the coating. This parameter is typically around 50% for HVOF. An experimental and numerical approach were both conducted to study the effect of the length of the converging part of the nozzle on the deposition efficiency, by Sakaki and Shimizu [128]. It was found that particle melting, could be enhanced by increasing the converging part of the nozzle, since the dwell time in the high temperature region increased. Even though the particle velocity decreased marginally as the length of the converging part increased the deposition efficiency increased. Increasing the length of the diverging part and the throat diameter caused the Mach disc to cut closer to the nozzle exit and the gas velocity reduced as revealed by Baik and Kim [87, 129].

The effect of spray distance on the particle behaviour was studied by Li and Christofides [66]. In this work the spray distance was in the range of between 200 to 300 mm and it was found that particles of less than 30 μm diameter experienced less velocity and temperature at the point of impact as the spray distance increased. Similar results were found by Dongmo et al. [77] and Eidelman and Yang [130]. In another study by Li et al. [48], the stagnation point of the flow on the substrate, created a radial flow parallel to the substrate and as a

result the particles were not sprayed perpendicularly, especially for small particles that have tendency to follow the flow.

2.6 Summary and Research Gaps

A literature review was conducted and presented in this chapter. It can be concluded that extensive work exists related to the modelling of the HVOF process. As previously presented, basic models with simplified geometries have been modelled, which mimic HVOF deposition, but these can provide only crude results. Modelling approach is known to be a complimentary one to the experimental approach. However, this depends on the detailed accuracy of the modelling technique used. crude models will not complement experimental data. However, the advantage of the computational modelling approach was not accompanied with a Design of Experiment (DOE) approach before. CFD modelling is time consuming and expensive therefore providing mathematical models allows experimentalists to use the equations for analysing HVOF systems. In this study both computational approach using ANSYS FLUENT, the available commercial software in Dublin City University, and the Design of Experiment technique using StatEASE Design Expert were applied to develop a statistical relationships between some of the important process variables. The study then considers two gun geometries developed recently in the HVOF industry.

Models and their assumptions applied in this study are well established models for physics involved in the HVOF process. The study only considered the multi phase physics of the process. The mathematical models were not adjusted and were applied as they are available in the ANSYS FLUENT code. A full description of the models can be found in the theory guide accompanied by the software. The models were applied by the majority of the authors in the literature especially by the most cited HVOF simulation work of Li et al. [66].

The simulation work of this study was validated against a measured data of the particle temperature at the substrate distance. The measuring system used in this work was Accuraspray unit developed by Oerlikon Metco [16].

Chapter 3

Research Methodolgy

3.1 Introduction

The methodology of this study is based on two techniques namely; CFD and DOE. The CFD technique was initially applied to simulate the multi-phase flow within the two nozzle geometries that are developed within the coating industry. The DOE technique is then applied on the results obtained from the CFD and statistical relations are developed between the parameters under investigation.

In this chapter, the methodology used behind the techniques are discussed and explained. The parameters under investigation are given. It is worth mentioning that this thesis is intended to be an applied thesis, so most of the mathematical techniques applied are well established models commonly used nowadays in the development of many industrial or engineering processes. However, a reasonable discussion is given about the reason for adopting a particular model or technique wherever necessary. Validation via experimental measurements were also included.

3.2 CFD Approach

The commercial software ANSYS FLUENT available in Dublin City University is used in this study to simulate the multiphase flow of the HVOF process [51]. The computational

simulation is applied to two geometries (DJ1050 and DJ2700) where each represent the first and second generation of the design development of the thermal spray gun or nozzle for HVOF deposition. These gun assemblies were developed by Oerlikon Metco [16] (formally known as Sulzer Metco). A schematic representation for each of the gun geometry and the boundary conditions applied are given in Figure 3.1. The dimension of the gun geometries were measured using vernier caliper and pin gauges.

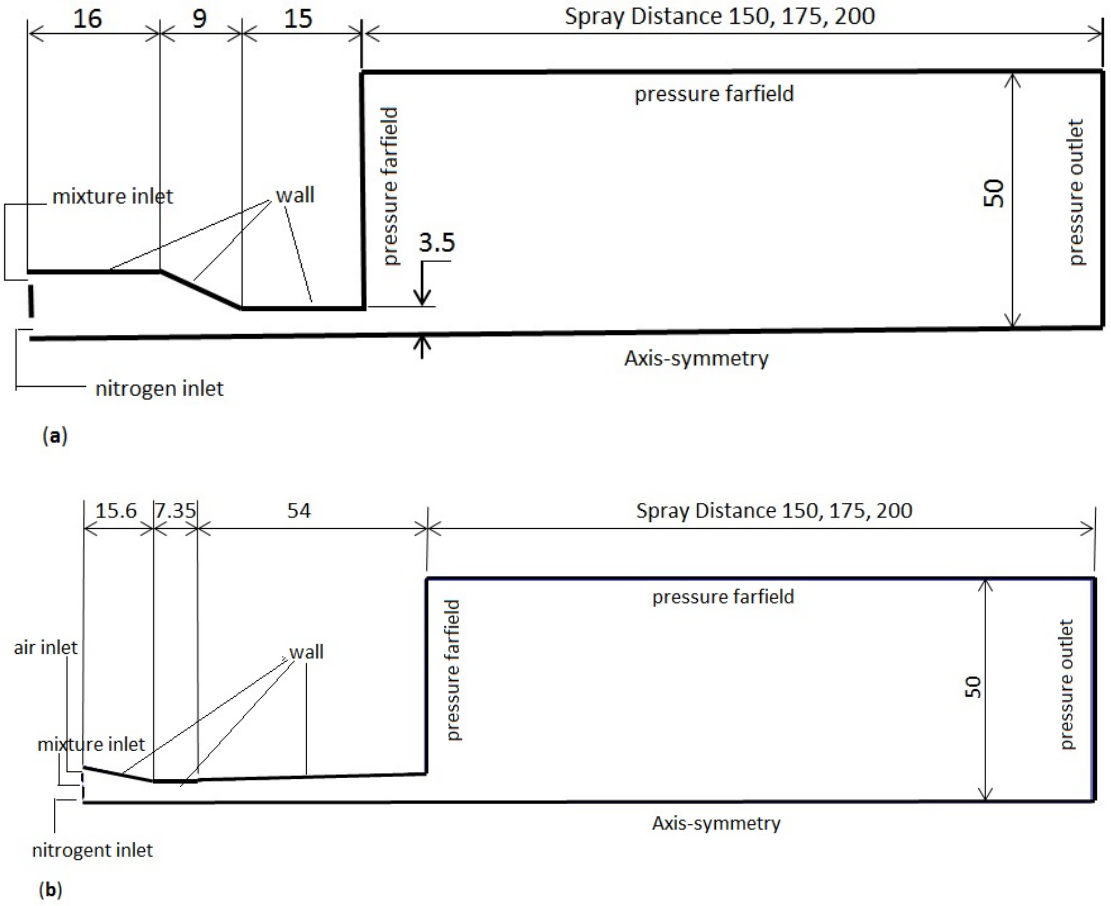

Figure 3.1: (a): Schematic diagram of the DJ1050 HVOF gun, (b): schematic diagram of the DJ2700 HVOF gun, dimensions in mm

3.2.1 Mathematical Models

For the gas flow dynamics, the continuity, momentum and energy equation in the averaged $(\kappa - \epsilon)$ form is used to account for the turbulence modelling, together with the equation of state. The previous mentioned equations can be referred to, from the last chapter Equation 2.13, Equation 2.14, Equation 2.15 and Equation 2.12, respectively. As mentioned

in the last chapter, the models adopted were those used by almost all the previous modelling research into HVOF and a detailed discussion can be found in Anderson et al. [81] and Versteeg et al. [83]. For the combustion modelling, the eddy dissipation model Equation 2.7 was adopted.

The Lagrangian formulation of the particle dynamic is applied to account for the momentum and trajectory calculation. The mathematical formula can be referred to as Equation 2.18. The drag coefficient for spherical particles developed by Morsi and Alexander is applied, which takes the form [96]:

$$C_D = a_1 + \frac{a_2}{Re} + \frac{a_3}{Re^2} \tag{3.1}$$

where where a_1 , a_2 , and a_3 are constants that apply over several ranges of Re, and finally in the case of thermal behaviour of the particle, the lumped capacity model in Equation 2.24 is applied. The particle dynamics and thermal models were applied on the tungsten carbide cobalt material WC-12%Co, one of most commonly used material in HVOF and thermal spray coating process in general for many different applications. The properties of WC-12%Co is given in Table 3.1

Table 3.1: Thermophysical properties of WC-12%Co [66]

Density, ρ_p (g/cm^3)	14.32
Heat capacity, C_{p_p} (J/kgK)	295.4
Latent heat of fusion, ΔH_m (J/Kg)	$4.2 * 10^5$
Surface emissivity, ϵ	0.4
Melting temperature of cobalt, T_m (K)	1768

3.2.2 Boundary and Operating Conditions

Eddy dissipation model is adopted to simulate the combustion process. The fuel involved in the process was propylene (C_3H_6). Higher temperatures of combustion, the products dissociate into some molecules and atoms [66, 77]. In general for such a combustion process

eight species are usually taken into account, and can be represented by the chemical equation as follows [77]:

$$C_3H_3 + 4.5\,O_2 \longrightarrow x_1\,CO + x_2\,CO_2 + x_3\,H + x_4\,H_2 + x_5\,H_2O + x_6\,OH + x_7\,O + x_8\,O_2 \tag{3.2}$$

where the mole coefficients $x_1 \rightarrow x_8$ in Equation 3.2 correspond to the equilibrium mole fractions for the combustion process under specific equilibrium pressure and temperature. In order to calculate the equilibrium mole fractions for the above reaction, temperature and pressure of the combustion can be applied from the minimization of Gibbs free energy method. The temperature and pressure during combustion was taken from the manufacturer Oerlikon Metco of the gun [16] and a programme developed by Gordon and McBride [131] is used to calculate the equilibrium compositions of the combustion reactions. A pressure of $5 \rightarrow 6$ bar and temperature of $3000 \rightarrow 3400$ K is documented by the manufacturer for both of the guns investigated in this study [16]. However, the pressure of 6 bar and the temperature of 3300 K were chosen for the calculation of chemical equilibrium compositions, and the values were substituted in the above formula and implemented in ANSYS FLUENT code. The chemical equilibrium reaction after this calculation therefore takes the form:

$$\begin{aligned} C_3H_6 + 4.5\,O_2 \longrightarrow\ & 1.803\,CO + 1.197\,CO_2 + 0.352\,H + 0.462\,H_2 + 1.994\,H_2O + \\ & 0.396\,OH + 0.740\,O + 0.703\,O_2 \end{aligned} \tag{3.3}$$

Equation 3.3 was applied in the combustion modelling for both the guns. Operating conditions for the flow rate of gases were taken from supplier of the gun [16]. The operating conditions for each gun are given in Table 3.2 and Table 3.3.

Table 3.2: Operating conditions for the DJ1050 HVOF , flow units in SLPM, ϕ representing the correspondent equivalence ratio ($\phi > 1$ = rich ; $\phi < 1$ = lean)

Case	C_3H_6	O_2	Air	N_2	ϕ
1	73	256	325	325	1.01
2	60	256	325	325	0.83
3	107	256	325	325	1.50

The operating conditions were supplied in SLPM, but the ANSYS FLUENT code does

Table 3.3: Operating conditions for the DJ2700 HVOF, flow units in in SLPM, ϕ representing the correspondent equivalence ratio ($\phi > 1$ = rich ; $\phi < 1$ = lean)

Case	C_3H_6	O_2	Air	N_2	ϕ
1	57	256	250	325	0.83
2	58	256	275	325	0.83
3	59	256	300	325	0.83
4	69	256	250	325	1.01
5	71	256	275	325	1.01
6	72	256	300	325	1.01
7	102	256	250	325	1.50
8	105	256	275	325	1.50
9	108	256	300	325	1.50

not accept a volumetric flow rate as a boundary condition. However, from the majority of previous simulation work there was less clarity on how the mass flow boundary conditions were calculated. It is well known that the state of the gas can be related to other thermodynamic properties via the equation of state (Equation 2.12) [132]. Such calculations were applied by Martinez et al. [133] to calculate the mass flow rate of gases, in which the volume flow rate was multiplied by gas density at standard conditions of 1 bar and 295.15 K. Effect of pressure and temperature on the density of gases at the mass inlet boundary conditions is investigated in this study, the results are presented and discussed in chapter 4. The nozzle wall temperature was assumed to be constant for both of the guns at 300 K. The other boundary conditions can be referred from Figure 3.1.

3.2.3 Numerical Calculation

Semi IMplicit Pressure Linked Equations (SIMPLE) that solve the conservative governing equations in segregated or sequential solver of ANSYS FLUENT code is applied in the simulation [51, 83]. The solver has an advantage that it links the velocity and pressure calculation through a pressure-correction equation so that their values satisfy the continuity or mass conservation. The solver is applied through one of the remarkable works of Li et al. [66] and validated against experimental results and good agreement was found. The disadvantage of the solver is that the calculation time might be slower due to the segregation

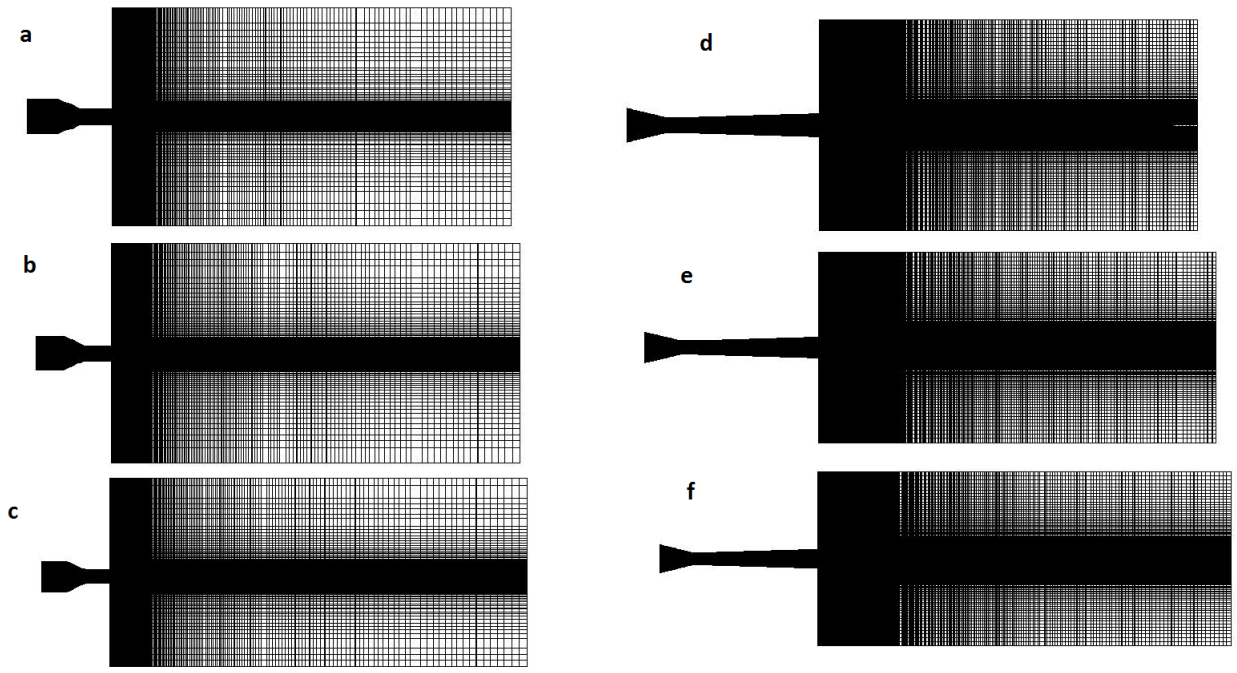

Figure 3.2: Quadrilateral mesh independent cells for DJ1050 gun (a = 38258 cells, b = 40321 cells, c = 42500 cells) and DJ2700 gun (d = 72444 cells , e = 75329 cells , f = 77138 cells).

or sequential order in which the governing equations are solved.

Regarding the discretization scheme, this work is guided the work of Kamnis et al. [67] in which a comparison between the second order and quadratic differencing scheme (QUICK) scheme was investigated. It was found that the second order discretization scheme was not able to capture the compressibility behaviour of the jet especially within the external domain. The grid or mesh independency were determined for the calculations domains in this study, as can be referred to Figure 3.2. Discrete Phase Model of ANSYS FLUENT based on the Lagrangian calculation of fourth order Rung-Kutta numerical scheme is applied to calculate the particle- thermal and dynamic behaviour in the continuum field of the gas. The model is applied because of the volumetric experimental particle loading in HVOF process, which is typically less than 10% [66].

3.3 Design of Experiment Approach

Improving the quality and sustainablilty of any engineering product is almost an aim in any engineering process. This aim is almost always achieved through experiments to

understand the process behaviour and to correlate its paramaters to the quality of the process. Engineering experiments generally go through three stages; exploration, estimation and confirmation. Determning the data required to characterize and quantify the process performance is done as an exploration stage followed by determining the effects of the process variables on the its quality and behaviour, which is reffered to as an estimation stage. Finally the confirmation stage in which verification of the estimated or predicted results of the experiment is obtained. [134]

Improving the quality of an engineering process can be conducted through changing one variable at a time (OVAT)technique, keeping all other variables constant during the experimentation process. The information obtained from such a technique is rather limited and the experimentation procedure is lenghty and costly. On the other hand, the experimentation could be based on some of the well established statistical principles. Experimenation approach based on such principles is known as Design of Experiments (DOE) [134]. Statistical based DOE approach has the advantage of correlating different parameters to the process efficiency and quality at time which reduce the time and resources required during the experimentation. In addition, the variables have important effects, can be efficiently determined as well as those that marginally affect the process.

DOE was first applied by Sir R. Fisher in the 1920's to correlate various kinds of fertilizers on different land areas. DOE has since been adopted and applied in many other fields such as biological, pharmaceutical, engineering etc. and recently in more developed technologies and industries. Most of the DOE work in thermally spraying has originated from DCU under Dr. Stokes supervision.

The best known methodolgy of DOE is Response Surface Methodolgy (RSM), developed in the 1950's by Box and Wilson [135]. Central Composite Design (CCD) and Box-Behnken Design (BBD) are considered the most commonly applied RSM methodologies. BBD methodology was adopted in this work and hence it is detailed in the next sections.

3.3.1 Response Surface Methodology (RSM)

The concept of optimization has almost become an inevitable part of the majority of technological development in order to gain the most efficient and desirable output [136]. RSM was chosen in this study to optimize some of the process parameters and relate them to one of the critical responses of HVOF process which is in-flight particle thermal and dynamic behaviour. RSM also specifies the relationships among one or more measured responses (interactions) and the essential controllable input factors [137]. If all independent variables are measurable and can be repeated with marginal error, the response surface can be mathematically expressed by:

$$y = f(x_1, x_2, x_k, ...) \tag{3.4}$$

where k is the number of independent variables

To optimize the response y, it is necessary to find an appropriate approximation for the true functional relationship between the independent variables and the response surface. Usually this is achieved through regression analysis to obtain a mathematical relation that might take a form of polynomial of a second order of the general form (Equation 3.5).

$$y = \sum b_i X_i + \sum b_{ij} X_i X_j + \sum b_{ij} {X_{ii}}^2 + \epsilon \tag{3.5}$$

As mentioned earlier, the utilized RSM designs in this work are based on BBD. The following are some details on this method.

3.3.2 Box-Behnken Design (BBD)

One of the most popular RSM designs are BBDs, which are based on three levels of each factor. These designs were developed by Box and Behnken in 1960 [138]. They are constructed by first combining two-level factorial designs with incomplete block designs and then adding a specified number of centre points. For three factors, the total number of points equal to 12 design points and 5 centre points therefore 17 experimental points. Although,

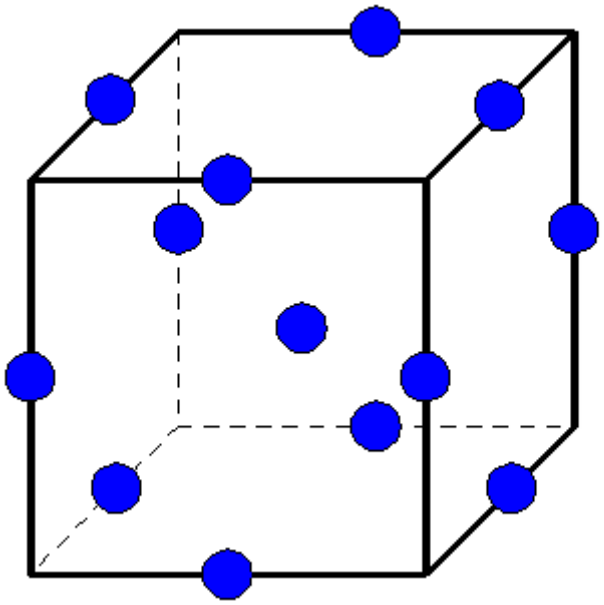

Figure 3.3: BBD representation of three factors [140]

the 12 unique combinations represent less than one-half of all possible combinations for three factors (3^3 or 27 combinations) with the same number of levels, they offer enough information to fit the 10 coefficients of the polynomial shown in Equation 3.5 [139]. Figure 3.3 presents a schematic diagram for BBD for three factors.

3.3.2.1 Analysis of the Design

To find out the ten coefficients in the polynomial Equation 3.5, the following equations can be used Equation 3.6 to Equation 3.8. The sum of squares for each term of BBD could be calculated by applying Equation 3.6 to Equation 3.12 for designs with 3 factors. Where A, B, C_i and D_i are constants and for a three factor design these constants equal to 1/8, 1/4, 1/16 and 1/4 respectively.

$$b_0 = \overline{Y_0} \tag{3.6}$$

$$b_i = A \sum_{u=1}^{N} X_{iu} Y_u \tag{3.7}$$

$$b_i i = B \sum_{u=1}^{N} X_{iu}^2 Y_u + C_1 \sum_{i=1}^{N} X_{ii}{}^2 Y - (\overline{Y_0}/S) \tag{3.8}$$

$$b_{ii} = D_1 \sum_{u=1}^{N} X_{iu} X_{ju} Y_u \tag{3.9}$$

$$SS_{b_i} = A \sum_{i=1}^{N} (X_i Y_i)^2 \tag{3.10}$$

$$SS_{b_{ij}} = D_1 \sum_{u=1}^{N} (X_{iu} X_{ju} Y_u)^2 \tag{3.11}$$

$$SS_{ii} = b_0 \sum_{u=1}^{N} Y - u + \sum_{u=1}^{N} b_{ii} X_{iu}^2 Y_u - \sum_{u=1}^{N} (Y_n)^2 / N \tag{3.12}$$

Notable features of BBD methodology can be summarized as follows [140]:

1. Has specific positioning of design points.
2. This design has 3 levels for each factor.
3. Created for estimating a quadratic model.
4. Provides strong coefficient estimates near the centre of the design space, but weaker at the corners of the cube, because there were not any design points.
5. Sensitive to missing data and a bad run.
6. Region of interest and region of operability are nearly the same.

3.3.3 General Steps in RSM

Sequential steps normally considered for carrying out a RSM problem are discussed next.

1. Identifying the critical process variables (or factors)

   These critical factors may be determined by referring to the previous studies or via

conducting a preliminary study (i.e. a screening study) based on factorial design or partial factorial design. In our case, the vital process factors were determined from the previous studies. The process input factors are equivalence ratio ϕ (Equation 2.3), particle size and spray distance, for DJ1050 and DJ2700 with an addition of the air flow rate for DJ2700 spray gun (therefore 3^4 equivalent design).

2. Finding the limits of each factor

Table 3.4: Process variables and experimental design used

Variables	Code	Unit	Limits coded/actual		
			-1	0	1
Equivalence ratio	A	dimensionless	0.83	1.01	1.50
Spray distance	B	mm	150	175	200
Particle size	C	μm	5	25	45
Air Flow (DJ2700 only)	D	SLPM	250	275	300

Previous studies and manufacturer specifications [16] were advised to find the limits of each factor which are given in Table 3.4

3. Design matrix development

The matrix depends on the type of RSM design selected, for BBD the design matrices in coded values are shown in Table 3.5 and Table 3.6 respectively. As stated earlier in the current work the matrix for each experiment is developed using the same statistical software. For three factors the experimental runs for BBD are 17 (based on 3^3) and 29 (based on 3^4) respectively [136,137]. Thus, the simulation runs are enough to estimate the coefficients in each case Equation 3.5.

4. Performing the experiment/simulation

The simulation were conducted according to the Design matrix Table 3.4 and Table 3.5 and in a random order to avoid any systematic error in the calculations.

Table 3.5: DOE operating conditions for DJ1050, where ϕ represents the correspondent equivalence ratio

Run No.	ϕ	Spray Distance(mm)	Particle Size(μm)
1	0.83	150	25
2	1.50	150	25
3	0.83	200	25
4	1.50	200	25
5	0.83	175	5
6	1.50	175	5
7	0.83	175	45
8	1.50	175	45
9	1.01	150	5
10	1.01	200	5
11	1.01	150	45
12	1.01	200	25
13	1.01	175	25
14	1.01	175	25
15	1.01	175	25
16	1.01	175	25
17	1.01	175	25

5. Recording the responses

   All responses, gas pressure, velocity and temperature; particle velocity and temperature at the substrate were modelled by ANSYS FLUENT code.

6. Development of the mathematical model

   The functional relationship representing any response of interest can be expressed as y = f (ϕ, PS, SD) and Equation 3.5 becomes as follows:

$$Y = b_0 + b_1\phi + b_2 PS + b_3 SD + b_{11}\phi^2 + b_{22}PS^2 + b_{33}SD^2 + b_{12}\phi PS + b_{23}PSSD \quad (3.13)$$

   where PS = Particle Size and SD = Spray Distance

7. Estimation of the coefficients in the model

   Regression analysis can be applied to specify the values of the coefficients in

Table 3.6: DOE operating conditions for DJ2700, where ϕ represents the correspondent equivalence ratio

Run No.	ϕ	Air Flow (SLPM)	Spray Distance(mm)	Particle Size(μm)
1	0.83	275	150	25
2	1.50	275	150	25
3	0.83	275	200	25
4	1.50	275	200	25
5	1.01	250	175	5
6	1.01	250	175	45
7	1.01	300	175	5
8	1.01	300	175	45
9	0.83	250	175	25
10	1.50	250	175	25
11	0.83	300	175	25
12	1.50	300	175	25
13	1.01	275	150	5
14	1.01	300	200	45
15	1.01	275	175	45
16	1.01	275	200	45
17	0.83	275	175	45
18	1.50	275	175	5
19	1.03	250	150	25
20	1.50	275	175	45
21	1.01	250	150	25
22	1.01	250	200	25
23	1.01	300	150	25
24	1.01	300	200	25
25	1.01	275	175	25
26	1.01	275	175	25
27	1.01	275	175	25
28	1.01	275	175	25
29	1.01	275	175	25

Equation 3.13. Equation 3.6 to Equation 3.9 were applied to evaluate the coefficients for BBD, and the calculations were performed by the StatEASE software.

8. Testing the adequacy of the models developed

   The analysis of variance (ANOVA) was used to test the adequacy of the models developed. The statistical significance of the models developed and each term in

regression equation were examined using the sequential F-test, lack-of-fit test and other adequacy measures (i.e. R2, Adj- R2, Pred. R2 and Adeq. Precision ratio) using the same software to obtain the best fit. The $Prob. > F$ (sometimes it called p-value) of the model and of each term in the model can be computed by means of ANOVA. If the $Prob. > F$ of the model and of each term in the model does not exceed the level of significance (say $\alpha = 0.05$) then the model may be considered adequate within the confidence interval of $(1 - \alpha)$. For the lack-of-fit test, the lack of fit could be considered insignificant if the $Prob. > F$ of the lack of fit exceeds the level of significance. Table 3.6 below is a summary of the ANOVA table.

Table 3.7: ANOVA table for full model

Source	SS	df	MS	$F_{cal} - Value$	P-Value or $Prob > F$
Model	SS_M	P	Each SS is divided by its df	Each MS is divided by MS_R	From table or software library
ϕ	SS_1	1			
Particle size	SS_2	1			
Spray distance	SS_3	1			
AB	SS_{12}	1			
AC	SS_{13}	1			
BC	SS_{23}	1			
A^2	SS_{11}	1			
B^2	SS_{22}	1			
C^2	SS_{33}	1			
Residual	SS_R	$N - P - 1$			from table
lack of Fit	SS_{lof}	$N - P - n_0$			from table
Pure Error	SS_E	n_{0-1}			from table
Cor Total	SS_T	$N - 1$			from table

Where: P: Number of coefficients in the model. N: Total number of runs.

$n0$: Number of centre points. $4df$: Degree of freedom. MS: Mean square

9. Development of the final reduced model

At this stage the final reduced model as determined by applying the above steps can be build-up. This model contains only the significant terms and the terms that necessary to maintain hierarchy. Also, a reduced quadratic ANOVA table can be produced.

10. Post Analysis

    When a final model is tested and checked and is found to be adequate, predicting any response within the range of factors using this model is possible. Also, producing some important plots such as 3D graphs, contours and perturbation plots to present the factors that affect and how they contribute in the response. Moreover, the possibility of employing the developed model for finding the optimal coating parameters setting at which the process could be optimized is a major goal for the study

3.3.4 Optimization

3.3.4.1 Desirability Approach

Many techniques are available in the statistics science for solving multiple response problems like overlaying the contours plot for each response, constrained optimization problem and desirability approach. Commonly used statistical software packages such as GPSS, NEMROD and Design-Expert were coded to implement a multiple response optimization techniques. The desirability method is recommended due to its simplicity, availability as a software and provides flexibility in weighting and giving importance for individual response. The desirability approach consists of transforming each estimated response, Y_i, into a unit less utilities bounded by $0 < d_i < 1$, where a higher d_i value indicates that response value Y_i is more desirable, if $d_i = 0$ this means an absolute undesired response or vice versa when $d_i = 1$ [141].

In the current work, the individual desirability for each response d_i is calculated using Equation 3.14 to Equation 3.18. The shape of the desirability function can be changed for each goal by the weight field wt_i. Weights are used to give added emphasis to the upper/lower bounds or to emphasize the target-value. Weights are ranged between 0.1 and 10; weights greater than 1 gives more emphasis to the goal, while weights less than 1 gives less emphasis to the goal. A weight value of 1, will make the $d_i^{'}$s vary from 0 to 1 in a linear mode. In the desirability objective function (D), each response can be assigned an importance (r), relative to the other responses. Importance varies from the least important a value of 1(+), to the

most important value of 5(+++++). If the varying degrees of importance are assigned to the different responses, the overall objective function is shown below Equation 3.18. Where n, is the number of responses in the measure and Y_i is the target value of ith response [5].

- For a goal of maximum, the desirability will be defined by:

$$d_i = \begin{cases} 0, & Y_i =< Low_i \\ (\frac{Y_i - Low_i}{High_i - Low_i})^{wt_i}, & Low_i \langle Y_i \langle High_i \\ 1, & Y_i => High_i \end{cases} \tag{3.14}$$

- For a goal of minimum, the desirability will be defined by:

$$d_i = \begin{cases} 1, & Y_i =< Low_i \\ (\frac{High_i - Low_i}{High_i - Low_i})^{wt_i}, & Low_i \langle Y_i \langle High_i \\ 0, & Y_i => High_i \end{cases} \tag{3.15}$$

- For a goal as a target, the desirability will be defined by:

$$d_i = \begin{cases} (\frac{Y_i - Low_i}{T_i - Low_i})^{wt_i}, & Low_i \langle Y_i \langle T_i \\ (\frac{Y_i - High_i}{T_i - High_i})^{wt_i}, & T_i \langle Y_i \langle High_i \\ 0, & \text{Otherwise} \end{cases} \tag{3.16}$$

- For a goal within range, the desirability will be defined by:

$$d_i = \begin{cases} 1, & Low_i \langle Y_i \langle High_i \\ 0, & \text{Otherwise} \end{cases} \tag{3.17}$$

- Objective Desirability Function:

$$D = (\prod_{i=1}^{n} d_i^{r_i})^{\frac{1}{\sum r_i}} \tag{3.18}$$

3.3.4.2 Optimization Approach in Design-Expert Software

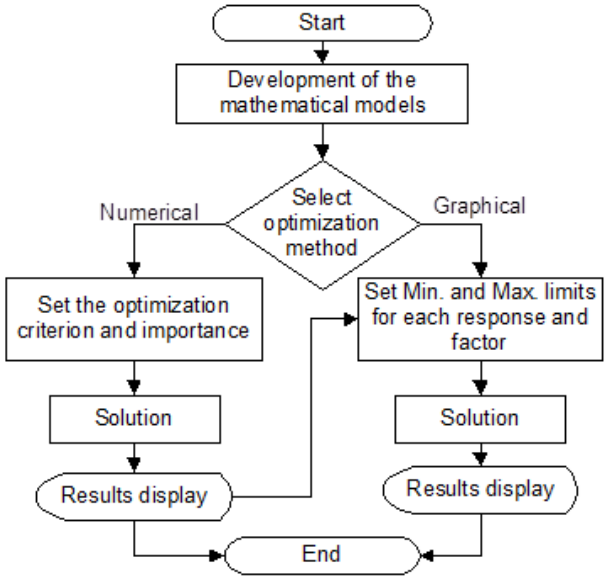

Figure 3.4: Optimization Steps flow process [141]

The optimization part in the Design-Expert software (Version-7) determines a combination of factor levels that simultaneously satisfy the requirements placed (i.e. optimization criteria) on each one of the responses and process factors (i.e. multiple response optimization). Numerical and graphical optimization methods were used in this work, by choosing the desired goals for each factor and response. As mentioned earlier, the numerical optimization process involves combining the goals into an overall desirability function (D). The numerical optimization feature in the design expert software package finds a point or more in the factors domain that would maximize this objective function. In the graphical optimization with multiple responses, the software defines regions where requirements simultaneously meet the proposed criterias, therefore superimposing or overlaying critical response contours on a contour plot. Then, a visual search for the best compromise becomes possible. In the case of dealing with many responses, it is recommended to conduct a numerical optimization first; otherwise, it could be impossible to uncover a feasible region. The graphical optimization displays the area of feasible response values whithin the factor space. Regions that do not fit the optimization criteria are shaded [138]. Figure 3.4 shows flow chart of the optimization steps in the Design-Expert software, which were implemented in this study.

Chapter 4

Results and Discussion

4.1 Introduction

The results of this work are divided into two parts, first is the CFD simulation results for both guns under investigation. The second is the DOE results which are based on the CFD results as that was the approach of this study. The parameters that were taken into account in the CFD calculations were the equivalence ratio (ϕ), spray distance and particle size for DJ1050 gun as can be referred to Table 3.5 and Table 3.6 for the DJ2700 in Chapter three. The same parameters were considered for DJ2700, with one exception of the inclusion of air flow rate.

Validation of the CFD results is conducted via Accuraspray-G3 which is able to measure and characterize the spray plume, average particle temperature and velocity. The device is based on cross-correlation of signals, dual-fibre optic, recorded at two closely spaced locations in the spray stream and the temperature is determined via two-colour pyrometry [43]. The device was available at Oerlikon Metco, Switzerland. The measurement was conducted together with Oerlikon Metco, in Switzerland [16]. The size range of the WC-12%Co particle sprayed during the experiment session was ($5\mu m \rightarrow 45\mu m$). The temperature profile of a $10\mu m$ particle yielded temperature of 1711 K, which was in a good agreement of that measured at 1750 K, as can be seen in Figure 4.1.

The output responses considered in this study are ; gas static pressure, gas static

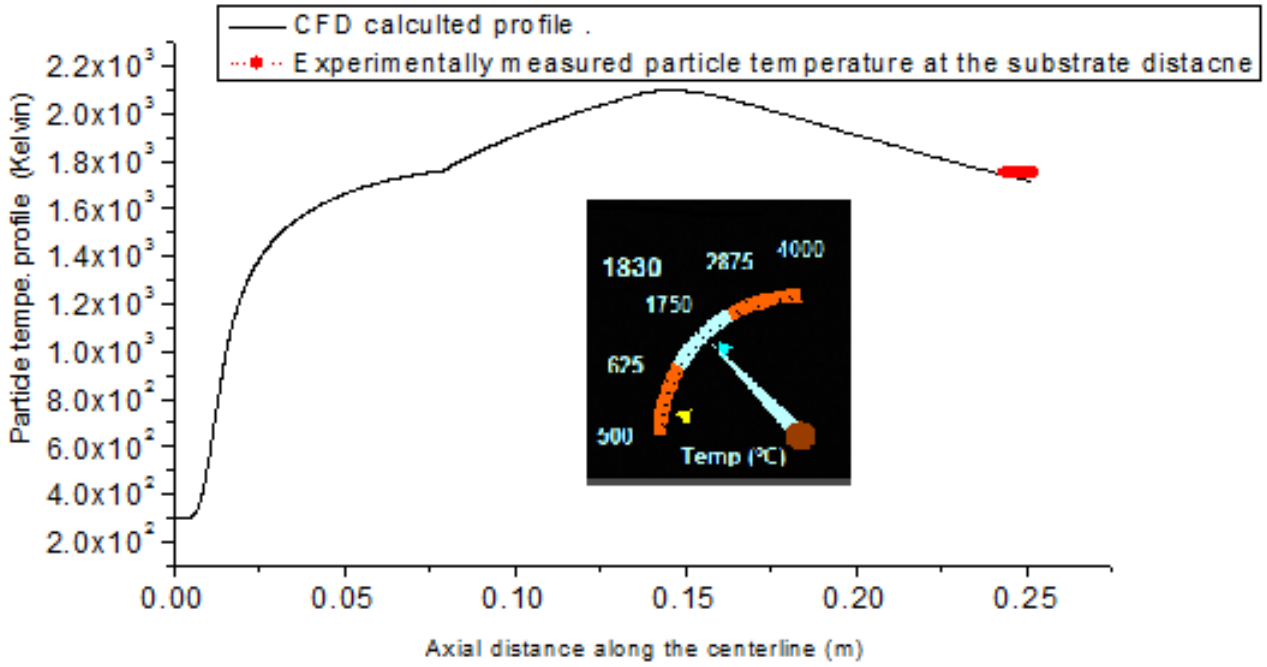

Figure 4.1: Computed temperature profile of a 10 μm WC-12%Co particle validated by a measured temperature over the stand-off distance

temperature, gas velocity magnitude, particle velocity and particle temperature. The responses of gas static pressure, gas static temperature and gas velocity were considered as the maximum values of the calculated outputs from the ANSYS FLUENT. While for the particle temperature and velocity were taken at the spray distance corresponding to the pressure outlet of the computational domain as in Figure 3.1. The results of the responses calculated in this study are summarized in Table 4.1 and Table 4.2. In the subsequent sections the discussion for the results of the responses considered in this study are given. The statistical methodology of BBD is applied on the calculated responses. The calculated responses in the following tables were given the abbreviations as follows; GP_{max}, GT_{max}, GV_{max}, PT, PV, PT_e, PV_e, are the maximum static gas pressure, the maximum static gas temperature, the maximum gas velocity, the particle temperature at the substrate, and the particle velocity at the substrate, the particle temperature at the nozzle exit and the particle velocity at the nozzle exit, respectively.

Table 4.1: Calculated responses for DJ1050

Run No	PG_{max} (bar)	GT_{max}(K)	GV_{max} (m/s)	PT(K)	PV (m/s)	PT_e(K)	$PV_e(m/s)$
1	3.56	3300	1860	1167	193	763	86
2	4.09	3100	1870	1152	209	815	89
3	3.68	3300	1850	1176	195	815	158
4	4.08	3200	1870	1161	208	815	89
5	3.65	3300	1860	1645	406	677	178
6	4.08	3200	1870	1622	420	687	181
7	3.65	3300	1860	724	141	600	63
8	4.08	3200	1860	937	151	606	69
9	3.76	3500	1900	1727	410	648	179
10	3.76	3500	1900	1405	334	617	264
11	3.76	3500	1910	921	143	594	70
12	3.76	3500	1900	1167	186	775	87
13	3.76	3500	1900	1176	199	779	87
14	3.76	3500	1900	1176	199	779	87
15	3.76	3500	1900	1176	199	779	87
16	3.76	3500	1900	1176	199	779	87
17	3.76	3500	1900	1176	199	779	87

4.2 Gas Pressure

Gas pressure behaviour in a varying area nozzle can be generally classified into three categories, depending on the static pressure at the nozzle exit; into an under-expanded nozzle, ideally expanded and over expanded [66]. Under expanded type, is where the static pressure at the nozzle exit is greater than the atmospheric/ambient pressure, an ideally expanded is where the static pressure is equal to the atmospheric pressure, an over expanded, is where the static pressure is less than the atmospheric pressure. In cases of under and over expanded types, shock waves are developed in the flow. In this study, the two nozzle geometries that were developed and commonly used in HVOF application are considered (Figure 3.1).

The nozzle geometry is taken as a basis to classify the development of HVOF process design within the first, second and third generations. In the first generation, nozzle design is characterized by a combustion chamber followed by a parallel sided barrel (DJ1050). The second generation, addition of converging part between the combustion chamber and the

Table 4.2: Calculated responses for DJ2700.

run	PG_{max} (bar)	TG_{max}(K)	VG_{max} (m/s)	PT(K)	PV (m/s)	PT_e(K)	$PV_e(m/s)$
1	3.62	3310	1870	1467	297	1297	212
2	4.49	2520	1710	1328	281	1111	194
3	3.62	3310	1870	1338	297	1244	210
4	4.49	3320	1710	1245	284	1087	194
5	4.12	3560	1870	1260	666	1087	193
6	4.12	3560	1870	1119	201	882	140
7	4.29	3580	1900	1226	673	1965	577
8	4.29	3580	1900	1101	205	889	141
9	3.24	3310	1870	1407	301	1263	211
10	4.2	2740	1700	1286	284	1087	193
11	3.8	3310	1870	1406	298	1315	208
12	4.9	3330	1720	1353	289	1175	203
13	4.2	3320	1890	1369	655	1852	565
14	4.29	3320	1900	1035	600	889	141
15	4.2	3570	1880	1119	201	886	141
16	4.2	3320	1870	1051	198	864	138
17	3.62	3310	1870	1089	209	912	145
19	4.49	3320	1710	1279	667	1875	562
20	4.12	3320	1890	1380	274	1195	200
21	4.49	3320	1700	1098	204	872	140
22	4.49	3320	1700	1098	204	872	140
23	4.12	3320	1890	1059	196	860	137
24	4.29	3320	1900	1366	278	1198	202
25	4.2	3570	1900	1411	288	1223	205
26	4.2	3570	1900	1411	288	1223	205
27	4.2	3570	1900	1411	288	1223	205
28	4.2	3570	1900	1411	288	1223	205
29	4.2	3570	1900	1411	288	1223	205

parallel sided barrel was involved (DJ2700). The third generation is of a typical de Laval nozzle type or a converging diverging nozzle. It is worth mentioning that the second and the third generation,(DJ2700 with adjusted pressure) designs are the most common ones used in HVOF applications nowadays.

4.2.1 CFD Results for Gas Pressure

One of the geometries considered in this study (DJ1050) is never computationally studied before in the literature. This might be attributed to the fact that a design such as this (DJ1050) has recently not been adopted by the majority of the manufacturers in HVOF industry. However, it was recently introduced as a novel design by [142], in which the combustion chamber can be operated for both liquid and gas fuel.

Before commencing the simulation of this study, the question of the state of the gases at their inlets to the nozzle is considered. In ANSYS FLUENT code, the recommended boundary condition for a compressible flow is of a mass flow inlet type (kg/s), as the code does not include a volumetric flow rate (m^3/s) as a boundary condition. It is noticed, in the majority of the previous modelling work of HVOF, that the given volumetric flow rate for the gases were converted into mass flow rate via the equation of state)(Equation 2.12), in which the calculation is based on the standard condition of 1 bar and 273.15 K.

The effect of pressure and temperature on the density of gases at their inlets were investigated in this study. The calculation of density was based on the equation of state; $P\dot{V} = \rho RT$ where P is the static pressure of the gas, $\dot{V}$ is the volumetric flow rate, ρ is the gas density to be calculated, R is the universal gas constant and T is the static gas temperature. The range of pressure and temperature operating conditions are given in Table 4.3. It could be concluded that changing the pressure and temperature within the range considered in this study has a marginal effect on the flow behaviour [1].

Table 4.3: Calculated responses for DJ2700.

P (bar)	$T(K)$	$\dot{V}_{mixture}$ (m^3/s)	$\dot{V}_{\mathrm{N}_2}$ (m^3/s)	$\dot{m}_{mixture}$ (kg/s)	$\dot{m}_{\mathrm{N}_2}$ (kg/s)
1.0 (baseline)	273	329	325	18	8
1.5 (case 1)	283	329	325	25	11
2.0 (case 2)	293	329	325	33	18
2.5 (case 3)	302	329	325	40	17

The results were presented and discussed in the International Thermal Spray Coating Conference, May, 2016, Shanghai, China. Professor Vardelle, leading researcher in CFD of

[1] Implementing the equation of state to account for the density variation at the inlet boundaries for high velocity oxy gas fuel process. M. Aldosari et al., ITSC 2016

HVOF, supported the importance of taking the variation of density with the thermodynamic state of the gas into account, while Professor Mostaghimi suggested that calculation based on the standard state of 1 bar and 273.15 K is sufficient in the modelling of the HVOF. Nevertheless, the range of pressure and temperature can be further widened, beyond that of this study and the effect on the flow behaviour could be pronounced. The effect of density variation on the pressure for DJ1050 gun is given in Figure 4.2.

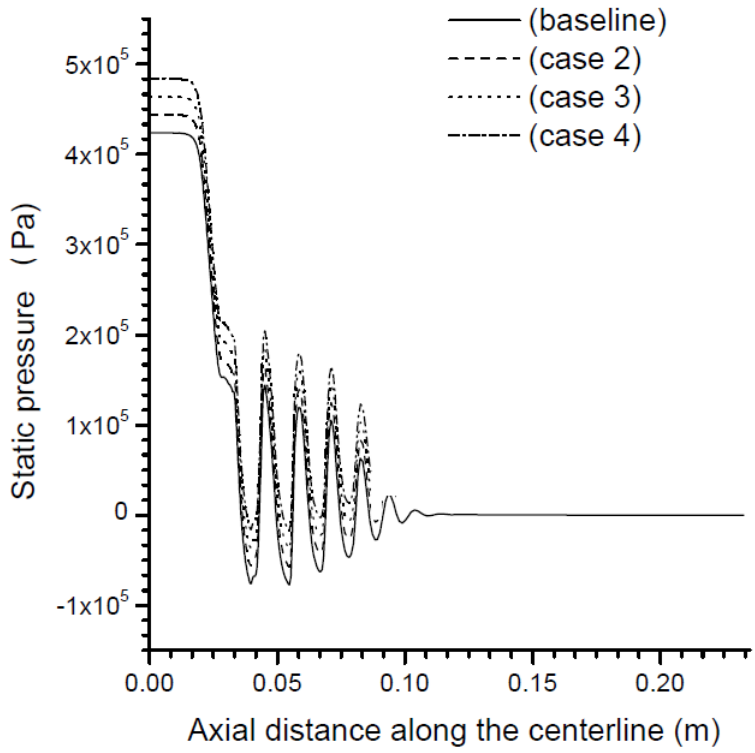

Figure 4.2: The effect of density variation on the pressure behaviour in a DJ1050 HVOF gun for the cases considered in Table 4.3

As the density of the gases increased, the static pressure in the combustion chamber increased and the compressibility behaviour changed marginally in the outside domain. The same behaviour was observed with other variables like temperature, velocity and density of the gas along the centreline axis of the nozzle. Due to the results obtained from this investigation, the density calculation of the gases is based on the standard ones at the 1 bar and 273.15 K and the data already available in the ANSYS FLUENT data base. Hence, in the subsequent results the mass flow rate was obtained by converting the volumetric flow rate to the mass flow rate by multiplying the volumetric flow rate by the standard corresponding density of the gas. The static pressure contour (at $\phi = 1.01$ and 175 mm spray distance

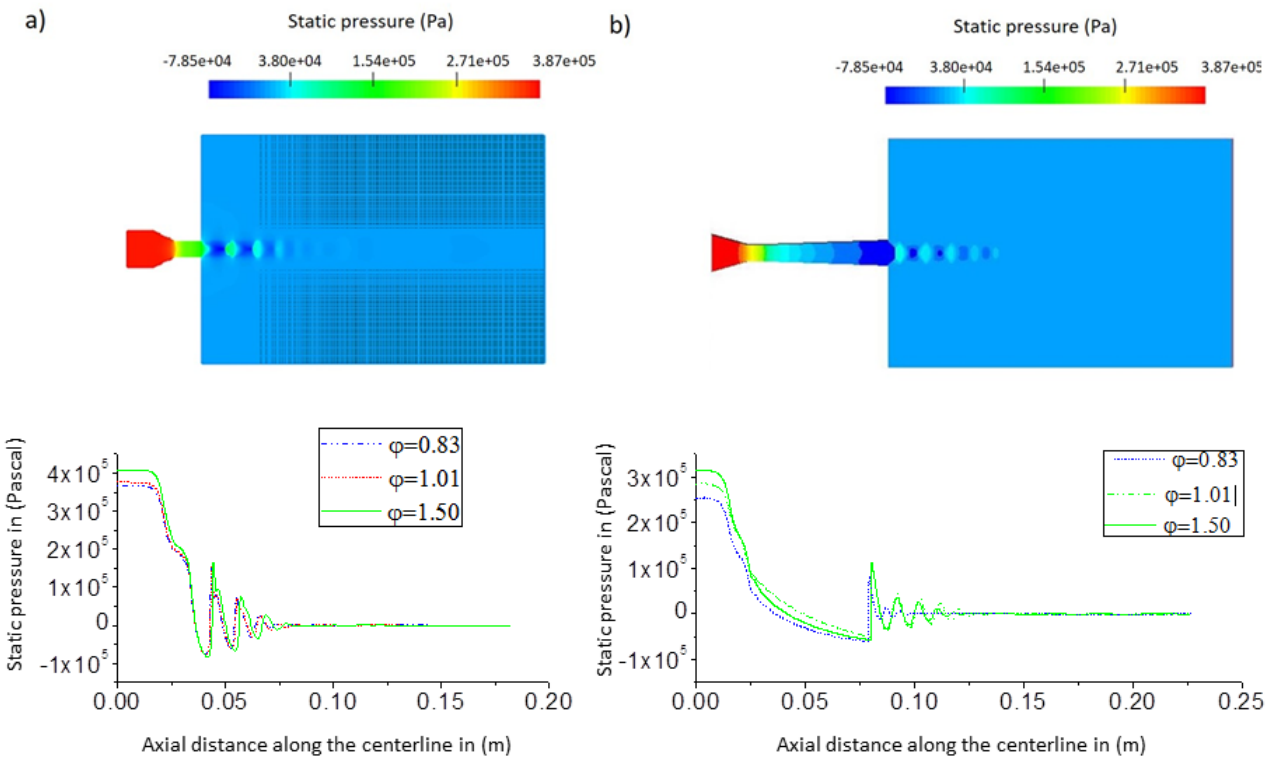

Figure 4.3: Static pressure along the centerline of [a]: under-expanded jet DJ1050 and [b]: over-expanded jet DJ2700 of the contours at $\phi = 1.01$ and 175 mm spray distance

only) and the plot of pressure variation along the centreline axis for 175 mm spray distance and for the range of ϕ in this study is given in Figure 4.3. In both guns, the compressibility behaviour was developed at the exit of the nozzle and the intensity of the shock waves reduced for $\phi = 1.01$. The static pressure, for the three cases of ϕ at the exit of the nozzle was around 1.5 bar for the DJ1050 gun, thus higher than the atmospheric pressure of 1 bar, which implies that the jet was of an under expanded type. While it was -78500 bar for DJ2700 and in this case the jet had an over expanded behaviour. It was noticed that increasing the equivalence ratio (ϕ) increased the static pressure inside the nozzle for the both guns (in the combustion chamber), as previously stated fuel rich provides more power output.

It was also noticed that under the same equivalence ratio the static pressure in the combustion chamber was almost the same for the both guns while it was different along the

centreline. It was also noticed that Mach disk was developed at the exit of the nozzle of DJ2700. The statistical results obtained by applying the BBD methodology on the responses of interest in this study are given in the subsequent sections.

4.2.2 DOE Results for Static pressure

Pressure is one of the key variables in any fluid flow, as it is quantitatively related to the other flow variables such as velocity and temperature through the general conservation mathematical models that describe the flow. The statistical results of this study were used to derive a quantitative or mathematical models to relate the maximum pressure obtained from the combustible jet of HVOF to the process parameters of equivalence ratio (ϕ) and spray distance. It was concluded that the combustion chamber pressure can have a significant effect on the flow behaviour [12], especially the compressibility behaviour of the flow which can affect the shock particle interaction in HVOF spray process. Nevertheless, the model developed in this study could be used as a guide in the design process of the gun to achieve a desired combustion chamber pressure.

Design-Expert V7 software is used to derive the mathematical model to show the effect of the considered input parameters on the maximum static pressure of the flow, which normally corresponds to the static pressure in the combustion chamber region. The step-wise regression method is used to derive the regression model for the pressure response.The ANOVA table (Table 4.4 for DJ1050 gun and Table 4.5 for DJ2700 gun) shows the analysis for this response . The ANOVA table shows also the adequacy measures of R^2, adjusted R^2 and predicted R^2 which were acceptable and indicate reliable relationships since their values are close to one and the difference between the $dj.R^2$ and $Pred.R^2$. was less than 0.2.

The final mathematical model for DJ1050 in terms of both coded and actual parameters were found to be as follows:

$$GP_{max} = 3.760 + 0.22 * A + 0.014B - 0.032 * A * B + 0.10 * A^2 \tag{4.1}$$

where GP_{max} is the coded maximum gas pressure, A and B are the coded equivalence ratio

Table 4.4: ANOVA analysis for Static pressure model for DJ1050.

Source	Sum of squares	DF	Mean squares	F value	$prob > F$	
Model	0.447	4	0.112	550.8	< 0.0001	significant
A (Equivalence ratio)	0.401	1	0.400	1971.8	< 0.0001	
B (Spray distance)	0.001512	1	0.0015	7.4461	0.0183	
AB	0.004225	1	0.004225	20.8	0.0007	
Residual	0.0024	12	0.00020			
Cor Total	0.450	16				
$R^2 = 0.99$				$Adj.R^2 = 0.99$		
$Pred.R^2 = 0.97$				$Adeq.Precision = 66.3$		

Table 4.5: ANOVA analysis for Static pressure model for DJ2700.

Source	Sum of squares	DF	Mean squares	F value	$prob > F$	
Model	2.43	2	1.22	61.9	< 0.0001	significant
A (Equivalence ratio)	2.11	1	2.11	107.8	< 0.0001	
D-Air flow	0.313	1	0.313	15.9	0.0005	
Residual	0.51	26	0.019			
Cor Total	2.94	28				
$R^2 = 0.82$				$Adj.R^2 = 0.81$		
$Pred.R^2 = 0.76$				$Adeq.Precision = 25.81$		

and spray distance respectively at min/max coded values of -1 or 1

$$GP_{max} = 3.25 + 0.56 * \phi + 0.005SD - 0.004 * \phi * SD + 0.10 * \phi^2 \tag{4.2}$$

where ϕ, SD are the actual factor value in their respective units (unitless, mm respectively) and the final mathematical models for DJ2700 in terms of both coded and actual parameters were found to be as follows:

$$GP_{max} = 4.16 + 0.42 * A + 0.16D \tag{4.3}$$

$$GP_{max} = 1.00 + 1.2 * \phi + 0.006D \tag{4.4}$$

For DJ1050: the coded models show order of effect on pressure as $A > A^2 >> -A * B > B$. So equivalence ratio having a significant effect both as itself (A) and squared (A^2) on pressure.

For DJ2700: $A >> D$; again equivalence ratio having significant effect on pressure.

One of the ANalysis of Variance (ANOVA) assumptions is the normality of the residuals (i.e. the residuals are normally distributed). Figure 4.4 is a normal plot for DJ1050 gun showing that the residuals have a linear relationship, which indicates that the residuals are normally distributed. Therefore, ANOVA can be carried out on observations for gas pressure.

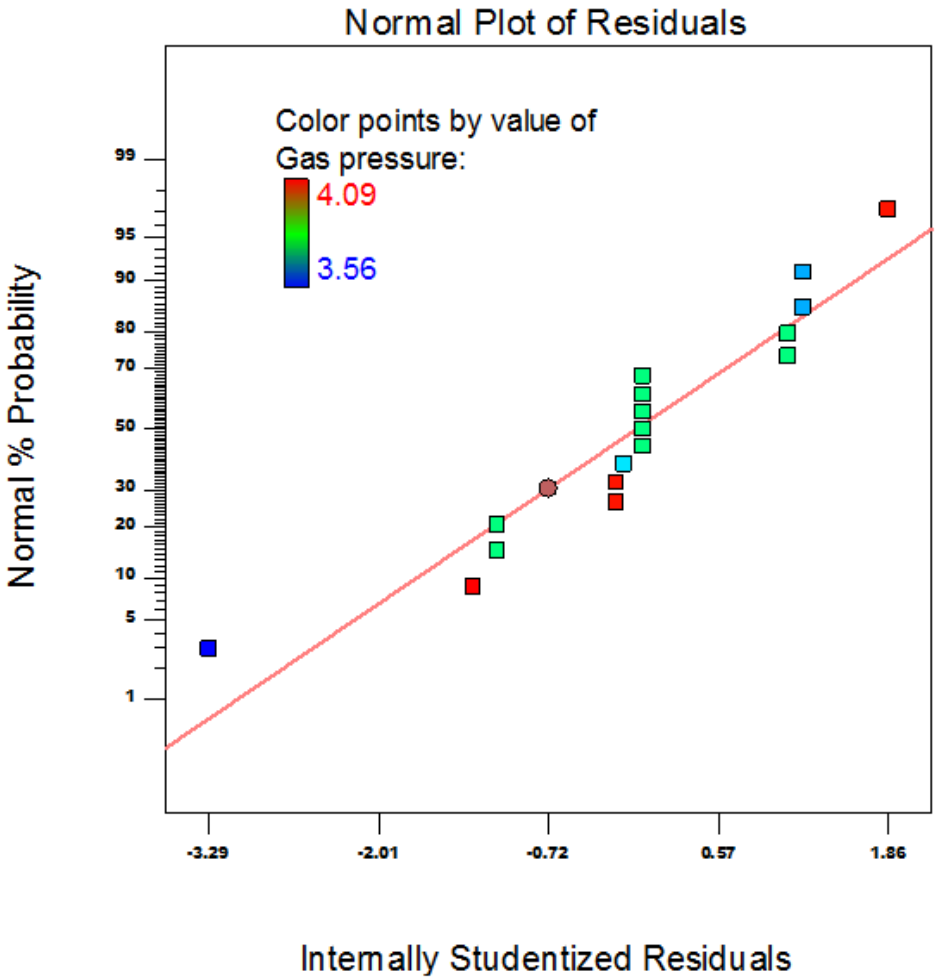

Figure 4.4: Normal plot of residuals DJ1050

In addition, the relationship between the actual and predicted value is linear which indicate that the difference between them is small as shown in Figure 4.5 for the DJ1050 HVOF gun. The same criteria was observed for the DJ2700 HOVF gun, and for the brevity it will not be included in the thesis.

It was observed from the models, that for the DJ1050 HVOF gun the equivalence ratio and the spray distance were found to have a pronounced effect on the maximum static gas

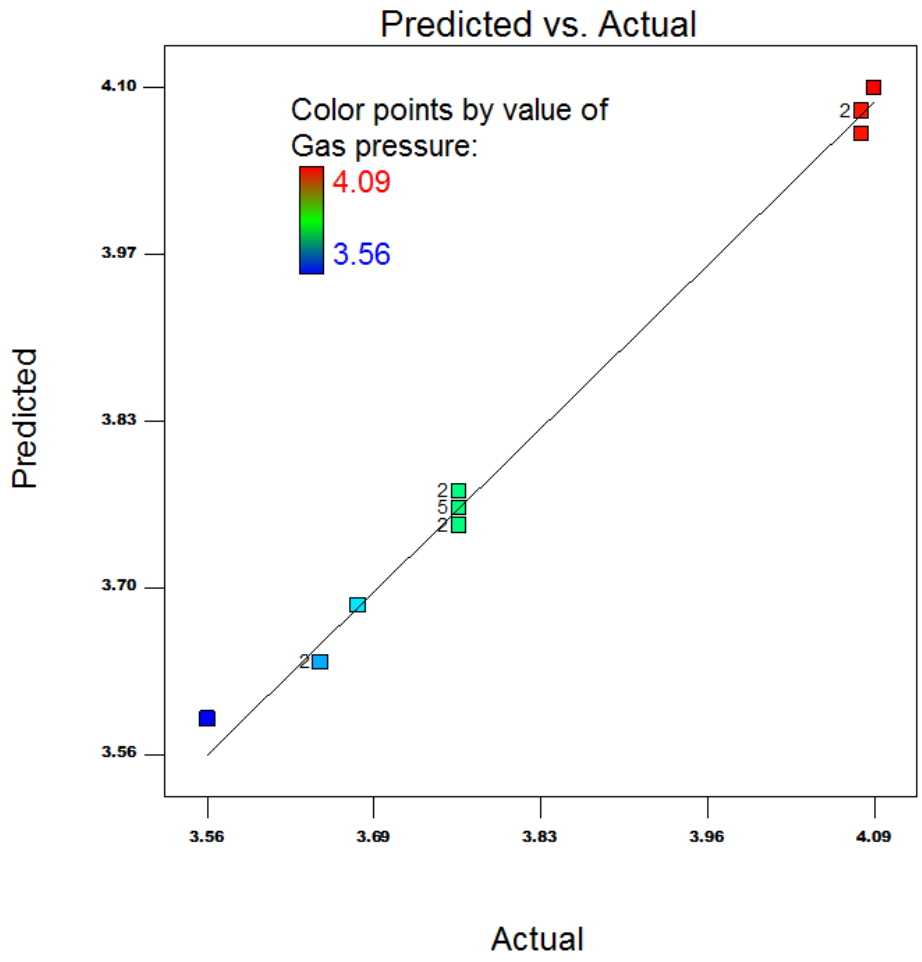

Figure 4.5: Predicted Vs actual values for DJ1050

pressure of the flow, while for the DJ2700 the equivalence ratio and the air flow rate had linear proportional effect on the pressure response. The equivalence ratio has a quadratic relationship to the response of pressure in the case of DJ1050. The difference could be attributed to the inclusion of air in modelling the DJ2700 gas dynamics. In the case of DJ1050, the relation between the equivalence ratio and the pressure response was of an exponential growth, while a slight linear increase in the pressure response was observed. As mentioned before, the static pressure of the combustion chamber which is considered as the highest pressure attainable in a combustible jet in a nozzle can have a considerable effect on the flow behaviour. The mathematical model relation developed in this study shows that the effect of the equivalence ratio on the static pressure is totally dependent on the geometry of the nozzle.

Figure 4.6 is a perturbation plot showing the effect of each factor on the gas pressure response. As the equivalence ratio increases the gas pressure increases in a quadratic manner

(A and A^2 terms in the coded equation), while the gas pressure increases slightly in a linear behaviour with increased spray distance.

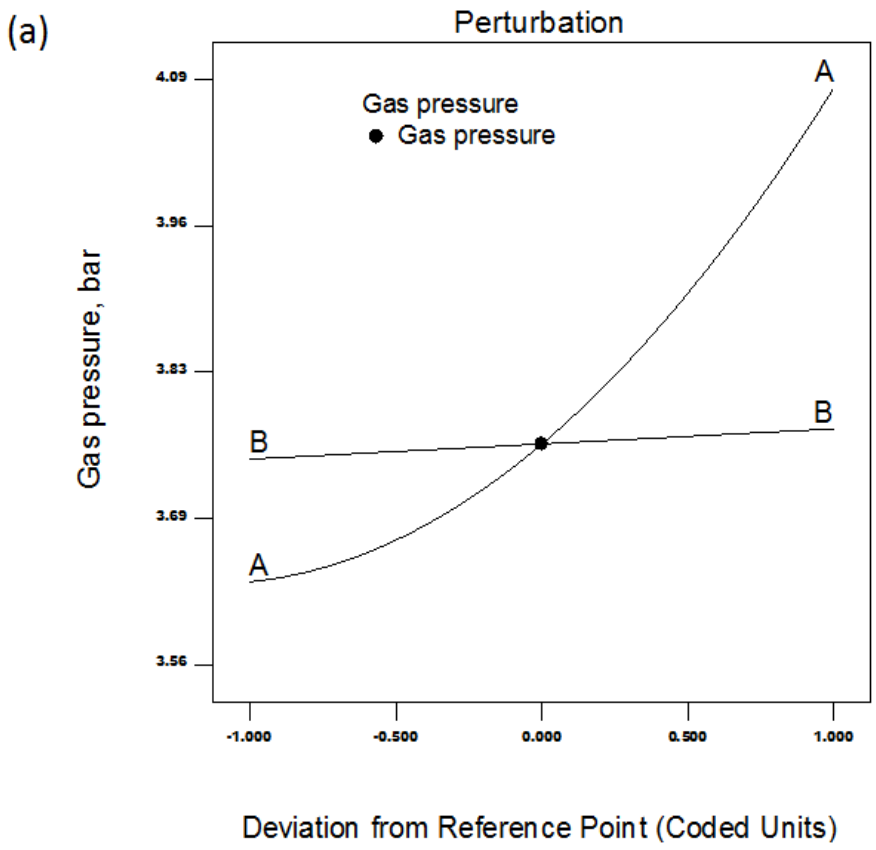

Figure 4.6: Perturbation plot for DJ1050 where A = equivalence ratio and B = spray distance for the pressure response

Figure 4.7 shows the interaction plot between the equivalence ratio and the spray distance at $\phi = 0.8$ (fuel-lean). It is clear that there is a significant difference between the two levels of spray distance at 150 mm and 200 mm. Applying $\phi = 0.8$ and spray distance of 200 mm would lead to a higher gas pressure response of approximately 3.76 bar. Whereas applying $\phi = 1.5$, less significant difference between the two levels of the spray distance were observed, due to the significant bars overlapping. The relationship or the interaction can be represented by the contour plot as in Figure 4.8. It is evident that the most significant factor is the equivalence ratio. As the equivalence ratio increases from 0.8 to 1.5 the gas pressure increases from 3.67 to 4.02, whereas the spray distance in the range of 150 to 200 mm had a marginal effect on this response.

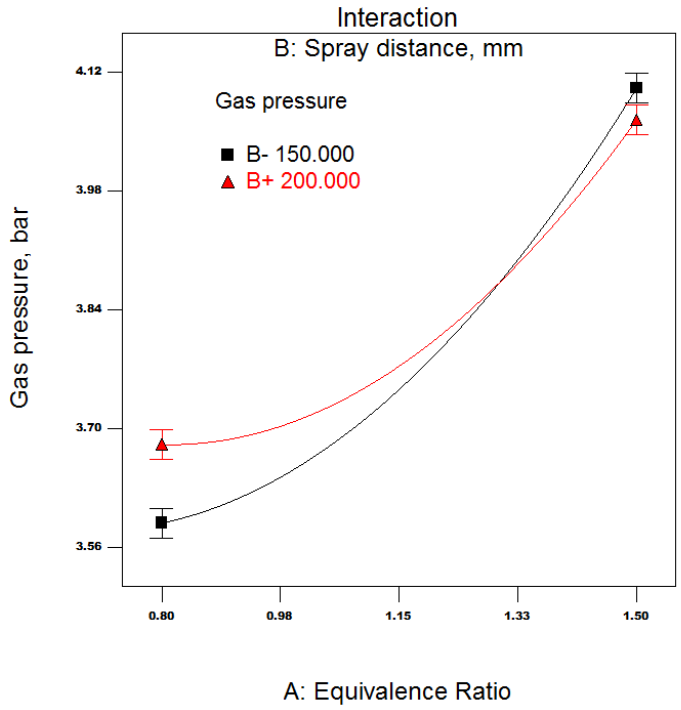

Figure 4.7: Interaction between the gas pressure response, equivalence ratio and spray distance DJ1050

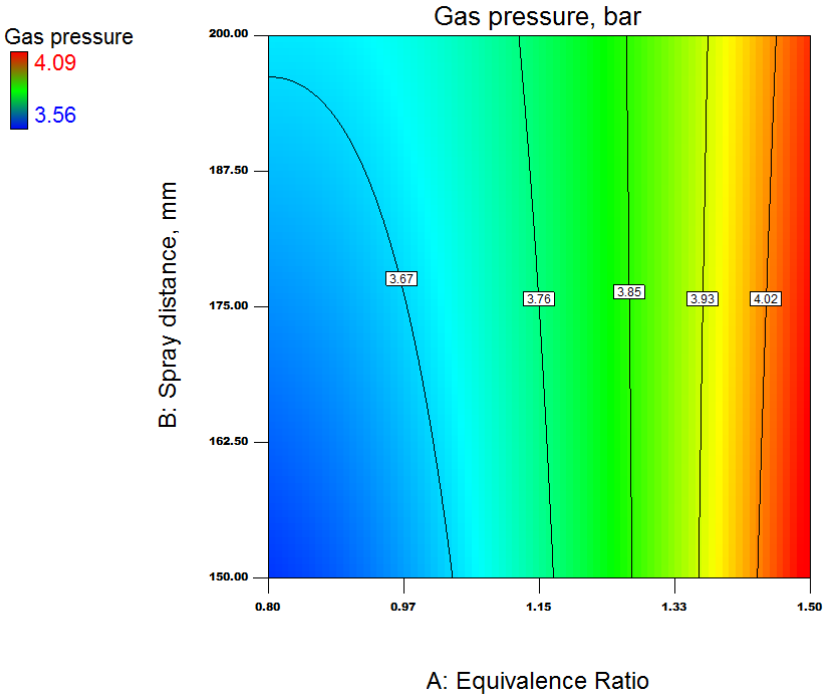

Figure 4.8: Contour plot of the gas pressure response Vs the equivalence ratio and the spray distance DJ1050

Figure 4.9 and Figure 4.10 present the perturbation and contour plot for DJ2700 which shows a linear relationship ($A >> D$ in the coded equation) between the equivalence ratio/air flow and the gas pressure response. The air flow had a marginal effect on the gas pressure

[102].

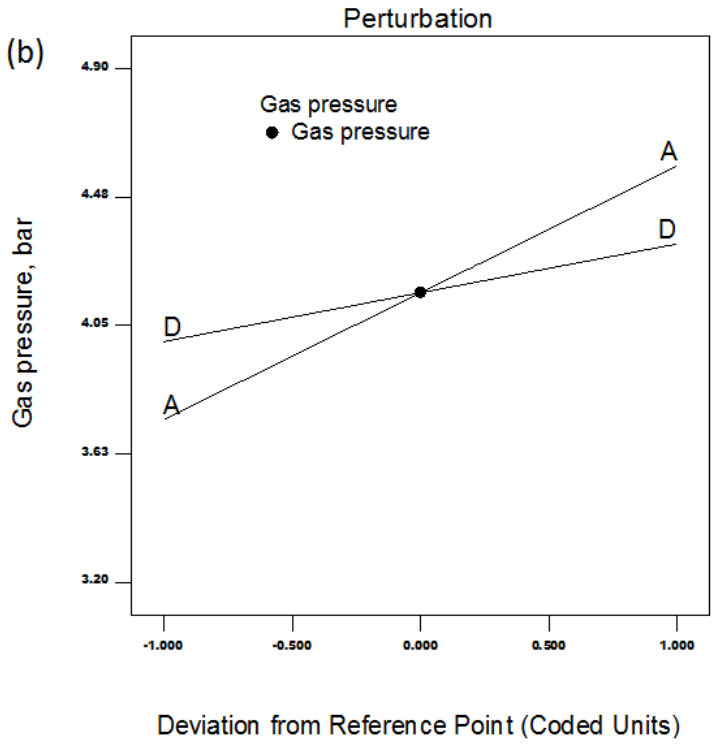

Figure 4.9: Perturbation plot for DJ2700 where A = equivalence ratio and D = Air flow for pressure response

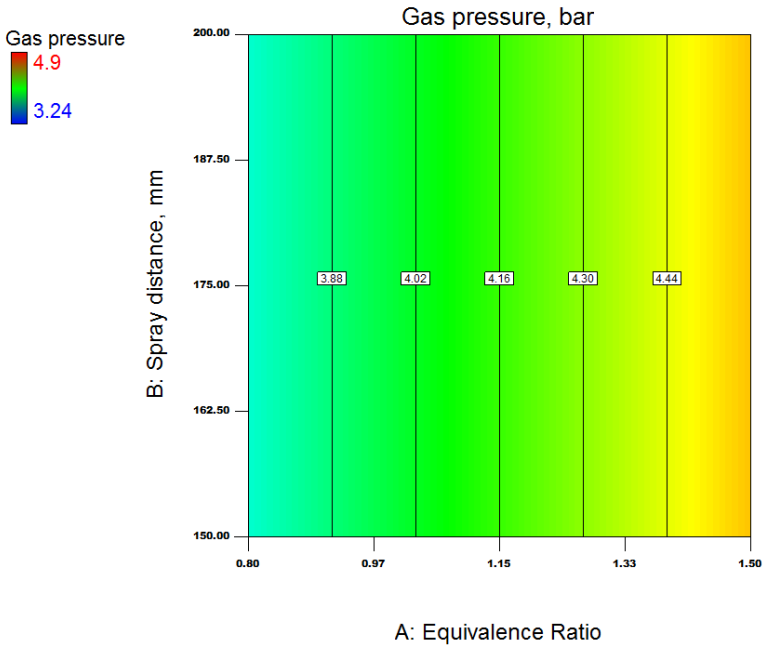

Figure 4.10: Contour plot for DJ2700 showing the relation between the gas pressure response, the equivalence ratio and spray distance.

4.3 Gas Temperature

Gas temperature is considered one of the most important variable within the HVOF process since the coating particles gain heat from the flame. The particles are typically in a semi molten or fully molten state upon the impact on the substrate surface. In this section the CFD results of the gas temperature followed by the DOE results for this response are presented and discussed.

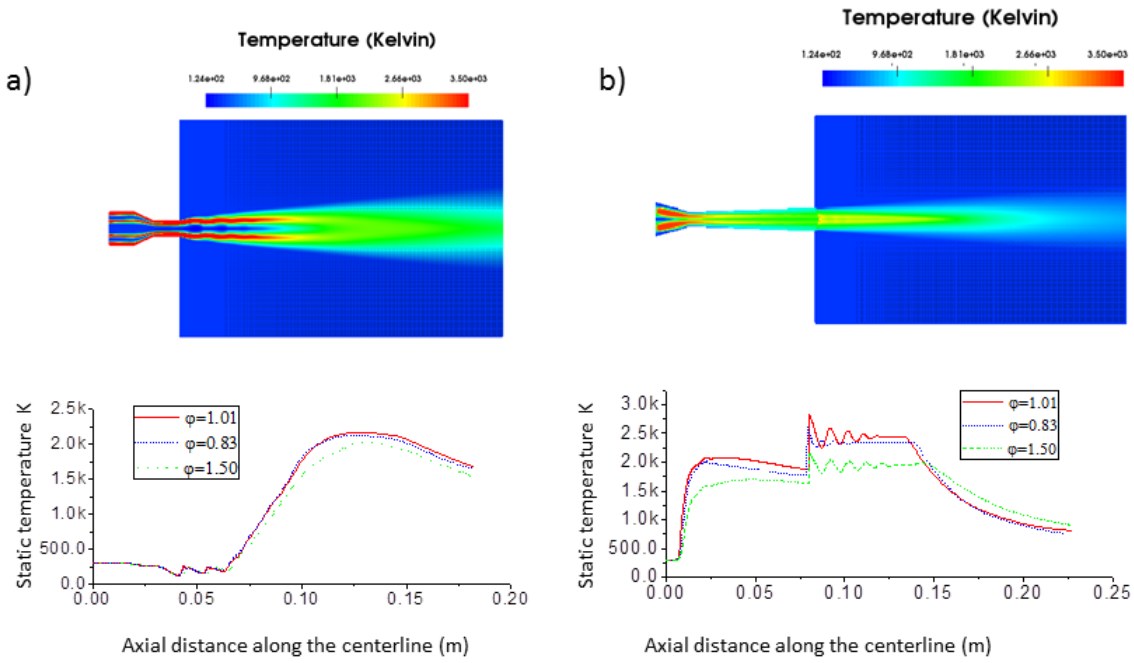

Figure 4.11: Static temperature along the centreline of [a]: DJ1050 and [b]: DJ2700. The contours are for $\phi = 1.01$ and 175 mm spray distance

4.3.1 CFD Results for Gas Temperature

Figure 4.11 shows the CFD results of the static gas temperature along the centerline for both the DJ1050 and DJ2700 HVOF guns. It was revealed that the geometry of the nozzle has a considerable effect on the temperature behaviour of the jet. For DJ1050 the nitrogen

inlet dimension was 5 mm in diameter and 1.5 mm in diameter for DJ2700. Both are located at the center of the nozzle inlet. Due to this difference in the nitrogen inlet dimension, the nitrogen flow had a considerable cooling effect on the temperature of the jet along the centerline inside the nozzle of DJ1050 gun in contrast with the DJ2700 as found by [102]. This was also in a good agreement with the previous studies that recommended to keep the nitrogen flow rate to a minimum due its effect on the jet temperature [12].

In case of DJ1050, temperature was almost constant along the centreline up to the nozzle exit and then started to increase to around 2000 K at a distance of around 125 mm along the axis line. The temperature then decreased to around 1500 K at a spray distance of 175 mm. On the other hand, the temperature profile of DJ2700 showed that the temperature started to increase inside the nozzle in the combustion zone, reached a peak at the nozzle throat for both ($\phi > 1$) and ($\phi < 1$) (for fuel-rich and fuel-lean conditions). The temperature then decreased slightly along the diverging part of the nozzle and the compressible behaviour began at the nozzle exit, before at some distance along the axis the temperature decreased to around 1000 K at the final spray distance.

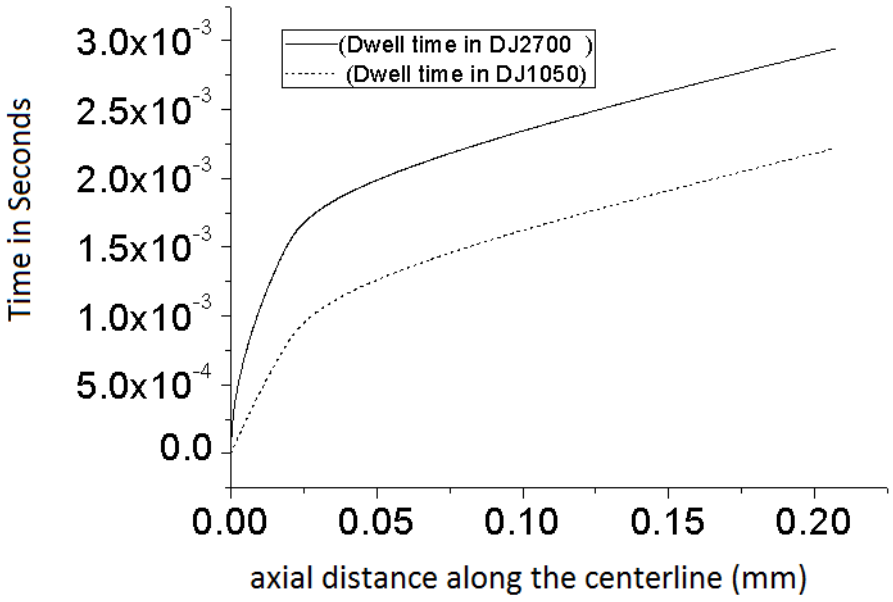

Figure 4.12: Residence time of 25μm particle in both DJ1050 and DJ2700 under the same operating conditions

It should be mentioned that there was a difference of approximately a milli-second in

the dwell time of a 25μm particle between the two guns (Figure 4.12). That was due to the fact that DJ1050 gun is shorter in length than DJ2700 gun, since the former does not contain a diverging section. This difference in the dwell time was also noticeable in the temperature profile of other particle sizes under the same operating conditions in the both guns. The difference of the dwell time, contributed to the temperature profile of the same size particle in both guns, as can be seen in Figure 4.13. Even though the jet temperature at the substrate distance is higher than in the case of DJ1050, the particle temperature at the substrate distance was higher in the case of DJ2700, at about 1416 K while it was 1100 K for the DJ1050 gun.

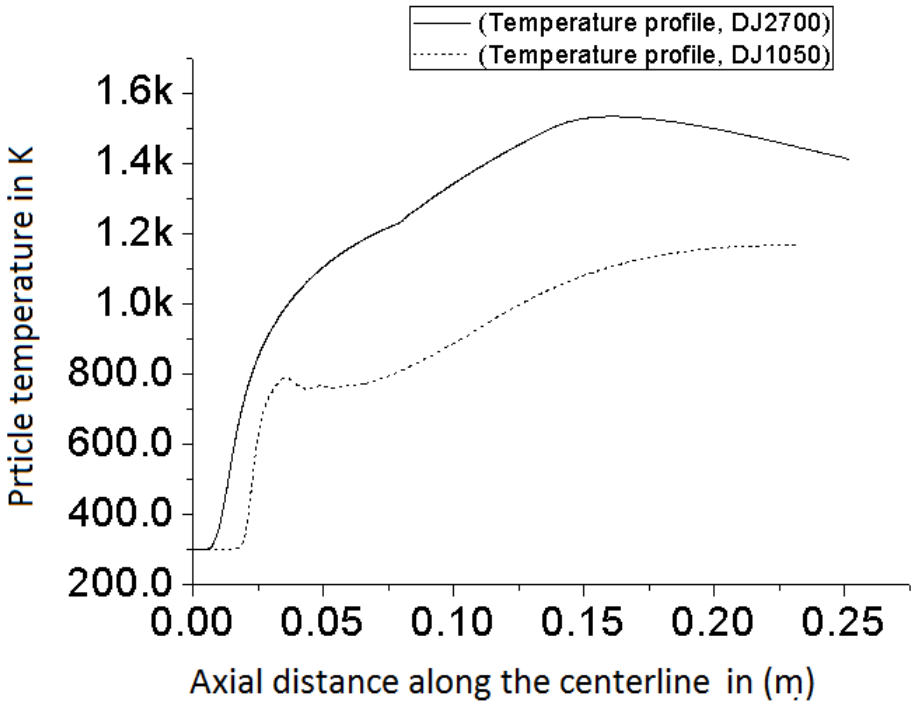

Figure 4.13: Particle temperature profile along the centerline axis for a 25μm particle for both the DJ1050 and DJ2700 HVOF guns under the same operating conditions

4.3.2 DOE Results for Gas Temperature

The statistical methodology that was discussed in Chapter 3 and similar to that applied for the pressure response, is also applied to the maximum static temperature range attained by the jet. The Design-Expert software is used to develop the statistical mathematical models to show the effect of the process parameters on this response. Unlike the maximum

static pressure which mostly affects the combustion chamber zone, the maximum static temperature could extends beyond this zone as was revealed by the CFD results. Table 4.6 and Table 4.7 provides the ANOVA tables which show the regression analysis of this response for both the DJ1050 and DJ2700 HVOF guns, respectively. As with the pressure response, the adequacy measures in ANOVA tables for the temperature response show adequate relations since their values are within reasonable ranges.

Table 4.6: ANOVA analysis for Static temperature model for the DJ1050 gun.

Source	Sum of squares	DF	Mean squares	F value	$prob > F$	
Model	326838	4	81709	261	< 0.0001	significant
A (Equivalence ratio)	31250	1	31250	100	< 0.0001	
B (Spray distance)	1250	1	1250	4	0.0687	
AB	2500	1	0.004225	20.8	0.0007	
A^2	291838	1	291838	934	< 0.0001	
Residual	3750	12	312.5			
Cor Total	330588	16				
$R^2 = 0.99$				$Adj.R^2 = 0.98$		
$Pred.R^2 = 0.95$				$Adeq.Precision = 39.11$		

Table 4.7: ANOVA analysis for Static temperature model for the DJ2700 gun.

Source	Sum of squares	DF	Mean squares	F value	$prob > F$	
Model	2.43	2	1.22	61.90	< 0.0001	significant
A (Equivalence ratio)	2.12	1	2.12	107.82	< 0.0001	
D-Air flow	0.32	1	0.32	15.97	0.0005	
Residual	0.51	26	0.020			
Cor Total	2.94	28				
$R^2 = 0.83$				$Adj.R^2 = 0.81$		
$Pred.R^2 = 0.76$				$Adeq.Precision = 25.81$		

The final mathematical models, in terms of the coded parameters derived for this response are as follows;

For the DJ1050 the maximum static temperature coded is:

$$GT_{max} = 3500 - 62 * A + 12.5 * B + 25 * A * B - 262 * A^2 \tag{4.5}$$

where A is the coded equivalence ratio and B the coded spray distance, both having minimum and maximum coded values of -1 and +1 respectively.

In terms of the maximum actual static temperature:

$$GT_{max} = 1358 + 425 * \phi - 2.78SD + 2.85 * \phi * SD - 2142 * \phi^2 \tag{4.6}$$

For the DJ2700, the models were as follows;

In terms of the coded variables,

$$GT_{max} = 3553 - 110 * A + 45.83 * B + 52.5 * D + 200 * A * D - 290 * A^2 - 184 * B^2 \tag{4.7}$$

where A is the coded equivalence ratio and B the coded spray distance and D is the air flow rate.

and in terms of the actual parameters:

$$\begin{aligned} GT_{max} = 770 - 3491 * \phi + 78 * SD - 17.28 * AirFlow \\ +22.86 * \phi * SD + 16 * \phi * AirFlow - 2373 * \phi^2 - 0.295 * SD^2 \end{aligned} \tag{4.8}$$

Based on coded results for DJ1050: $-A^2 >> -A > A * B$; equivalence ratio has both a squared (A^2) and single (A) negative effect on temperature. For DJ2700: $-A^2 > A * D > -B^2 > -AA >> D > B$ after negative equivalence ratio squared, the interaction of this with air flow followed by negative spray distance squared interactions affect the temperature. The DOE explains their complex interactions to allow interpretation of the results.

It was deduced that from the models of the DJ1050, the spray distance had a linear mathematical relation with the gas temperature while the equivalence ratio has a quadratic one in terms of both coded and actual variables. As for the DJ2700, both the equivalence ratio and the spray distance were linear and quadratic relation with this response in terms of both coded and actual variables of the models. Finally the effect of air flow in the case of DJ2700 had a linear relation with the the response.

The validity of the models were also statistically assisted through the assumption of the

normality of the residuals and the difference between the actual and predicted values for both cases as in. However, for brevity the plots for the DJ1050 was only given in the thesis as in Figure 4.14 but the same results was observed for the DJ2700 gun. The relationship was linear for the residuals and the difference between the predicted and actual values were minimal which is validated within the ANOVA table methodology. Similar relations were observed for the residuals and the difference between the actual and predicted values plots for the DJ2700, which also justified the application of ANOVA analysis.

In the next discussion, the analysis of the perturbation and interaction plots for the both cases are given. It should be noted that the Air flow was just included in the case of the DJ2700 only. The approach was followed based on the geometrical design of both guns since the air is included the flow in the DJ2700 and to investigate the effect of air on the combustion modelling especially on the reaction modelling.

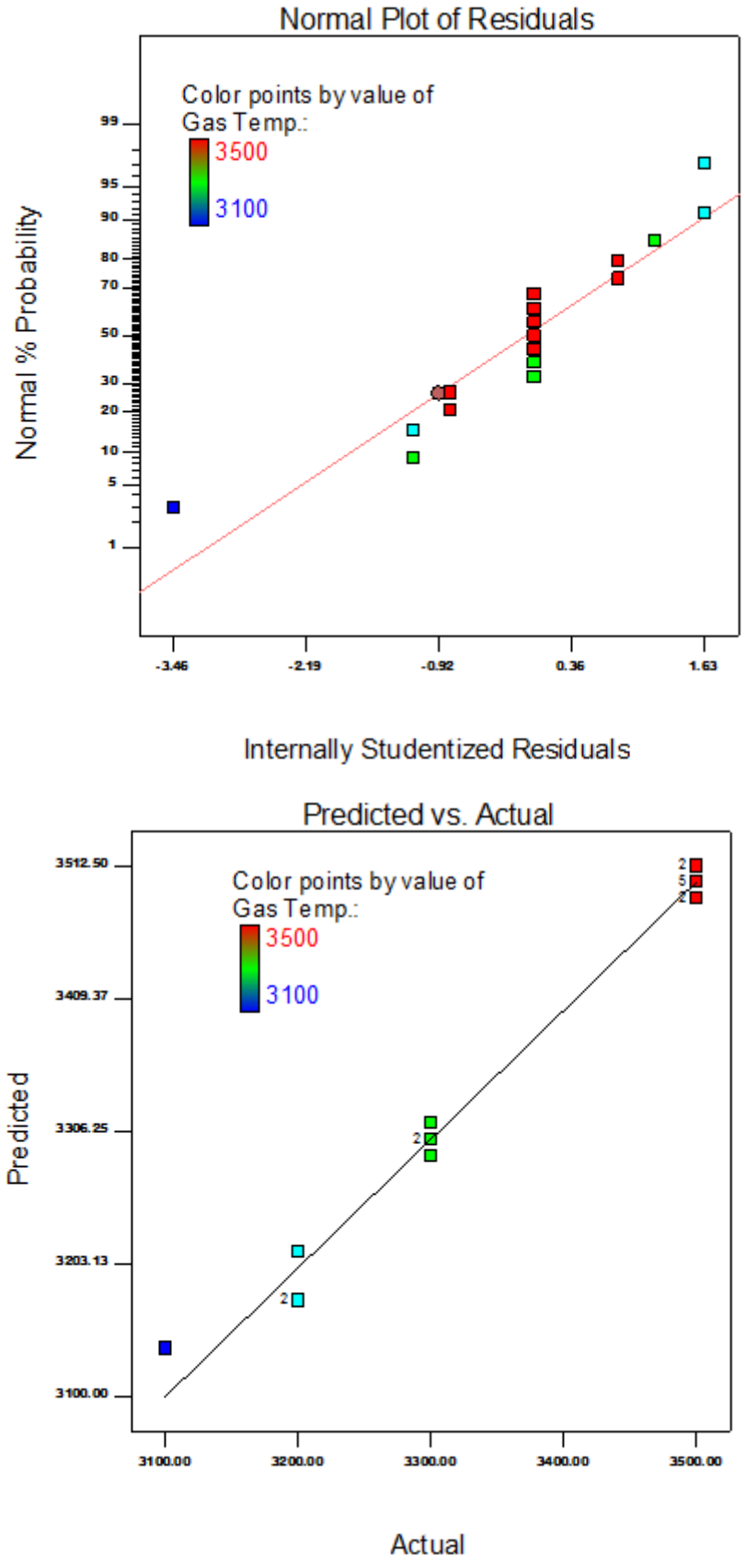

Figure 4.14: Normal plot and predicted vs actual values for gas temperature response in the DJ1050 gun

The perturbation plot Figure 4.15 shows the effect of the equivalence ratio and spray distance on the response of the temperature for the case of DJ1050. It was noticed that the behaviour of the temperature took the form of a parabolic profile ($-A^2 and - A$ effect) which is in an agreement with the temperature behaviour in most of the combustion of the hydrocarbon fuel as was discussed in Figure 2.10 [56]. As the equivalence ratio increases, the gas temperature increased up to an inflection point of around 3500 K at around the stoichiometric ratio and then decreased dramatically with further increasing the equivalence ratio. On the other hand, increasing the spray distance had a slight effect on the temperature response. The temperature increased marginally as the spray distance increased in the range between 150 to 200 mm, which might indicate that the spray distance in the range under investigation (150 to 200 mm) had a marginal effect on the temperature response.

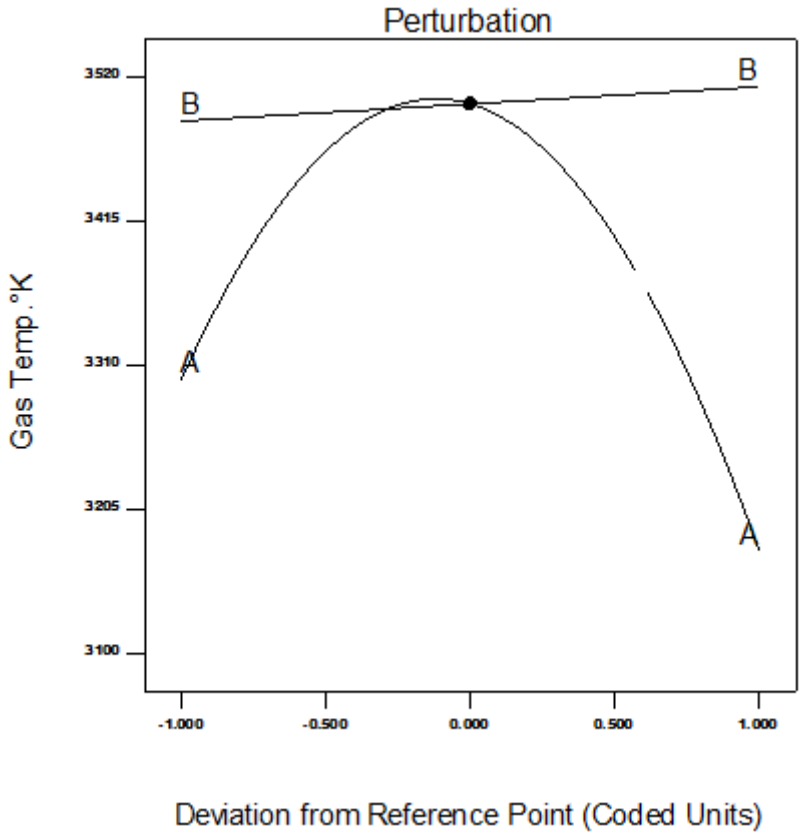

Figure 4.15: Perturbation plot showing the effect of the A = equivalence ratio and B = spray distance on the maximum attainable gas temperature for the DJ1050 gun

The effect of the equivalence ratio and the spray distance on the temperature response can be further depicted via the contour plot of Figure 4.16, in which the temperature changed between 3100 and 3500 K and it peaked (3495 K) around the stoichiometric ratio as the

equivalence ratio was increased from 0.8 to 1.5. The contour also shows the marginal effect of the spray distance in the range of 150 to 200 mm on the gas temperature response.

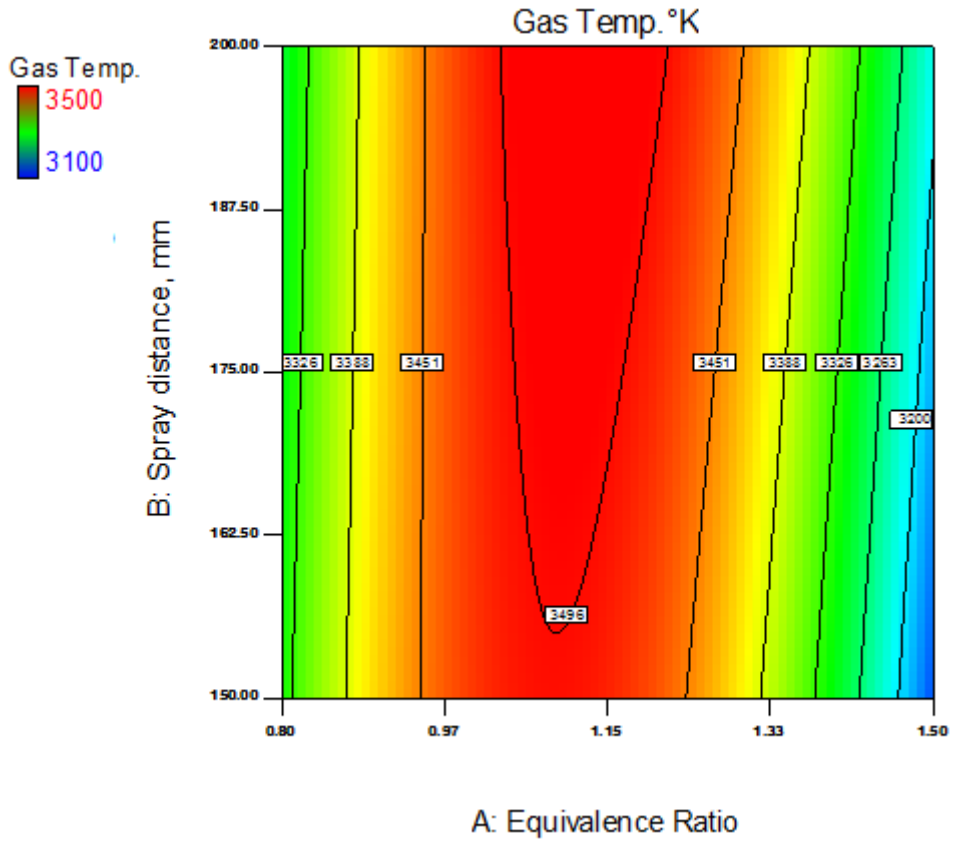

Figure 4.16: Temperature contour showing the relationship between the spray distance and equivalence ratio for the DJ1050 gun

The equivalence ratio effect was noticeable when the spray distance was 150 mm, such that the equivalence ratio of 0.8 and 1.5 corresponded to a temperature of around 3300 K and 3150 K, respectively while became less significant when a 200 mm spray distance was applied as the temperature changed between 3200 and 3300 respectively, as shown in Figure 4.17. No physical meaning could be deduced from such an interaction, but it could be attributed to the computational aspects since the computational calculation of the static temperature might be affected when changing the computational domain of static temperature, however as the difference in temperature corresponding to the two levels of interactions was slight, the difference of two interaction levels could be only attributed to the equivalence ratio.

In the next discussion, the DOE results for the DJ2700 are presented. As mentioned the effect of the air flow rate was added in the computational modelling for this case, as a

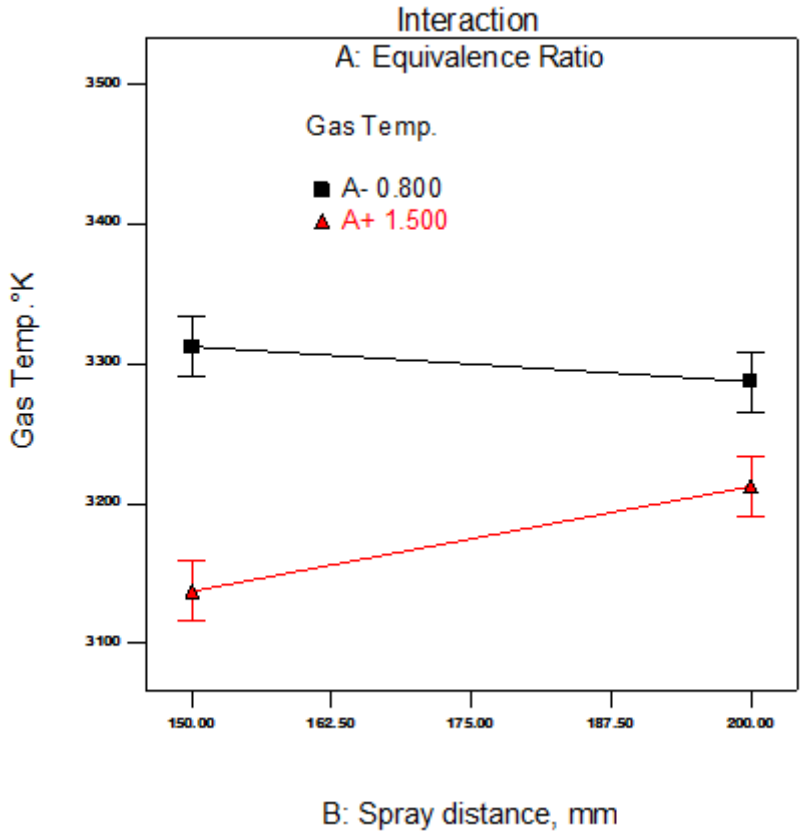

Figure 4.17: Interaction plot of the temperature with the spray distance and the equivalence ratio for DJ1050. (A = the equivalence ratio)

result of geometrical aspect of design of the nozzle and the inclusion of air flow in the process in the flow domain. The parabolic quantitative behaviour (given by the $-A^2$ and $-B^2$ in the coded equation) of the temperature versus the equivalence ratio was also observed in the case of the DJ2700, the only noticeable difference was that the range of the temperature was narrower. The temperature peaked at around the equivalence ratio of 1 as in the case of the DJ1050.

In addition, the temperature behaviour was of a parabolic form as the spray distance increased from 150 to 200 mm, but still the variation of the temperature versus the spray distance was over a narrow range as can be seen in Figure 4.18. The effect of air flow on the temperature response was found to be of minimal effect as the temperature variation was over a narrow range of almost less than 50 K as the air flow rate was changed from 250 to 300 SLPM. The effect of air flow on the temperature in this study was in a good agreement with the results of a key previous study by modelling HVOF process of Gu et al. [102]. The reason might be attributed to reaction of air with the flame, or fuel in the

computational domain. Figure 4.19 depicts a contour plot that shows the effect of spray distance and equivalence ratio on the temperature response. A peak temperature at $\phi = 1$ and spray distance of 175 mm is formed to yield a gas temperature of 2580 K.

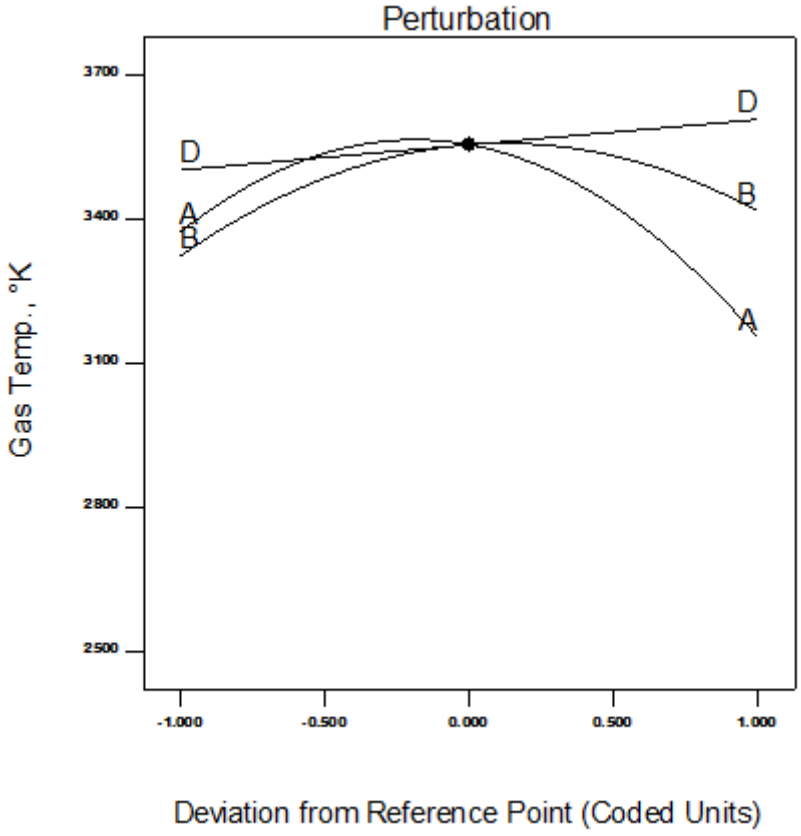

Figure 4.18: Perturbation plot showing the effect of A = equivalence ratio, B = spray distance and D = air flow rate on the gas temperature response for DJ2700

Figure 4.20 shows the interaction plot ($-A^2$ in the coded equation) between the equivalence ratio and the spray distance on the gas temperature. It is evident that at an equivalence ratio of 1.5, there is a difference between the two levels of the spray distance (150 to 200 mm) on the gas temperature, applying a spray distance of 200 mm would result in a higher temperature at a fuel-rich condition ($\phi > 1$) which corresponds to 1.5 on the plot, while applying 150 mm spray distance would result in a higher temperature in the case of fuel lean ($\phi < 1$) condition. It was noticed that the difference in the temperature is greater in case of the fuel rich condition than in the fuel lean condition, which supports findings by Gu et al. [102], however at 200 mm it has the opposite effect.

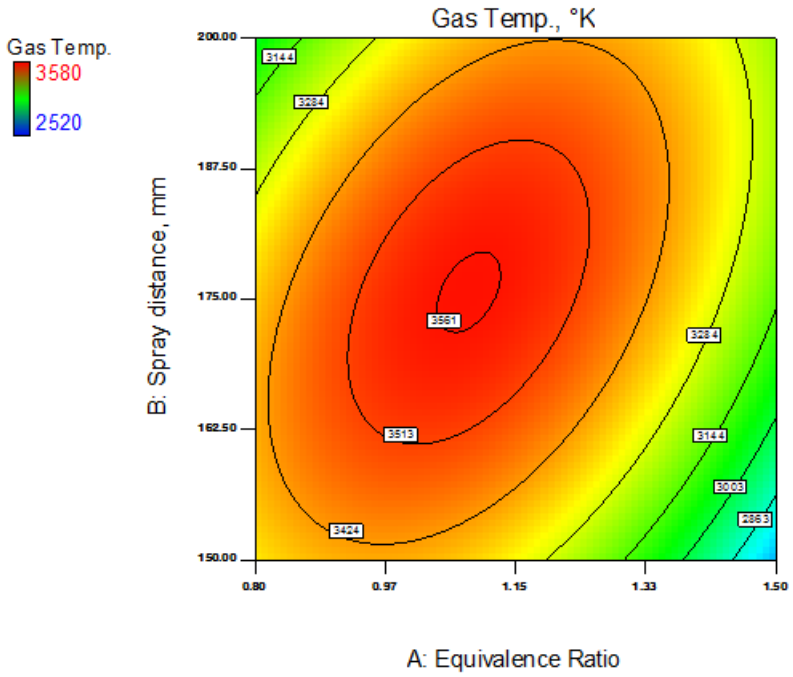

Figure 4.19: Contour plot of the gas temperature response vs the spray distance and the equivalence ratio for DJ2700

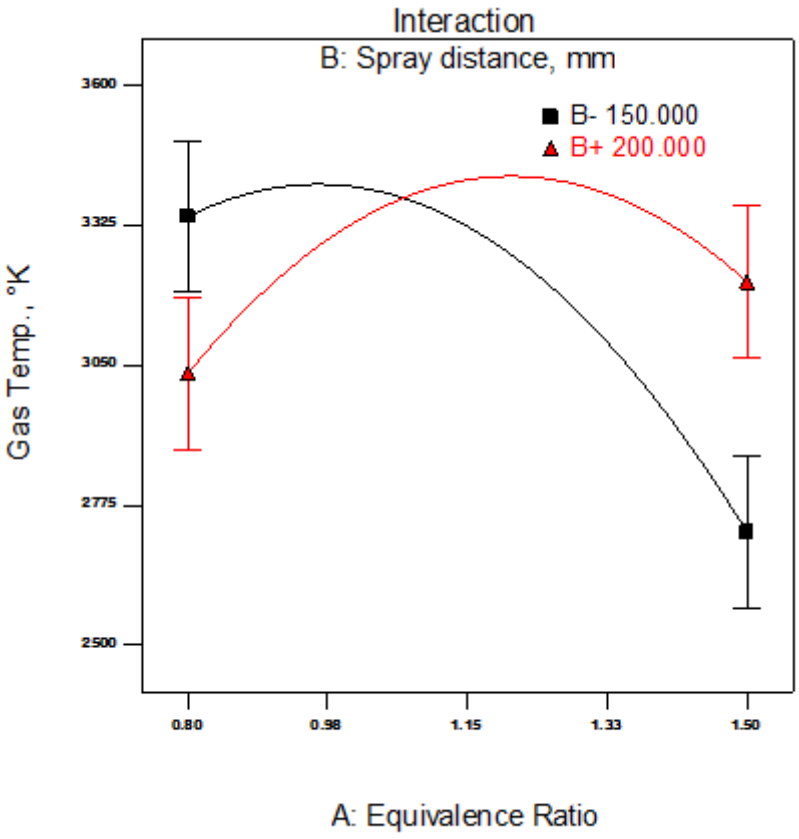

Figure 4.20: Interaction plot of the temperature with spray distance and equivalence ratio of DJ1050: A = the equivalence ratio, B = spray distance, D = air flow

The interaction ($-A^2 > A * D > -B^2$ in the coded equation) between equivalence ratio the air flow on the gas temperature is shown in Figure 4.21. It is evident that at an equivalence ratio of 1.5 there is statistically considerable difference between the two levels of the air flow (250 and 300 SLPM) on the gas temperature. Applying an air flow rate of 300 SLPM would result in a higher temperature and this is due to the fact that the excess air would react with the excess fuel in the case of the fuel-rich mixture (supported by Equation 2.27 and x tending towards a value of 16.7) according to Li et al. [18–20, 66], while applying an equivalence ratio of 0.8 the excess air would act as a coolant or reduce the combustion temperature. However, in the case of applying an equivalence ratio of 0.8 the difference between the two levels of air flow and the gas temperature is less significant. Finally, at around the stoichiometric ratio ($\phi = 1$) both levels of air flow had the same effect on the gas temperature.

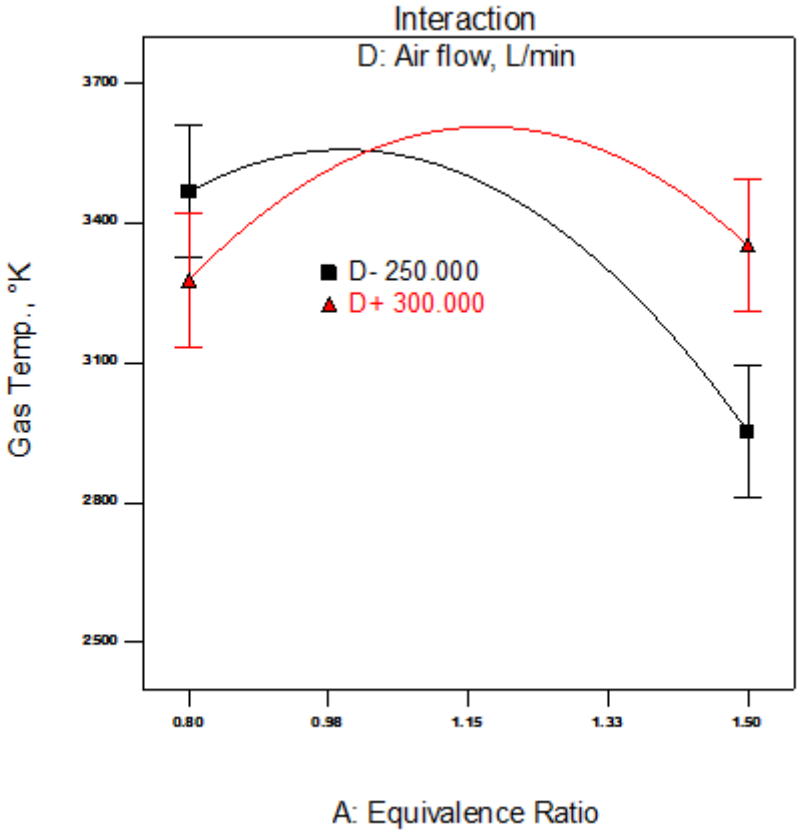

Figure 4.21: Interaction plot of temperature with spray distance and equivalence ratio for DJ2700: A = the equivalence ratio and D = air flow

4.4 Gas Velocity

As with the gas static pressure and static temperature, the CFD calculation for gas velocity was applied to both guns under investigation. The velocity of the combustible jet or the flame is considered as important as the temperature, since it is the physical quantity that affects the momentum transfer between the continuum and the particle. The main difference between the two cases is the compressibility behaviour and sonic condition developed at two different locations within each geometry.

4.4.1 CFD Results of Gas Velocity

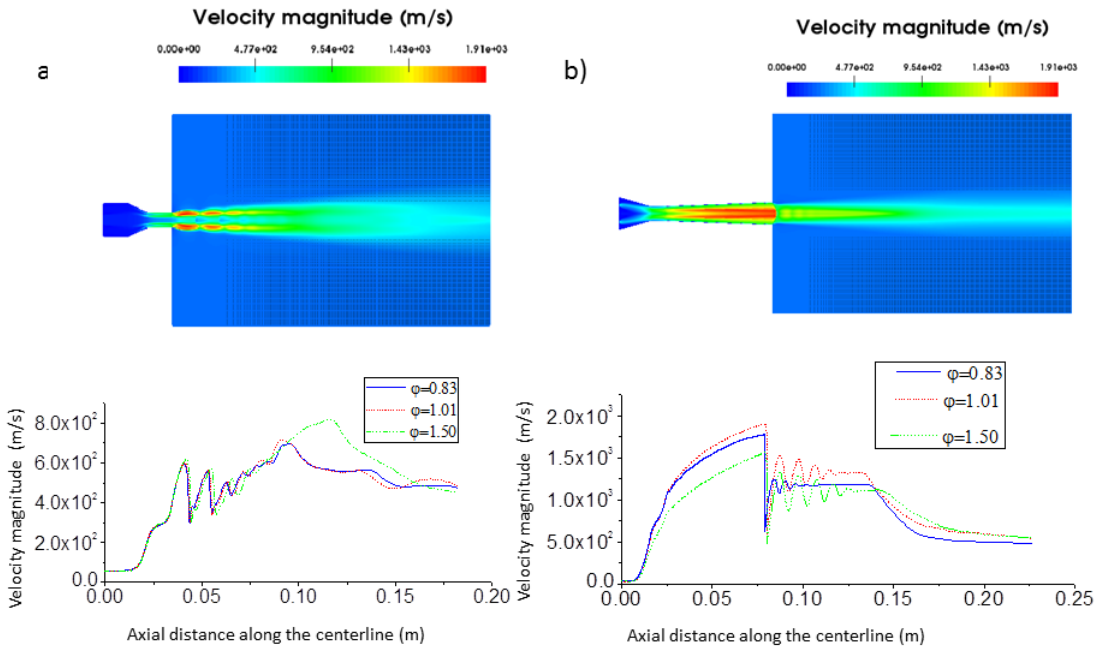

Figure 4.22: Contour of velocity magnitude and its profile along the centerline for a): DJ1050 and b): DJ2700, the contours are for the case of $\phi = 1.01$ for both guns

For the DJ1050 gun the sonic condition occurred at the nozzle exit, while for the DJ2700 it occurred at the nozzle throat, which corresponds to the minimum area = 0.024 m^2 along the nozzle. The flow was supersonic at the diverging part of the DJ2700 nozzle while it was supersonic at the outer domain exactly from the beginning of the nozzle exit before reducing

down to subsonic condition Figure 4.22

The nitrogen flow had a significant effect on the velocity behaviour in the case of DJ1050 since the inlet diameter was about 5 mm, while it was only 1.5 mm in the case of DJ2700, supported by Gu et al. [102]. It was noticed that the nitrogen flow caused a reduction in the flow velocity magnitude along the centerline of the jet, creating areas of low velocity zones between repeating high velocity zones of the jet before the jet velocity reduced back to the subsonic condition. In the DJ2700 gun, the flow initiated its supersonic behaviour at the nozzle throat, expands supersonically, during which the velocity magnitude becomes almost uniform over the diverging section, and therefore a Mach disk develops at the exit of the nozzle, which corresponds the sharp shock wave at the nozzle exit. Shock waves developed prior to the flow velocity reduced back to its subsonic condition.

4.4.2 DOE Results of Gas Velocity

Like before, (pressure and temperature) statistical methodology was applied to the maximum velocity magnitude, calculated by CFD modelling, regardless of the velocity vector field over the computational domain. The general trend in thermal spray coating industry is toward increasing the velocity of particle to minimize the porosity within the resultant coating, the maximum velocity achievable by the jet can be taken as an indication to satisfy this general aim. Table 4.8 and Table 4.9 provide the ANOVA or regression analysis of the velocity response for both the DJ1050 and DJ2700 guns, respectively. Both tables show adequate relations between the parameters considered since the adequacy measures are within the acceptable ranges (as discussed within the previous responses of pressure and temperature).

Mathematical models developed by the statistical analysis for the velocity response are as follows;

In terms of the coded variables for DJ1050:

maximum gas velocity magnitude:

Table 4.8: ANOVA analysis for gas velocity response model for the DJ1050 gun.

Source	Sum of squares	DF	Mean squares	F value	$prob > F$	
Model	6564	3	2188	150	< 0.0001	significant
A (Equivalence ratio)	200	1	200	13	< 0.0001	
A^2	6314	1	6314	434		
Residual	189	13	14.25			
Cor Total	6752	16				
$R^2 = 0.97$				$Adj.R^2 = 0.96$		
$Pred.R^2 = 0.94$				$Adeq.Precision = 26.29$		

Table 4.9: ANOVA analysis for gas velocity response model for the DJ2700 gun.

Source	Sum of squares	DF	Mean squares	F value	$prob > F$	
Model	154795	6	25799	4041	< 0.0001	significant
A (Equivalence ratio)	81675	1	81675	1280	< 0.0001	
C-Particle size	75	1	75	1.17	0.0005	
D-Air flow	833	1	833	13	0.0015	
AC	225	1	225	3.52	0.0738	
A^2	71632	1	225	71632	1122	
C^2	326	1	326	5.11	0.0340	
Residual	1404	22	63			
Cor Total	156200	28				
$R^2 = 0.99$				$Adj.R^2 = 0.98$		
$Pred.R^2 = 0.97$				$Adeq.Precision = 53.39$		

$$GV_{max} = 1901 + 5 * A - 2.5B - 38.6 * A^2 \tag{4.9}$$

where A is the coded equivalence ratio, B the coded spray distance, at maximum and minimum values of -1 and +1 respectively. The effect of all parameters can be ordered as follows: $-A >> A > -B$

In terms of the actual parameters or variables

$$GV_{max} = 1485 + 739 * \phi - 0.1 * SD - 315\phi^2 \tag{4.10}$$

For the DJ2700 gun, in terms of the coded variables the mathematical model of regression analysis is:

For maximum gas velocity magnitude:

$$GV_{max} = 1895 - 82.5 * A - 2.5C + 8.3 * D - 7.5 * A * C - 101.8 * A^2 - 6.8 * C^2 \quad (4.11)$$

where A, C and D are the coded (-1 to +1), equivalence ratio, particle size and air flow respectively. The effect of each parameters can be ordered as follows $-A^2 > -A >> D > -A * C > -C^2 > C$.

In terms of the actual parameters:

$$GV_{max} = 936 + 1703 * \phi + 1.96 * PS + 0.33 * AirFlow - 1.071 * \phi * PS - 831 * \phi^2 - 0.017 * PS^2 \quad (4.12)$$

The statistically developed models were validated based on the same analysis applied to the previous responses as can be seen in Figure 4.23, for the DJ1050. gun. The same was observed for the DJ2700 gun, but for brevity was not included in the thesis.

For the DJ1050, the quantitative relation developed by the regression analysis showed that the most effective factor on the gas velocity response was the equivalence ratio since the gas velocity had a negative proportional relation with the square of equivalence ratio (A^2). The same quantitative relation between the gas velocity and the equivalence ratio ($-A^2$) was observed for the DJ2700, but the particle size showed a relation to the gas velocity in addition. This relation could have a statistical meaning but not computational since the CFD model was assumed to be one way coupling multi-phase flow, which means that the particle modelling calculation or discrete phase does not influence the continuum field of the flow.

The velocity magnitude response increased with increasing the equivalence ratio up to an inflection point at around the stoichiometric ratio before decreasing again with further increasing of the equivalence ratio (Figure 4.24).

The same quantitative pattern was observed for the temperature response too. It could be concluded that the velocity and temperature of the flow had the same relation with the

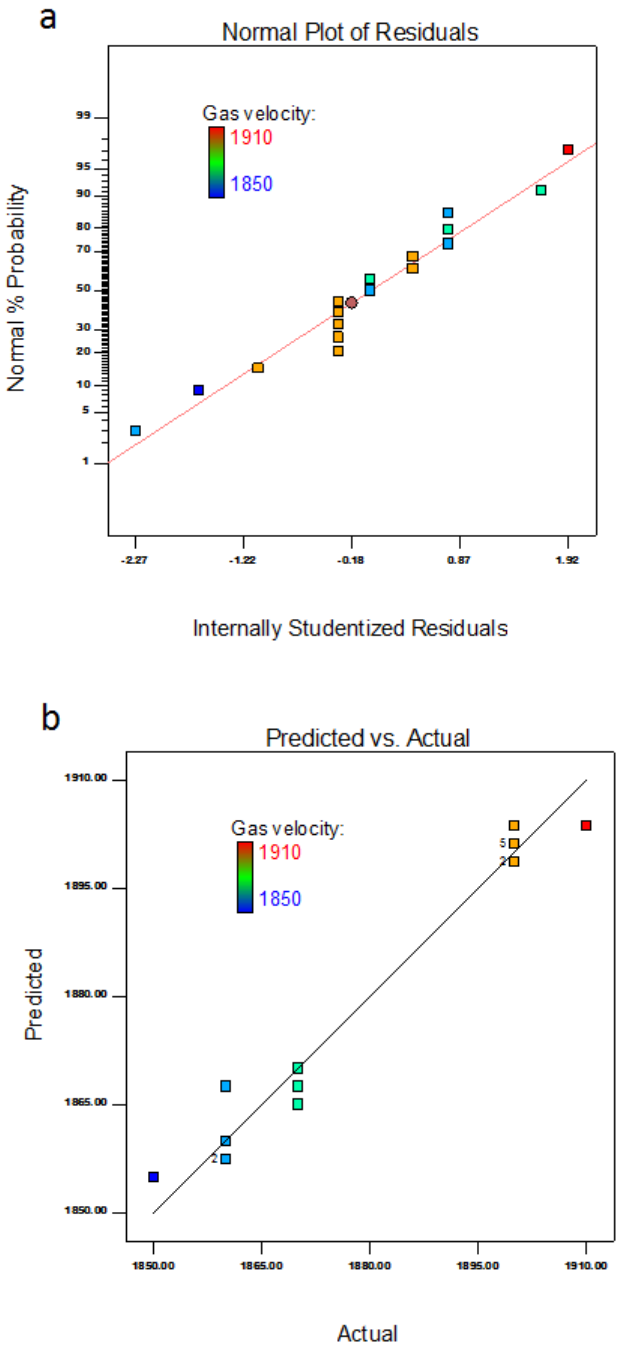

Figure 4.23: Normal plot residuals (a) and difference between actual and predicted values (b) for the gas velocity response for DJ1050

equivalence ratio parameter. The spray distance range under investigation in this study, decreased the velocity response slightly as it was increased. It could be recommended that increasing the spray distance beyond the upper limit of this range (200 mm) is desirable.

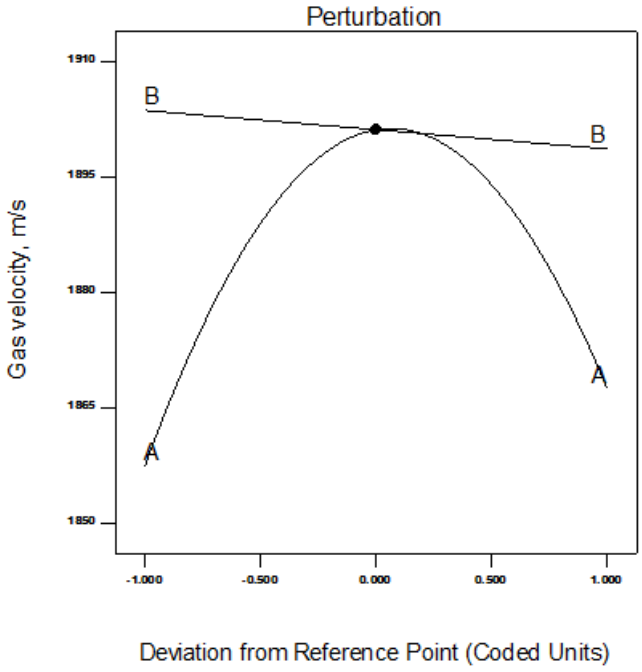

Figure 4.24: Perturbation plot for velocity response for DJ1050; A = equivalence ratio and B = spray distance

Figure 4.25 is a contour plot that shows the maximum velocity (1900 m/s) just over the stoichiometric ratio (fuel rich $\phi > 1$) and a dominant effect of this parameter on the velocity of the jet in contrary to the minimal influence of the spray distance on the same response, as fuel-richness provided more power but less efficiency. Within Figure 4.26 perturbation plot for the DJ2700 gun, the most noticeable observation was that the considered range of the spray distance had no influence on the velocity response of the jet. The equivalence ratio was still the most dominant parameter, that affected the velocity response, the only difference was that the velocity increased slightly as the equivalence ratio was increased up to an inflection point and then decreased sharply as the equivalence ratio increased further toward the upper limit of 1.5. The particle showed a statistical influence on the gas velocity in this case but it was indeed negligible and could be attributed only to the statistical calculation not to any physical or realistic calculation. Since an one way coupling approach was adopted in the CFD modelling, the air flow effect was still negligible as increasing the air flow rate resulted in a slight increase in the velocity response. This marginal effect on the velocity of the jet was even concluded by the previous study of modelling HVOF such as Li et al. [18].

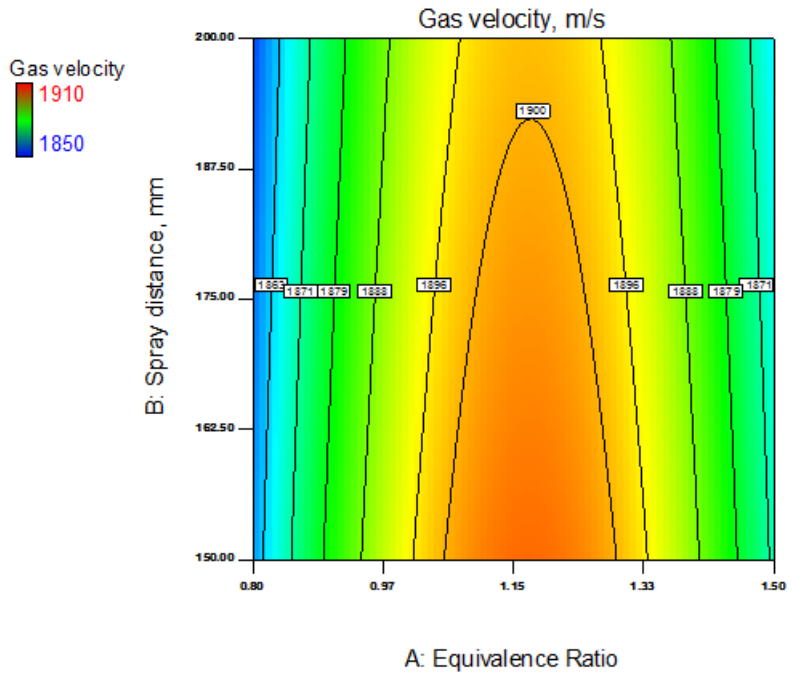

Figure 4.25: Contour plot of the velocity response for the DJ1050

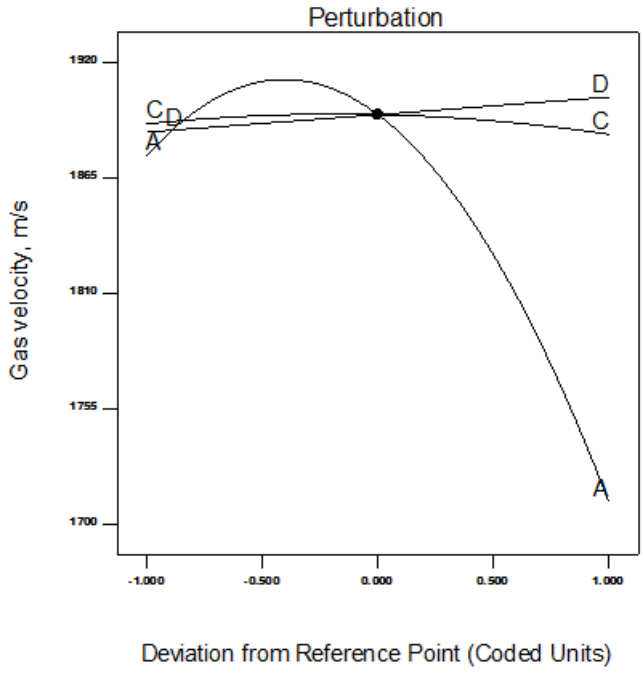

Figure 4.26: Perturbation plot of DJ2700; D = air flow, A = equivalence ratio, C = particle size

4.5 Particle Temperature and Velocity

4.5.1 CFD Results

Particle thermal and dynamic behaviour is the most crucial physics within the HVOF process, since the coating quality is totally dependent on the particle physical state upon impact of the substrate. Hence particle temperature and velocity can be considered as the most important parameters influencing HVOF coating. It is desirable to heat the particle to a molten or semi-molten state and accelerate it to a high velocity possible impact a surface with enough kinetic and thermal energy to mechanically adhere the particle to the asperities of the substrate. One of the main critical parameter that affect the temperature and velocity of the particle is its size. The size range of 5 to 45 μm is commonly used in the HVOF industry, one related to the nanostructured size powders and the other respective to micro sized powders. WC-12%Co was the material chosen in this study due to the fact that it is one of most commonly used material in the industry for many different industrial applications.

Figure 4.27 and Figure 4.28 are the particle temperature profiles along the centerline of the nozzle for the DJ1050 and DJ2700. It can be seen that particles of 5 μm, in both cases, attained higher temperatures than the other two sizes. In general it was concluded that the larger the size of the particles the less heat it could gain from the flame. The same results were concluded in one of the key publication on the modelling of HVOF process by Li et al. [66]. The most important difference between the particle thermal behaviour in the two nozzle geometries was that in case of DJ2700 the particles of all sizes achieved higher temperatures than in the case of DJ1050, which can be considered a remarkable advantage of the DJ2700 nozzle design. However, over heating can lead to recrystallization of the powder, forming new phases or even decarburization which can result in a poor coating.

Only particles of 5 μm were able to reach a fully molten state since the melting temperature of cobalt is 1768 K within WC-12%Co. Therefore the DJ1050 gun can melt the cobalt binder but protect the WC phase as WC melting temp is approximately 3000 K. The DJ2700 gun at 5 μ m could cause recrystallization but should be safe at 2350 K maximum temperature.

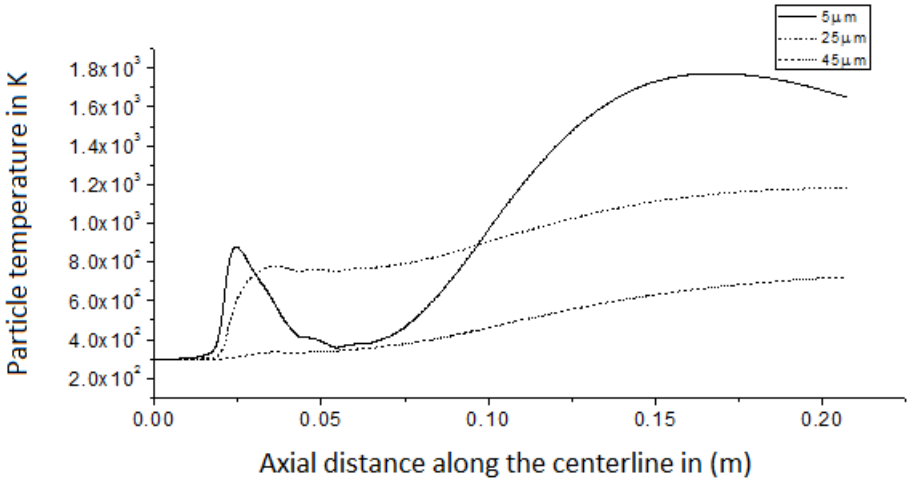

Figure 4.27: Particle temperature profile for three particle sizes along the centerline of the nozzle for DJ1050

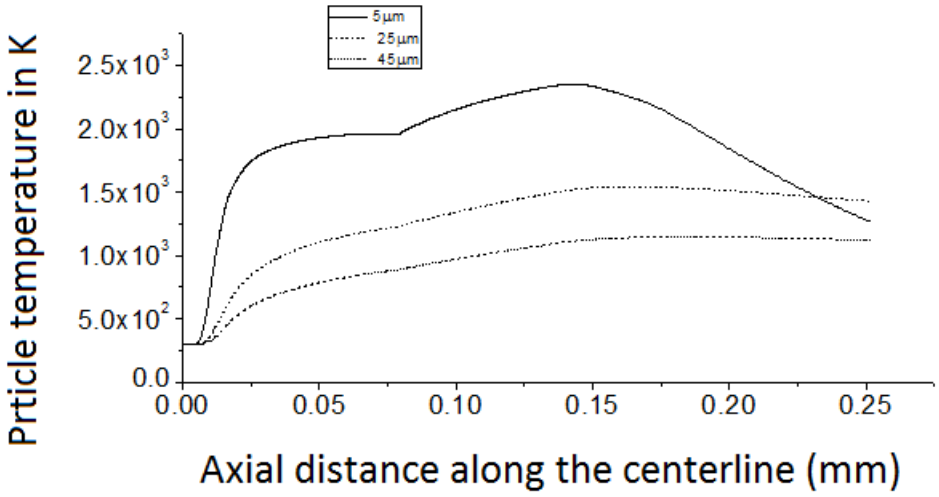

Figure 4.28: Particle temperature profile for three particle sizes along the centerline of the nozzle for DJ2700

Particle velocity was also observed to be significantly dependent on the particle's size in the same manner as the particle temperature. Such that, if the particle size increased the particle had more sluggish or slow dynamic response to the flow, and small size particles had higher velocities as shown in Figure 4.29 and Figure 4.30, which supports the finding by Yang and Eidelman [103].

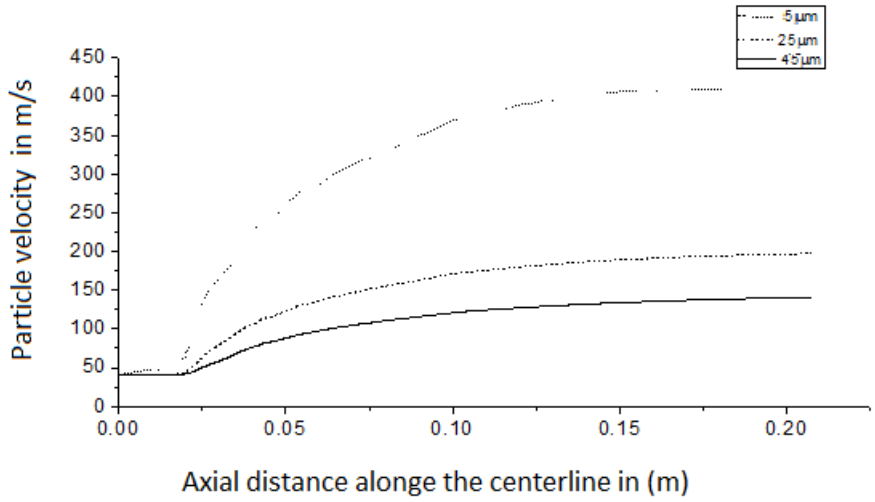

Figure 4.29: Particle velocity profile for three particle sizes along the centerline of the nozzle for DJ1050

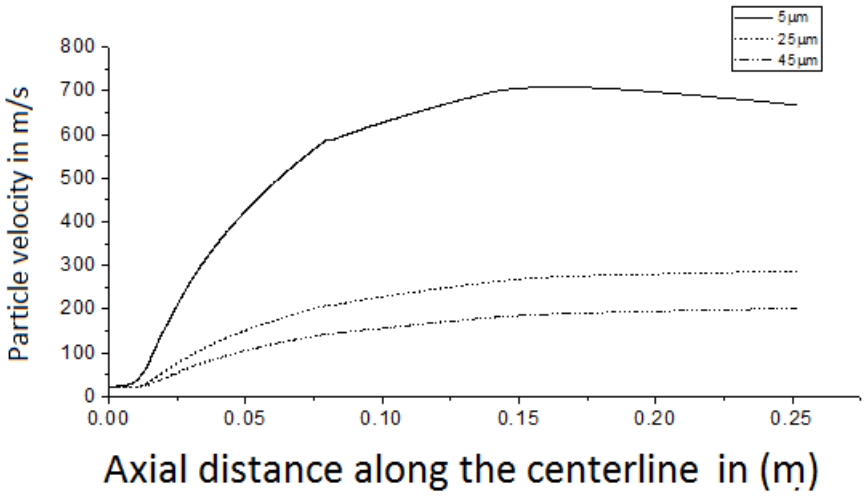

Figure 4.30: Particle velocity profile for three particle sizes along the centerline of the nozzle for DJ2700

4.5.2 DOE Results of Particle Temperature

Having validated the CFD model via the measurement of particle temperature for DJ2700 (as was shown in (Figure 4.1). The DOE technique was applied to the particle range of 5 μm to 45 μm in order to derive quantitative relations to show the effect of the process parameters and particle size on its thermal and dynamic behaviour. The range is chosen based on the size of the spray particle commonly used in the HVOF process. The ANOVA analysis is presented in Table 4.10 and Table 4.11 for both the DJ1050 and DJ2700 guns respectively.

Both tables showed adequate measures of R^2, $Adj.R^2$, $Pred.R^2$, and $Adeq.Precision$ and these were within adequate values.

Table 4.10: ANOVA analysis for particle temperature model for DJ1050.

Source	Sum of squares	DF	Mean squares	F value	$prob > F$	
Model	1000396	4	2500995	40	< 0.0001	significant
B-Spray distance	435	1	435	0.069	0.7959	
C-Particle size	878239	1	878239	141	< 0.0001	
BC	80968	1	80968	13	< 0.0001	
C^2	40753	1	40753	6.55	0.0250	
Residual	1404	12	63			
Cor Total	156200	16				
$R^2 = 0.93$				$Adj.R^2 = 0.90$		
$Pred.R^2 = 0.74$				$Adeq.Precision = 22.14$		

Table 4.11: ANOVA analysis for particle temperature model for DJ2700.

Source	Sum of squares	DF	Mean squares	F value	$prob > F$	
Model	476777	10	476777	20.51	< 0.0001	significant
A - Equivalence ratio	20740	1	20740	8.92	< 0.0001	
B - Spray distance	875723	1	87572	37.68	< 0.0001	
C - Particle size	12701	1	12701	5.46	< 0.0001	
D - Air flow	3954	1	3954	1.70	0.2085	
AC	55745	1	55745	24	0.0001	
BC	17820	1	17820	7.67	0.0126	
BD	13393	1	13393	5.76	0.0274	
B^2	41244	1	41244	106	< 0.0005	
C^2	247411	1	24741	106	< 0.0001	
D^2	18536	1	18536	7	0.0112	
Residual	41824	18	41824			
Cor Total	518601	16				
$R^2 = 0.91$				$Adj.R^2 = 0.87$		
$Pred.R^2 = 0.68$				$Adeq.Precision = 14.67$		

As with the previous responses, mathematical models were developed via regression analysis that correlate the responses to the process parameters. The mathematical model that correlate the process parameters to the particle temperature for DJ1050 took the form:

Coded form of maximum particle temperature at the substrate:

$$PT = 1170 - 7.37B - 331C + 142BC + 98C^2 \tag{4.13}$$

where B, C are the coded spray distance and the particle size within (-1 to +1) as before. The order of the effect can be shown to be $-C^2 >> B * C > C^2 >> -B$. In terms of the actual parameters or variables:

$$PT = 1170 - 7.40SD - 78.62PS + 0.28SD * PS + 0.24 * PS^2 \tag{4.14}$$

As for the DJ2700 gun, the same mathematical models for particle size in terms of the coded parameters was of the form for the particle temperature at the substrate:

$$PT = 1412 - 41.6A - 85.4B - 32.53C + 18D - 118AC + 57BD - 78B^2 - 191C^2 - 52D^2 \tag{4.15}$$

where A, B, C and D are the coded values of equivalence ratio, spray distance, particle size and air flow respectively in the range of -1 to +1. The effect order can be written as $-C^2 > -AC > -B > -B^2 > BD > -D^2 > -A > -B > -D$ and terms of the actual parameters or variables:

$$\begin{aligned} PT = -3945 + 302\phi + 11.6SD + 18PS + 30 * AF - 16\phi * PS + 0.133SD * PS \\ +0.09SD * AF - 0.12 * SD^2 - 0.47PS^2 - 0.08 * AF^2 \end{aligned} \tag{4.16}$$

The statistical analysis revealed that the spray distance had a slight effect on the particle temperature in case of the DJ1050, while the particle size ($-C$) was the only factor that affected the particle temperature response as shown (Figure 4.31). However, the influence of the spray distance on the particle temperature was better observed through the interaction plot in Figure 4.32.

It was concluded that at a particle size of 5 μm spraying at a distance of 200 mm resutls in a reduced particle temperature, however, compared to that of 45 μm sprayed at

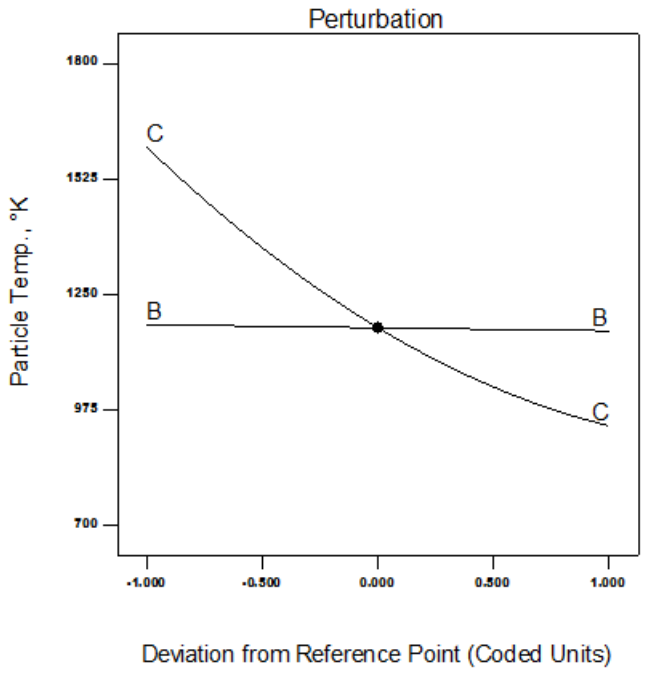

Figure 4.31: Perturbation plot for particle temperature response; C = particle size and B = spray distance for DJ1050

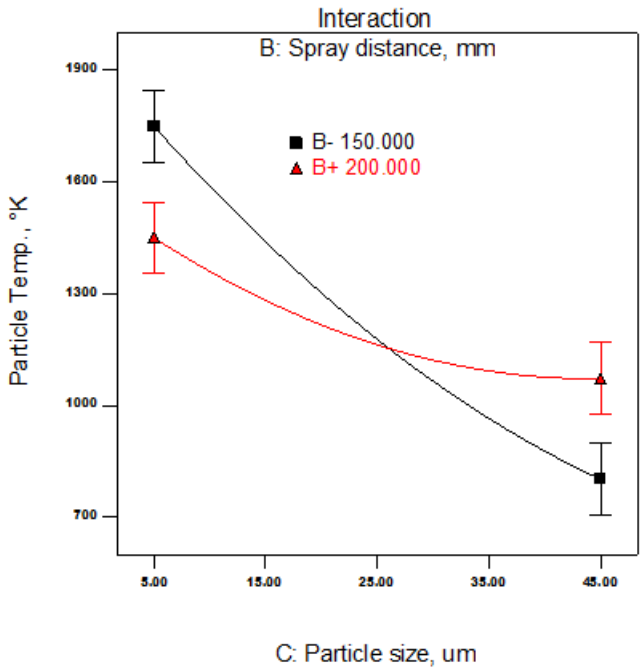

Figure 4.32: Interaction of the particle temperature response with particle size and spray distance

equivelant distance, the 5 μm particles retain a higher particle temperature. The reason is due to the difference in the thermal response of the particle, which is considerably affected by the particle size [100]. Such that particle of smaller size has rapid change in its thermal

behaviour. It was also revealed that at around 25 μm particle size, both of the spray distance had the same effect on the particle temperature.

On the other hand, there was an influence of each process parameters on the particle temperature in the case of the DJ2700. But the most influential factor was found to be the negative square of the particle size ($-C^2$), followed by the negative interaction of spray distance and the equivalence ratio($-AC$), the negative of the spray distance ($-B$), the negative of the square of the spray distance ($-B^2$), the negative interaction of the spray distance and the air flow ($-BD$), the negative interaction of the air flow ($-D^2$), the negative interaction of the equivalence ratio($-A$), the negative interaction of the spray distance ($-B$), and finally, the negative interaction of the air flow ($-D$).

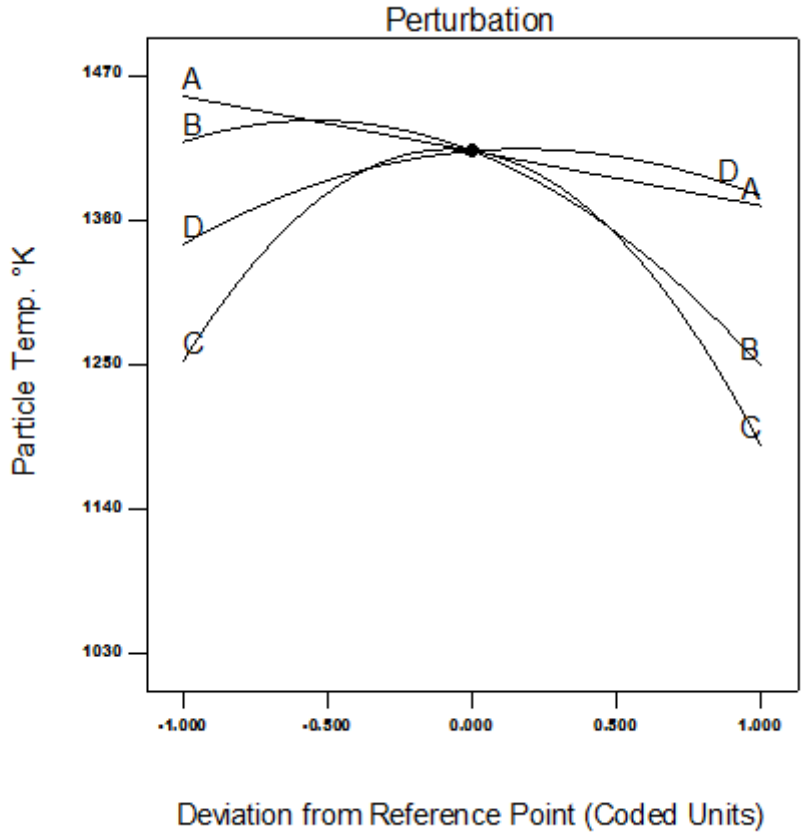

Figure 4.33: Perturbation plot for particle temperature response; C = particle size , B = spray distance, A = equivalence ratio and D = air flow rate for DJ2700

It can be seen from the perturbation plot of the individual factors in Figure 4.33, for the DJ2700 that as the particle size was increased the particle temperature increased up to a maximum point and decreased for further increasing in particle size. As for the spray

distance, it was obvious that the relationship was inversely proportional, such that as the spray distance increased, the particle size decreased over all the ranges of the spray distance. As the equivalence ratio increased the particle temperature decreased, but over a narrow range of temperature. The air flow had a quite similar influence of the particle size, but its temperature variation was marginal.

4.5.3 DOE Results of Particle Velocity

The final results of this study were those associated to the particle velocity response at substrate distance. The DOE methodology adopted in this study was applied to the particle velocity at the location of the substrate. As the case with the temperature, the location was chosen due to the importance of the particle velocity at the point of impact. The particle deforms kinetically under the influence of the momentum transfer due the gas dynamics. The particles can be even sprayed without a heat source under the influence of the high velocity and the high kinetic energy, gained from the high velocity of the gas such as in cold spray coating, normally not suitable for WC−Co however. The velocity of the particle is a main factor in reducing the porosity of the coating, since the particle can mechanically adhere to the surface via the adiabatic shear stresses due to the velocity.

Table 4.12 and Table 4.13 show the associated ANOVA tables for the particle response for DJ1050 and DJ2700 respectively. As per the other previous responses, the adequacy measures showed reasonable statistical values. The mathematical model which correlates the process parameters involving particle velocity for DJ1050 at the substrate distance location took the form:

$$PV = 200 - 4.17B - 29.8B * C + 73.73C^2 \tag{4.17}$$

where B, C are the coded spray distance and particle size respectively within (-1 to 1). Order of the factors effect was $C^2 > BC >> B$.

In terms of the actual parameters or variables:

$$PV = 753 - 16SD - 25PS + 0.6SD * PS + 0.1PS^2 \tag{4.18}$$

Table 4.12: ANOVA analysis for particle velocity response model for DJ1050.

Source	Sum of squares	DF	Mean squares	F value	$prob > F$	
Model	139507	4	34876	161	< 0.0001	significant
B-Spray distance	139	1	139	0.64	0.4382	
C-Particle size	3556	1	3556	16.43	< 0.0001	
BC	80968	1	80968	13	0.0016	
C^2	23028	1	23028	106	< 0.0001	
Residual	2596	12	216			
Cor Total	142104	16				
$R^2 = 0.98$				$Adj.R^2 = 0.97$		
$Pred.R^2 = 0.92$				$Adeq.Precision = 37.23$		

For the DJ2700, the mathematical model in terms of the coded variables was of the form for particle temperature at the impact location:

$$PV = 282 + 27A - 182C - 123A * C + 113C^2 \tag{4.19}$$

where A, C are the coded equivalence ratio and the particle size within the same range of (-1 to +1). Effect of the variables took the order $-C > AC >> C^2 >> A$

In terms of the actual parameters or variables:

$$PV = 53 + 551\phi - 1.6PS - 19\phi * PS + 0.28PS^2 \tag{4.20}$$

Figure 4.34 is the perturbation plot for the particle velocity in the case of DJ1050. It was revealed that the square of particle size (C^2) is the most dominant factor affected the particle velocity in this case, and as the particle size was increased the particle velocity decreased, supported by Kamnis et al. [116] and Li et al. [18, 66].

From the interaction plot in Figure 4.35, it can be seen that if processing particles of 5

Table 4.13: ANOVA analysis for particle velocity response model for DJ2700.

Source	Sum of squares	DF	Mean squares	F value	$prob > F$	
Model	568149	4	142037	33.57	< 0.0001	significant
A-Equivalence ratio	9227	1	9227	2.18	0.1527	
C-Particle size	398052	1	398052	94.08	< 0.0001	
AC	69915	1	69915	16.52	0.0004	
C^2	90953	1	90953	21.49	< 0.0001	
Residual	101534	24	4230			
Cor Total	669684	28				
$R^2 = 0.84$				$Adj.R^2 = 0.82$		
$Pred.R^2 = 0.55$				$Adeq.Precision = 23.27$		

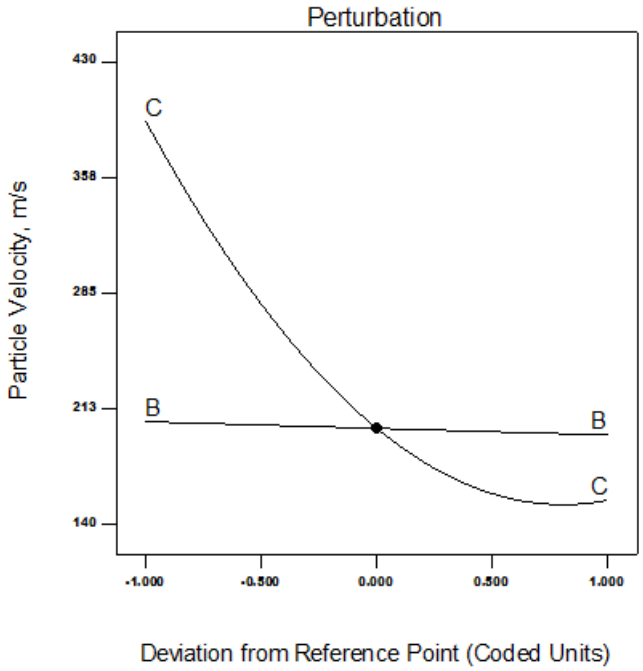

Figure 4.34: Perturbation plot for particle velocity response C = particle size and B = spray distance for DJ1050

μm the lowest level of the spray distance of 150 mm gives higher velocity, while in case of the 45 μm the higher level of spray distance of 200 mm gives a higher velocity. This could be attributed to the dynamic response of the particle which becomes more rapid as the particle size reduced. At a particle size of around 25 μm the spray distance levels does not have an effect on the particle velocity.

For DJ2700, the same results were found regarding the particle velocity relation to the particle size ($-C$). Increasing the equivalence ratio (A) had a negligible effect on the particle

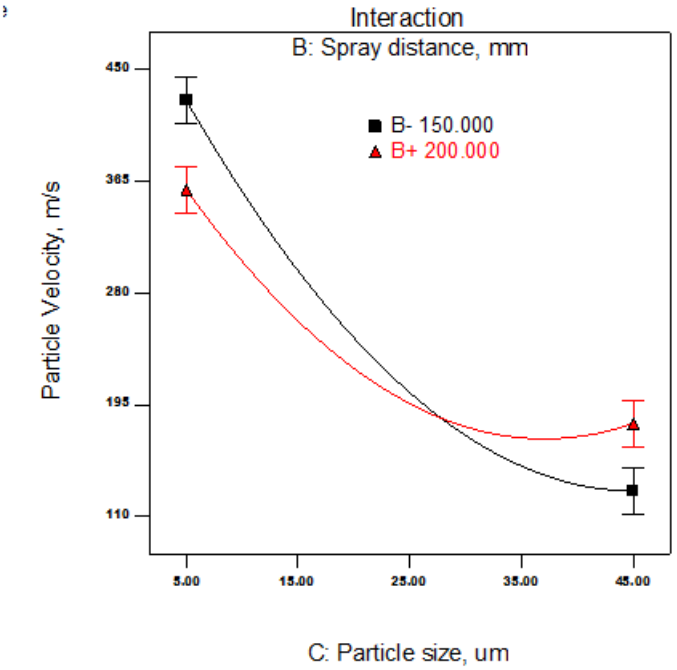

Figure 4.35: Interaction of the particle velocity response with the particle size and spray distance for DJ1050

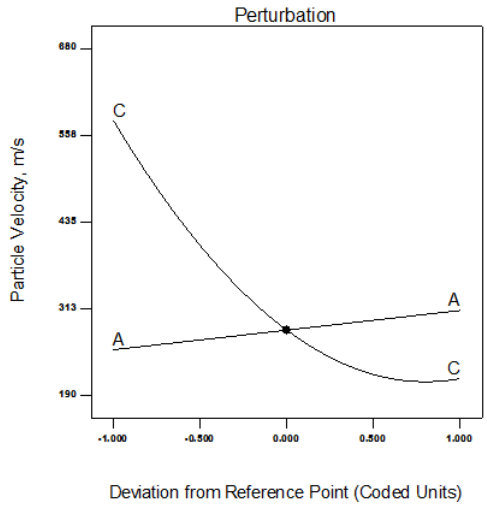

Figure 4.36: Perturbation plot for particle velocity response C = particle size and A = air flow rate for DJ2700

velocity as in Figure 4.36. From the interaction plot in Figure 4.37, that correlates particle velocity to the equivalence ratio and its size, It was concluded that when spraying 5 μm particles the equivalence ratio of the lowest level would give lower velocity. The opposite effect was found for spraying 45 μm particles, but the difference between the velocity levels was smaller. At around 30 μm the effect of equivalence ratio showed no difference in the velocity levels.

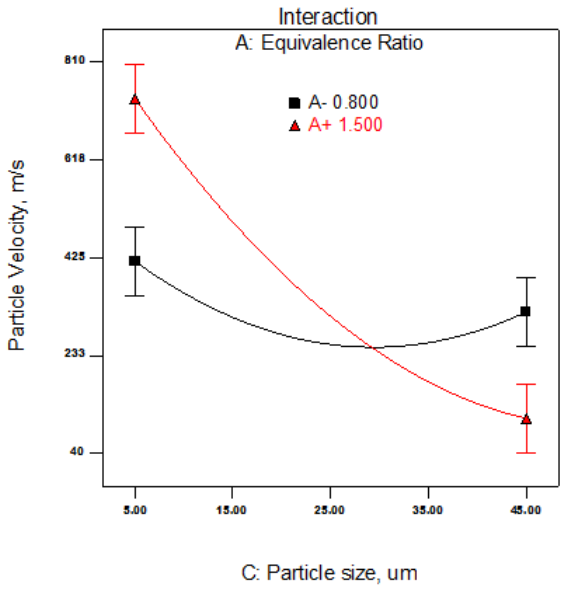

Figure 4.37: Interaction plot of particle velocity response with the equivalence ratio and particle size for DJ2700

4.5.4 DOE Results of Particle Temperature at the Nozzle Exit

The statistical analysis was also applied to the particle temperature at the nozzle exit. The aim of this investigation was to reveal the effect of the process parameters on the particle temperature at two different locations. In other words, to determine if the relation of the process parameters on the particle temperature, is affected by location. Table 4.14 and Table 4.15 are the ANOVA tables for the particles temperature response at the nozzle exit for both DJ1050 and DJ2700 guns. The tables show the adequacy measures which were in an acceptable ranges as in the previous responses.

The statistical model developed for the DJ1050 in terms of the coded variables is as follows: for the particle temperature at the nozzle exit:

$$PT_{exit} = 789 + 25 * B - 6.76 * C + 52.9 * B * C - 138.59 * C^2 \tag{4.21}$$

where B and C are the spray distance and the particle size respectively, where $-C^2 > BC > -C > B$ was the order of the factors effect within the (-1 to +1) range. In terms of the actual variables it was in the form:

$$PT_{exit} = 867 - 1.6 * SD - 1.5 * PS + 0.1SD * PS - 0.34 * PS^2 \tag{4.22}$$

Table 4.14: ANOVA analysis for the particle temperature response at the nozzle exit response model for DJ1050.

Source	Sum of squares	DF	Mean squares	F value	$prob > F$	
Model	98054	4	24513	22.93	< 0.0001	significant
B-Spray distance	5101	1	5101	4.77	0.04957	
C-Particle size	366	1	366	0.34	0.5691	
BC	11230	1	11230	10.50	0.0071	
C^2	81357	1	81357	76.12	< 0.0001	
Residual	12825	24	1068			
Cor Total	110880	16				
$R^2 = 0.88$				$Adj.R^2 = 0.84$		
$Pred.R^2 = 0.55$				$Adeq.Precision = 14.036$		

Table 4.15: ANOVA analysis for particle temperature at the nozzle exit response model for DJ2700.

Source	Sum of squares	DF	Mean squares	F value	$prob > F$	
Model	1888793	7	269827	12.31	< 0.0001	significant
A-Equivalence ratio	30.14	1	30.14	0.0013	0.9708	
B-Spray distance	163317	1	163317	7.45	0.0125	
C-Particle size	745771	1	745771	34.04	< 0.0001	
D-Air	155247	1	155247	7.08	0.0146	
AC	413624	1	413624	18.88	0.0003	
BC	220934	1	220934	10.08	0.0046	
CD	189866	1	189866	8.66	0.0077	
Residual	460003	21	21904			
Cor Total	2348796	28				
$R^2 = 0.80$				$Adj.R^2 = 0.73$		
$Pred.R^2 = 0.48$				$Adeq.Precision = 15.09$		

The statistical model developed for DJ2700 in terms of the particle temperature coded variable is as follows:

$$\begin{aligned} PT_{exit} = 1183 - 1.5 * A - 116 * B - 249 * C \\ +113.74 * D - 321 * A * C \\ +235 * B * C - 217.86 * C * D \end{aligned} \tag{4.23}$$

where A, B, C, and D are the equivalence ratio, spray distance, particle size and air flow rate

respectively. The order of influence of the factors was $-BC > -AC > BC > -C > D > -A$ in the same range of (-1 to +1) and in terms of the actual variables it was of the form:

$$\begin{aligned} PT_{exit} = 1 - 1194.61 + 1143.92 * \phi - 16 * SD \\ -77 * PS + 15 * AirFlow - 45.9 * \phi * PS \\ +0.47 * SD * PS - 0.43 * PS * AirFlow \end{aligned} \tag{4.24}$$

It could be seen from the mathematical models that the particle size (C) is still a dominant

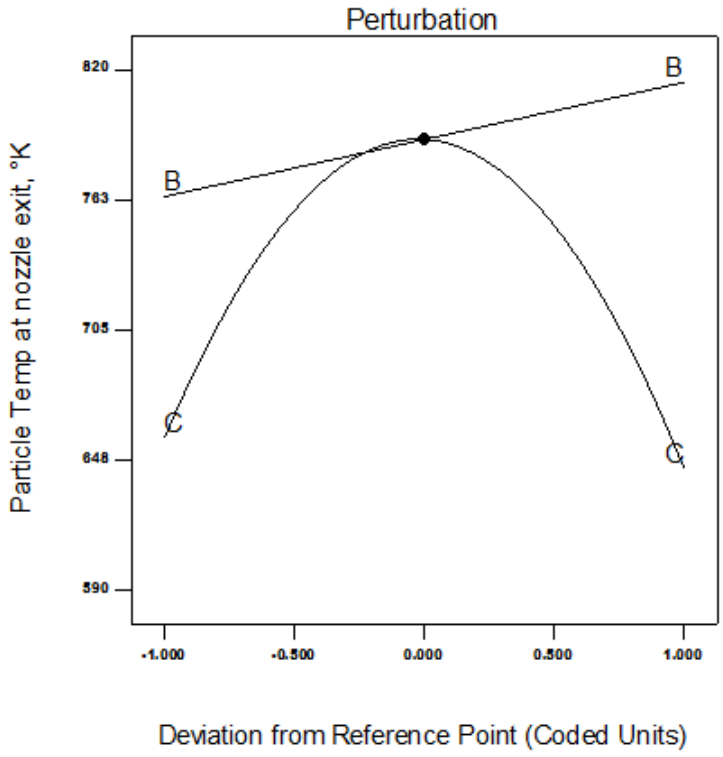

Figure 4.38: Perturbation plot shows the relation between the particle temperature at the nozzle exit with the spray distance and particle size for B = spray distacne and C = particle size: DJ1050

factor regarding the particle temperature, which was the same result found at the other location of the spray distance. The main difference in the particle temperature at the two location was their temperature behaviour. Figure 4.38 is the perturbation plot showing the relation between the particle temperature at the exit of the nozzle and its size and the spray distance. It was noticed that the particle size effect on its temperature at this location was of a quadratic form (C^2). The particle temperature increased with increasing particle size to a maximum point of around 790 K and decreased after that. All particle sizes were much

less than the melting temperature of 1769 K at that location. On contrary, perturbation plot for the particle temperature response with spray distance in Figure 4.31, shows that the particle temperatures for similar different sizes were much closer to the melting point.

The spray distance had the same effect on particle temperature response at this location as the spray distance location (BC). Based on this difference in the value for particle temperature response at both locations, it could be revealed that the design of the DJ1050 provides a good and desirable behaviour of the particle temperature along the jet, since the temperature was found to be closer to the the melting point at the spray distance (substrate location). This is important as it is well known that melting the particle at the point of impact on the substrate would decrease the porosity of the coating [66].

The interaction plot in Figure 4.39 shows that when applying a spray distance of 150 mm, the particle temperature decreased with increasing the particle size, and the opposite effect was found when applying the upper level of spray distance which is 200 mm. This could be attributed to the fact that thermal behaviour of the smaller particles change more rapidly than that of the larger ones [116]. The same interaction was found in case of particle temperature at the spray distance location. The only noticeable difference was that temperature values, at the spray distance location (substrate) were much higher. Moreover, the gap between the two particle temperature levels in the case of nozzle exit was larger due to the fact that temperature of the gas at this location changes rapidly, due to the compressibility effect.

In case of DJ2700, the relationship between particle temperature at nozzle exit and the process parameters were linear. In comparison with the same response behaviour at other location (over the spray distance) in Figure 4.33. First, the equivalence ratio effect on the particle temperature decreased and became negligible. For spray distance the relation took an inverse proportional linear relation ($-B$) rather than quadratic one with the other location. Air flow had a linear direct proportional relation (D) with the particle temperature response at this location as shown in the perturbation plot in Figure 4.40. This may be attributed to increase of the oxygen content in the reaction. The particle size was of negative or inverse linear relation with the particle temperature at this location ($-C$). On contrary to the particle temperature behaviour at the spray distance which was increasing

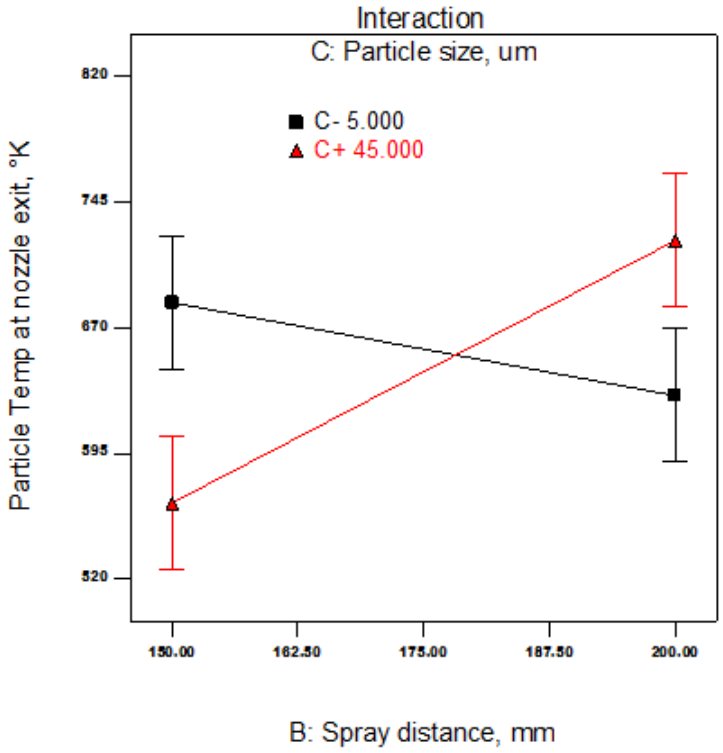

Figure 4.39: Interaction of the particle velocity temperature at the nozzle exit with the particle size and spray distance for DJ1050

and decreasing at a specific particle size, the particle temperature at the nozzle was always decreased whenever the particle size increased. This difference might be attributed to the thermal response of the particle was affected by location. It should be noted that the particle temperature range at both locations was not large, which indicates that particle temperature was more uniform in comparison to that in the case of DJ1050.

In the case of DJ1050, the particle temperature range was roughly between 900 K to 1600 K at the spray distance location due to the effect of the process factor of the particle size and spray distance location. Whereas, for DJ2700 it was between 650 K to 820 K under the influence of the same factors at the nozzle exit location. On the other hand, particle temperature ranges at the two locations were 1200 K to 1460 K and 1000 K to 1450 K for the spray distance and the nozzle exit location respectively.

The interaction between the particle temperature at the nozzle exit and both the spray distance and particle size for the DJ2700 is shown in Figure 4.41. It was evidenced in the case of lean mixture, which corresponds to the equivalence ratio of 0.8, the higher level particle

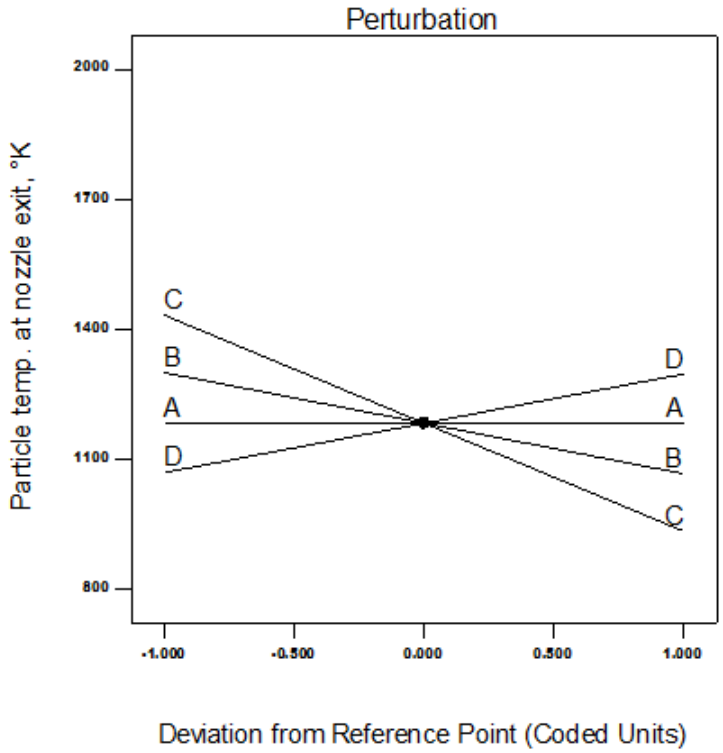

Figure 4.40: Perturbation plot for particle temperature at the nozzle exit response C = particle size and B = spray distance A = equivalence ratio and D = air flow rate for DJ2700

size had higher temperature than the lower one, Plus in case of the fuel rich mixture, which corresponds to 1.5 equivalence ratio, the opposite effect was revealed. The same variation with the same process parameters were found at the spray distance location. The obvious difference was that the temperature of the two particles levels overlapped at 0.8 equivalence ratio in this location, which was not observed at the other location. At the equivalence ratio of 1.5 there was a significant difference in the particle temperature over the two levels. The particle temperature of the higher size decreased as the equivalence ratio increased, while the particle temperature increased for the lower size level. The reason might be attributed to the difference in the thermal response out along the flame corresponding to the different equivalence ratios (fuel rich/lean).

4.5.5 DOE Results of Particle Velocity at the Nozzle Exit

The particle velocity response to process variables at the nozzle exit was also investigated. The motivation for this investigation was the same with the previous response of the particle temperature at the nozzle exit, which was considering the effect of location (at the nozzle

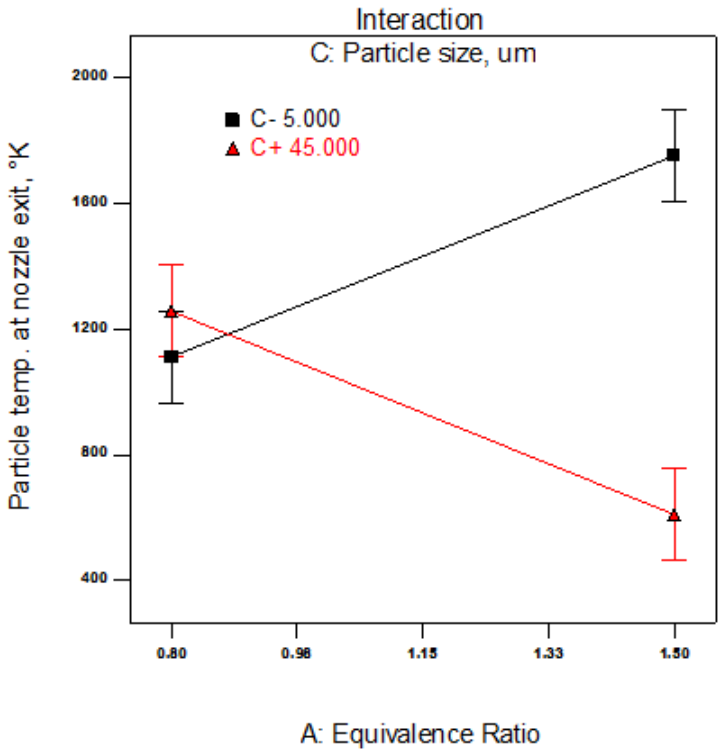

Figure 4.41: Interaction plot of particle temperature at the nozzle exit response with particle size and equivalence ratio for DJ2700

exit and at the substrate location) on the response. ANOVA tables for these responses are presented in Table 4.16 and Table 4.17. The applicability of the ANOVA tables can be verified by the values of the adequacy measures as with the previous responses.

Table 4.16: ANOVA analysis for particle velocity at the nozzle exit response model for DJ1050.

Source	Sum of squares	DF	Mean squares	F value	$prob > F$	
Model	49205	7	7029	44.83	< 0.0001	significant
A-Equivalence Ratio	404	1	2.58	0.1425	0.04957	
B-Spray distance	3873	1	3873	24.70	< 0.0001	
C-Particle size	33265	1	33265	212.	0.5691	
AB	1294	1	1294	8.25	0.0184	
BC	1096	1	1096	6.99	0.0267	
B^2	2115	1	2115	13.49	0.0051	
C^2	81357	1	81357	76.12	< 0.0001	
Residual	1411	9	156	0.0010		
Cor Total	50616	16				
$R^2 = 0.97$				$Adj.R^2 = 0.95$		
$Pred.R^2 = 0.80$				$Adeq.Precision = 22.93$		

Table 4.17: ANOVA analysis for particle velocity at the nozzle exit(response model for DJ2700).

Source	Sum of squares	DF	Mean squares	F value	$prob > F$	
Model	319932	7	45704	9.63	< 0.0001	significant
A-Equivalence Ratio	7504	1	7504	1.58	0.2222	
B-Spray distance	4.21	1	4.21	4.21	0.0528	
C-Particle size	137328	1	137328	28.95	0.5691	
BC	11230	1	11230	10.50	< 0.0001	
D-Air Flow	17556	1	17556	3.70	0.0680	
AC	56840	1	56840	11.98	0.0023	
CD	36483	1	36483	7.69	0.0114	
C^2	81357	1	81357	76.12	< 0.0001	
Residual	99603	21	4743			
Cor Total	419536	28				
$R^2 = 0.88$				$Adj.R^2 = 0.84$		
$Pred.R^2 = 0.55$				$Adeq.Precision = 14.036$		

The mathematical model developed for DJ1050 in terms of the coded variables is as follows for particle velocity at the nozzle exit was

$$PV_{exit} = 85 - 7.11 * A + 22.00 * B - 64 * C - 17.98 * A * B \\ -16.55 * B * C + 22.38 * B^2 + 39.85 * C^2 \tag{4.25}$$

where, A, B and C are the equivalence ratio, the spray distance and the particle size respectively. And the order of the influence was $C^2 > B^2 > -AB > -BC > C > B > A$

In terms of the actual variables:

$$PV_{exit} = 635 + 339 * \phi - 8.46 * SD - 2.4 * PS - 2.005 * \phi * SD - \\ 0.003 * SD * PS + 0.035 * SD^2 + 0.099 * PS^2 \tag{4.26}$$

As for the DJ2700 gun the mathematical model in terms of the coded variables:

$$PV_{exit} = 223 + 25 * A - 40 * B - 106 * C + 38 * D - 119 * A * C \\ +105 * B * C - 95 * C * D \tag{4.27}$$

where A, B, C and D are the equivalence ratio, spray distance, particle size and air flow rate respectively. The order of influence of the variables was $AC > BC > CD > C > B > A$.In the actual variables was:

$$PV_{exit} = -743 + 497 * \phi - 6.89 * SD + 29.9 * PS + 6.3 * AirFlow - 17.02 * \phi * PS \\ +0.21 * SD * PS - 0.19 - PS * AirFlow \tag{4.28}$$

Figure 4.42 shows the perturbation plot, based on the effect of the process parameters on the particle velocity at the nozzle exit. In comparison to the response behaviour at the spray distance/substrate location, the statistical analysis showed that the equivalence ratio had an effect on the particle temperature at this location in addition to the effect of the spray distance and particle size. The particle velocity had the same velocity behaviour as that of the spray distance location, as can be referred to in Figure 4.34.

As the particle size increased the particle temperature decreased. However, the particle velocity was almost 50% lower at the nozzle exit location, which is desirable, as the higher the particle velocity at the point of impact, the denser the coating. The particle velocity at the nozzle exit was found to be considerably higher than that at the substraate location. The reason could be attributed to the intrinsic high gradient of all flow variables at the nozzle exit [18]. Nevertheless, increasing the spray distance would increase the particle velocity at this location in the nozzle, which means that under this design (DJ1050) the jet velocity increased as the spray distance increased. The effect of the equivalence ratio on the particle velocity at this location had a marginal effect that could be ignored, as the equivalence ratio increased the particle velocity decreased slightly.

Figure 4.43 shows the interaction plot shows the effect of the spray distance and the equivalence ratio on the particle velocity at the nozzle exit. Under fuel lean mixture ($\phi < 1$)

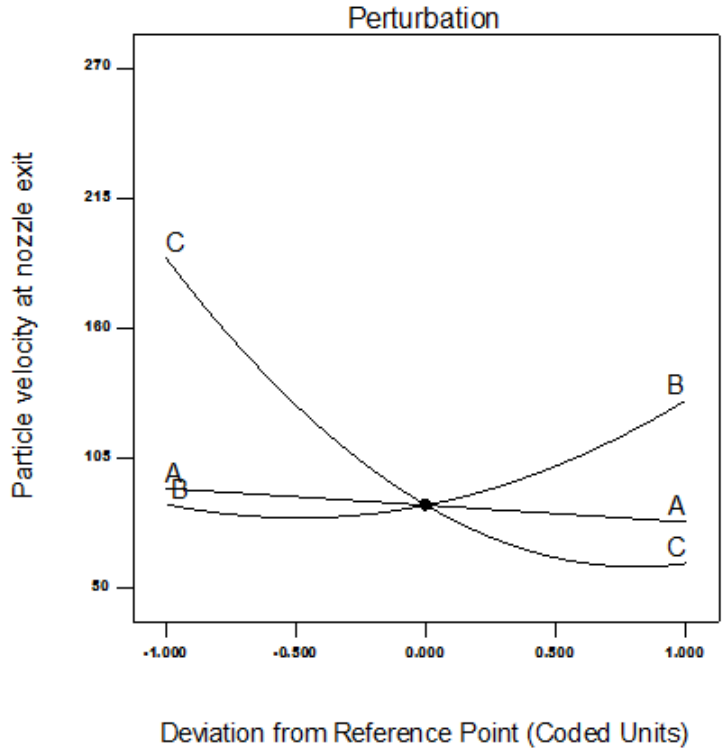

Figure 4.42: Perturbation plot shows the relation between the particle temperature at the nozzle exit where; B = spray distance and C = particle size and A = equivalence ratio: for DJ1050

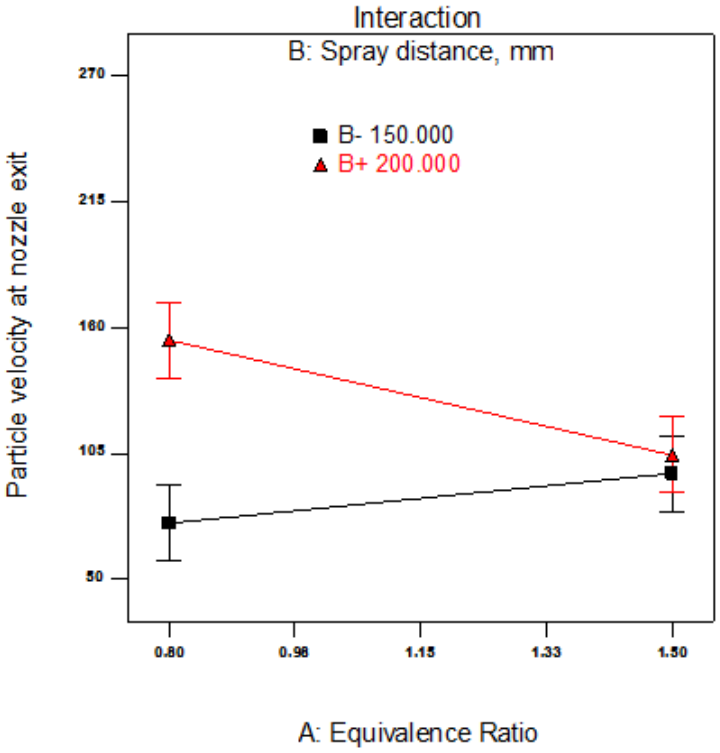

Figure 4.43: Interaction plot between the spray distance, equivalence ratio and particle velocity at nozzle exit for DJ1050

operating condition, the spray distance increased particle velocity. Such that the higher level of the spray distance corresponded to a higher particle velocity at the exit of the nozzle. While in the case of the fuel-rich condition, no influence on the particle velocity by the spray distance was found at the exit of the nozzle. It could be deduced that operating at a fuel lean mixture resulted in higher variation in of the flow velocity at this location as the spray distance changed from 150 mm to 200 mm.

Another statistical interaction was developed to show the effect of particle size and spray distance on the particle velocity at the nozzle exit for the DJ1050 as shown in Figure 4.44. The interaction showed that processing lower level of the particle size would result in increased velocity as the spray distance increased. Whereas, no influence of increasing the spray distance was observed, when the process used higher levels of particle size. This

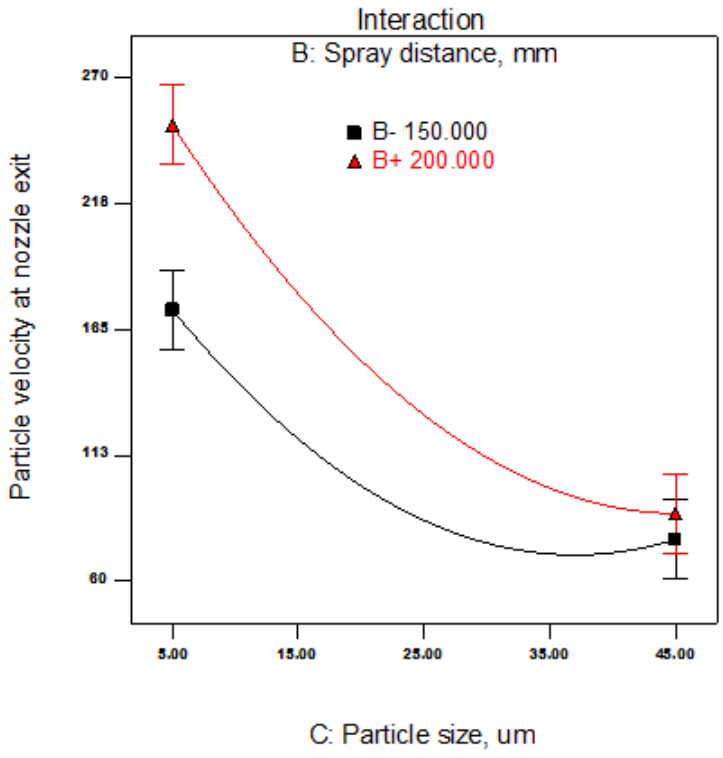

Figure 4.44: Interaction plot between the spray distance, particle size and particle velocity at nozzle exit for DJ1050

could be attributed to the fact that smaller particle size would have higher response to high gradient velocity field of the jet at this location than at the spray distance location with a lower gradient velocity field. Increasing the spray distance would not have an effect on the particle velocity at this location due the sluggish response of the particle to the high gradient

region of the gas flow field at this location.

Finally, the perturbation plot showing the relationship between the process parameters and particle velocity response at the nozzle exit for the DJ2700 gun is given in Figure 4.45. It was clear that all process parameters variables had an effect on the particle velocity at this location. The influence of the particle size was the greatest one while the equivalence ratio had a minimal effect on this response at this location of nozzle followed by the air flow rate effect. The spray distance was shown to have reducing effect on the particle velocity in

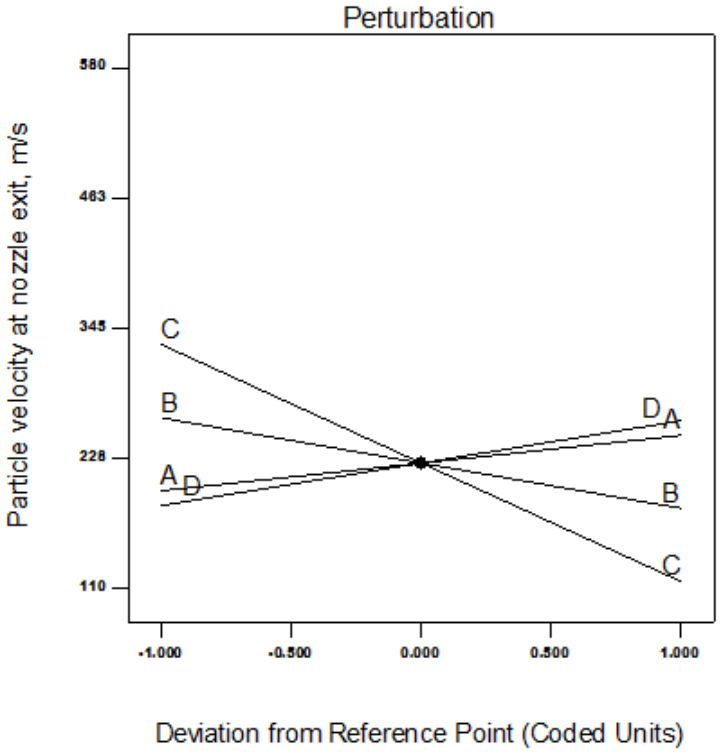

Figure 4.45: Perturbation plot showing the relation between the particle temperature at the nozzle exit where; B = spray distance , C = particle size A = equivalence ratio and D = air flow: for DJ2700

this case in contrary to what was found in the case of the DJ1050 at the same location of the nozzle exit. This result revealed that increasing the spray distance decreased the velocity gradient at the exit of the nozzle for the the DJ2700 gun. It was also revealed that the particle velocity reduced linearly with increasing particle size at this location. While it was reduced quadratically against increasing the same factor at the spray distance location.

Around a mean point of all process variables, the perturbation plot showed not effect on the particle velocity at this location. It should be mentioned that it would be very

controversial to physically describe any of the process variable behaviour at this location due to the difficulty of the measurement at this location.

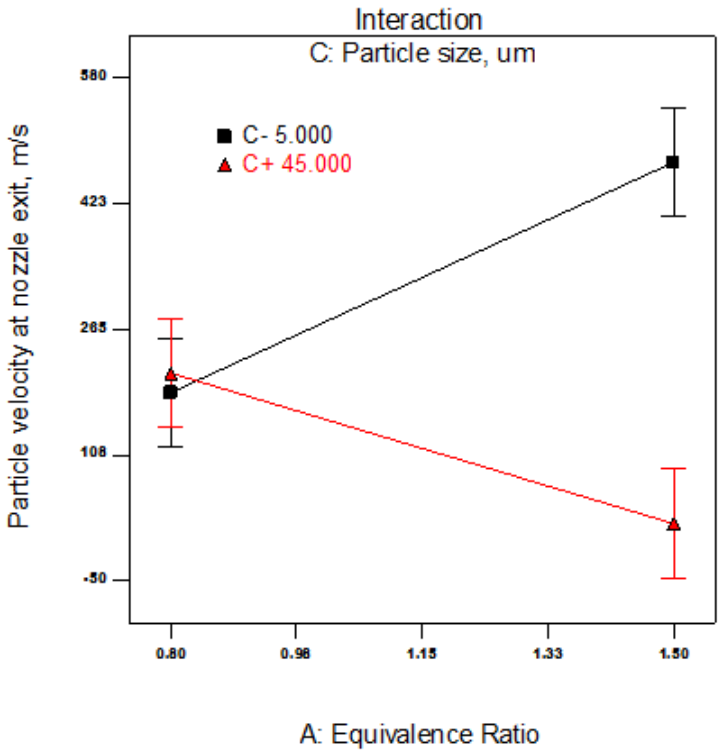

Figure 4.46: Interaction plot between the spray distance, particle size and particle velocity at nozzle exit for DJ2700

An interaction between three process variables and response was developed in this case. The reason could be attributed to high variation of the process parameters at this location in the flow. Additionally, applying one way coupling modelling between the flow variables and particle in flight dynamic behaviour, the interaction between the process variables could be higher.

First interaction showed the effect of the equivalence ratio and the particle size on the particle velocity as shown in (Figure 4.46). When applying an equivalence ratio of 0.8 (fuel lean mixture), there was no significant influence of the two levels of the particles sizes at this particle velocity. While in the case of applying an equivalence ratio of 1.5, there was a considerable difference in the particle size effect on particle velocity. Therefore smaller particle size was shown to possess much higher velocity than the higher one counterpart [103, 108]. The result was in a good agreement with the axiomatic behaviour of the small particle size of high response to the flow, especially at such high flow gradient location in

the flow.

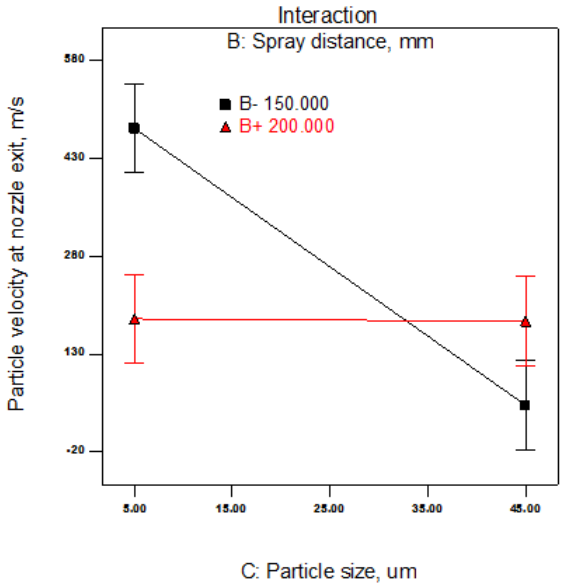

Figure 4.47: Interaction plot between the spray distance, particle size and particle velocity at nozzle exit for DJ2700

The spray distance and particle size effect on the particle velocity response at the nozzle exit is shown in the interaction plot as in Figure 4.47. Processing particle size at the lower level showed that the lower spray distance resulted in a much higher particle velocity. In case of spraying particle for the higher size level, the effect of the spray distance reduced considerably. Moreover, the effect of spray distance of 200 mm had no effect on the particle velocity for the both size level.

4.6 Validation of the Statistical Models

To validate the statistical work of this study, a set of operating conditions applied during the experiment work conducted in Oerlikon, Metco, Switzerland were substituted into the model developed for particle velocity as a function of actual variables as in Equation 4.20 which takes the form:

$$PV = 53 + 551\phi - 1.6PS - 19\phi * PS + 0.28PS^2$$

One of the operating parameters conducted through the experiment, using DJ2700 gun, was as follows:

- Air flow rate = 350 SLPM
- Oxygen flow rate = 230 SLPM
- C_3H_6 = 57
- $\phi = 0.84$
- SD = 270 mm

Substituting the previous values with a particle size diameter of 10 μm into the statistical model developed for the particle velocity yielded a particle velocity of 515 m/s, which was 14% of the experimentally measured value of around 600 m/s. Hence, the CFD and statistical models were deemed reliable.

4.7 Optimization of Process Parameters

The last section of the results in this study is about optimizing the parameters according to a well-known criterion within the HVOF industry. The optimization is based on the desirability approach as discussed in Chapter 3. Particle temperature and velocity are known to be critical parameters in thermal spray processes. The main motivation of developing a HVOF process is to increase the gas/particle velocity while heating it to a low to medium

temperature. Higher velocity and low to medium temperature is known to be the main factor for producing a coating with low porosity, which is desirable in many application such as corrosion and wear resistance. The optimization of this study then was about aiming to achieve this criteria. The desirability approach is based on setting a desirable target of the considered output as maximum, minimum or specific value. Then the software (StatEASE) applies and solves Equation 3.14 to Equation 3.18, depending on the setting of the desired values, to obtain the process parameter that would satisfy the target. The target applied in this study was to obtain; maximum gas temperature, maximum gas velocity, maximum particle temperature and maximum particle velocity. The values of the range of each operating parameter and the desirable targets can be represented on these targets for DJ1050 case gun as in Table 4.18. The solution for the parameters that satisfy such a target value are given in Table 4.19 for this case.

Table 4.18: Optimization criterion (i.e. Quality) low to medium gas / particle temperature and high velocity of gas /particle as the targets for the DJ1050 gun

Constraint name	aim	Lower limit	Upper limit	Lower weight	Upper weight	Importance
ϕ	is in range	0.8	1.5	1	1	3
SD	in range	150	200	1	1	3
PS	in range	5	45	1	1	3
GT	min.	3100	3500	1	1	5
GV	max.	1850	1910	1	1	5
PT	maxi.	724	1722	1	1	5
PV	max.	420	3300	1	1	5

Table 4.19: Solution of the operating parameters for the DJ1050 gun

Solution Number	ϕ	SD	PS	GT	GV	PT	PV	Desirability
1	1.44	150	17	3229	1880	1375	272	0.48
2	1.45	150	19	3204	1877	1314	250	0.48
3	1.44	199	7	3295	1875	1408	332	0.46
4	0.87	199	7	3380	1870	1409	333	0.38
5	0.88	199	9	3391	1872	1364	306	0.38

It can be seen from the results in Table 4.19 that 5 solutions of the operating parameters can be applied to achieve the desired target of the maximum values for gas temperature, gas velocity, particle temperature and particle velocity. It was noticed that the calculated optimum spray distance for the target was varied between 150 and 199 mm. The optimum

particle size was in the range of 7 to 19 μm. The equivalence ratio was in a range of 0.87 to 1.45. Solution number 1 and 2 gave the highest desirability factor of 0.48. The desirability factor indicated how close the solution is to the target. The two highest desirability factor cases were correspondent to fuel- rich condition of around 1.44 1.45, a spray distance of 150 mm and particle size range of 17 to 19 μm, in order to achieve the maximum gas velocity and minimum to medium gas temperature. The result of the optimum operating parameters can be further depicted in Figure 4.48

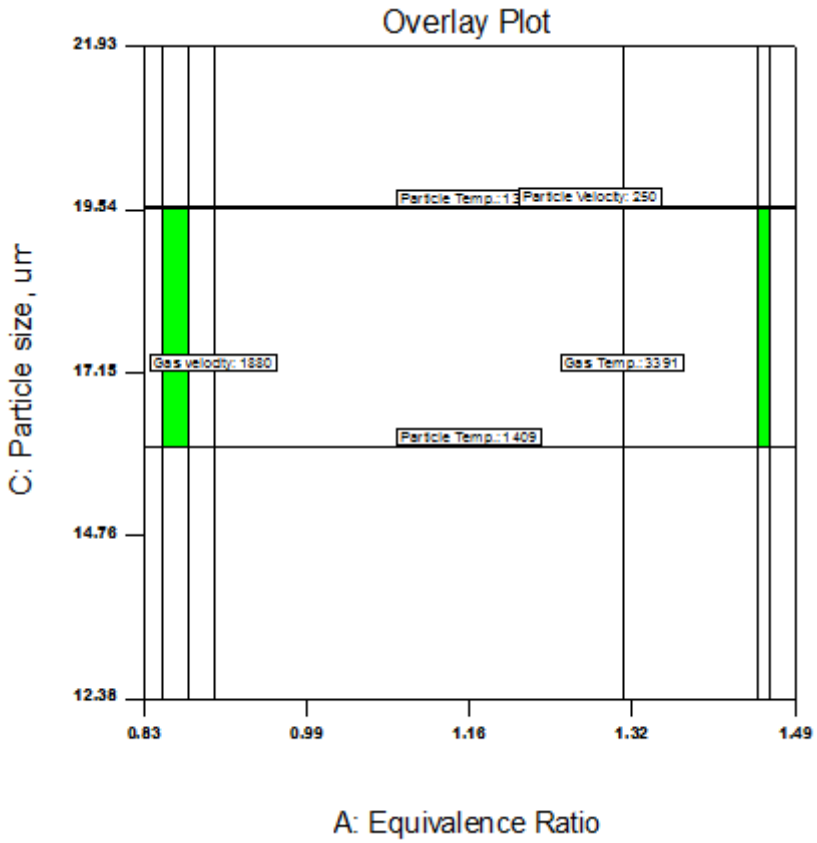

Figure 4.48: Overlay plot for the first target for the DJ1050 gun

The same approach was applied to the DJ2700 gun, and the same two criteria were applied (Table 4.20). It must be mentioned that air flow rate was included as a parameter in this case.

The solution for the DJ2700 gun (Table 4.21) showed that the optimum parameters were shown to have reasonable desirability factor at around 0.5, which means that the operating conditions considered in this study can roughly satisfy 50% of this target. In addition, again the fuel rich operating condition was shown to have been an apparent optimum solution. The optimum solution for the particle size was almost constant at 5 μm in this case, and

Table 4.20: optimization criterion (i.e. quality) low to medium gas / particle temperature and high velocity of gas /particle as the targets for the DJ2700 gun

Constraint name	aim	Lower limit	Upper limit	Lower weight	Upper weight	Importance
ϕ	in range	0.8	1.5	1	1	3
SD	in range	150	200	1	1	3
PS	in range	5	45	1	1	3
$AirFlow$	in range	250	300	1	1	3
GT	min.	2520	3580	1	1	5
GV	max.	1700	1900	1	1	5
PT	min.	1034	1467	1	1	5
PV	max.	195	672	1	1	5

the air flow rate was more close to the highest value of operating condition. And in this case, it could be concluded that, fuel-rich particle size of 5 μm, spray distance of around 150 mm and air flow rate of 290 - 299 SLPM should be applied in order to achieve the desired target under such criteria, of medium gas/particle velocity and low to medium gas/particle temperature.

Table 4.21: Solution of the optimized operating parameters for the DJ2700 gun

Solution Number	ϕ	SD	PS	$AirFlow$	GT	GV	PT	PV	Desirability
15	1.31	150	5	299	3240	1843	1271	647	0.55
16	1.31	150	5	296	3222	1841	1288	652	0.55
17	1.27	150	5	250	3065	1840	1342	637	0.54
18	1.35	151	5	299	3208	1820	1282	671	0.54
19	0.80	150	5	299	3253	1872	1159	418	0.54
20	1.33	171	5	250	3251	1812	1253	664	0.53

The optimized solution for the DJ2700 gun can be also depicted by the overlay plot in (Figure 4.49). It can be noticed from both overly plots of both guns that DJ2700 has wider window of optimum parameters than DJ1050. In addition, both optimum parameters had a desirability factor at around 50%.

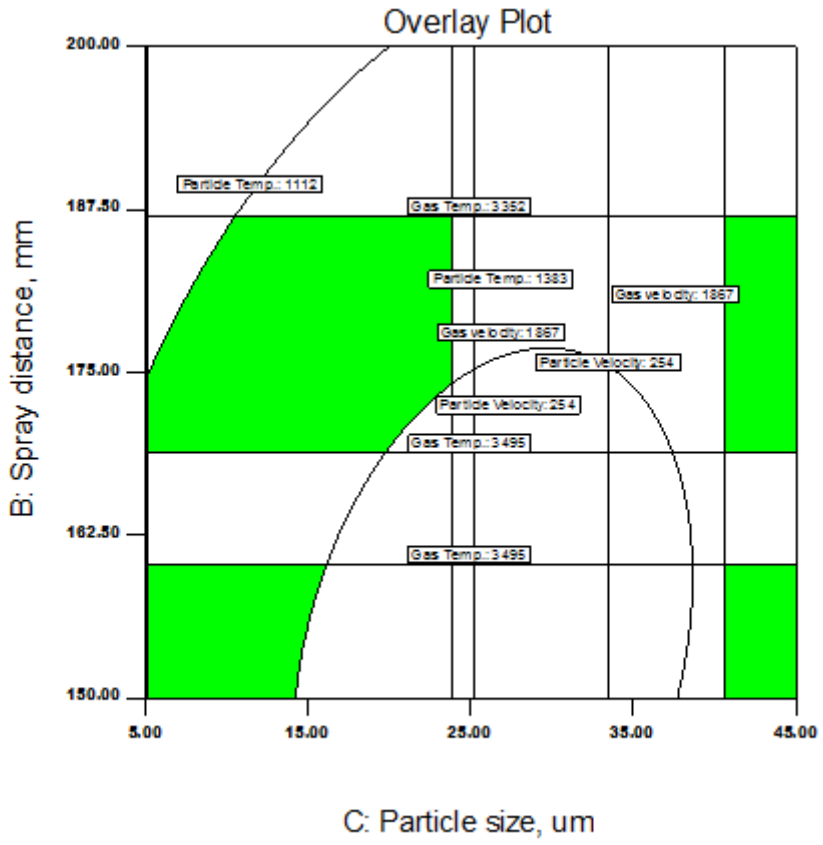

Figure 4.49: Overlay plot for the first target for the DJ1050 gun

The frequent optimum equivalent ratio for both gun were fuel rich. DJ1050 show more optimum values for the particle size, while for DJ2700 optimized particle size was shown to be fixed at 5 μm (Nano structured size). The high level spray distance was noticed to be more optimum for the DJ1050, while the opposite was observed for the DJ2700. In general, it could be concluded that gun geometry plays an important role in the performance of the HVOF thermal spray process.

Chapter 5

Conclusion and Recommendation for Future Work

5.1 Conclusion

The main findings from the research was that both the CFD and DOE results for the both guns, displayed results (temperature and velocity) that were highly dependent on the equivalence ratio (particularly fuel-rich), square of the equivalence ratio or interactions of equivalence ratio with other factors. The CFD and DOE were within 14% percent agreement with the experimental measurements.

The mathematical models developed through the statistical approach in this study, are a good guide in the design of the HVOF process. One of main contributions of this work is the fact that for the first time the effect of the density variation on the gas dynamic behaviour has been investigated. However, the results show that under the range of the pressure and temperature of the gases at the inlet of the nozzle, there was no noticeable effect on gas flow.

The main difference and advantage of the second generation nozzle design over the first generation was found to be in the particle temperature at the point of impact over the spray distance, which was found to be higher. Lower temperature particles at the point of impact is highly desirable in the HVOF process since it gives less porous coating and increases the deposition efficiency of the process. In addition, the second generation was found to give

higher particle velocity, which is also desirable due to the same reason.

Due to the dynamic and thermal influence from the flame of both the DJ1050 and DJ2700 HOVF guns, the DJ1050 demonstrates its usefulness in applying dense coatings for micro-sized powders (7 to 19 μm). Whereas, the DJ2700 favours 5 μm sized powders, therefore is a better contender for the deposition of Nano-structured WC-12%Co powders which are promising new powder feedstocks in use in today's thermal spray industry.

The novelty of this research is the provision of models both through CFD and DOE equations which can be used to predict the dynamic and thermal influences experienced by a WC-Co particle when deposited by either a DJ1050 or DJ2700 HVOF gun, something new to the thermal spray community.

5.2 Recommendation for Future Work

Based on the results of this study and the literature survey conducted herein, model refinement and improvement is further required in the modelling of HVOF. It should be mentioned that there were many models (especially for the particle dynamics) that had to be applied. However, one of the challenges in modelling the HVOF is the experimental validation since measuring some aspects of the process is still beyond the capability of the current instruments, especially the dynamics inside the nozzle. The results of this research allows HVOF thermal spray users to predict and understand the complex interactions within the process therefore this work will complement future studies.

The PIMPLE solver is a free open source code of OpenFoam, which could be applied to simulate the whole process at once. To date this solver has never been used to do so. The author highly recommends the application of the solver, since such a simulation would quantitatively reveal more in-depth aspects of the HVOF process, taking into account the particle/coating build up

Future nozzle designs have not been investigated in the literature. It is in this context that it might be innovative to investigate such designs, through such methodologies presented in this thesis, which would be totally a novel approach for the HVOF process. Micro size

nozzles might provide a possibility to spray particles sizes less than 5 μm and nano structured powdered, which is currently the lowest limit achievable.

Publications

1. M. Aldosari, J. Stokes, K. Benyounis Comparative Study Between Two Nozzle Assemblies For High Velocity Oxy Fuel (HVOF) Thermal Spray Coating Process Under preparation.
2. M. Aldosari, J. Stokes, K. Benyounis Modelling particle velocity and temperature via a combined CFD and DOE approaches for HVOF process Under preparation.
3. M. Aldosari, J. Stokes, K. Benyounis Multi-phase flow modelling for HVOF process Under preparation as a chapter book.

References

[1] J Stokes. The theory and application of Sulzer Metco HVOF(High Velocity Oxy-Fuel)Thermal Spray Process, Dublin City University, Ireland. A book, ISBN 1-87232-753-2,2008.

[2] D Cheng, G Trapaga, JW McKelliget, and EJ Lavernia. Mathematical Modelling of High Velocity Oxygen Fuel thermal Spraying of Nanocrystalline Materials: an Overview. Modelling and Simulation in Materials Science and Engineering, 11(1):R1, 2002.

[3] B Bhushan and Balkishan K Gupta. Handbook of tribology: materials, coatings, and surface treatments. 1991.

[4] S Hasan. Design of experiment analysis of high velocity oxy-fuel coating of hydroxyapatite, MEng thesis, Dublin City University. 2009.

[5] J Stokes. Production of coated and free-standing engineering components using the HVOF (High Velocity Oxy-Fuel)process. PhD thesis, Dublin City University, 2003.

[6] L Pawlowski. The science and engineering of thermal spray coatings. John Wiley & Sons, 2008.

[7] Flame Spray Technologies. Available online: www.fst.nl. (Accessed 09/2017)

[8] M Oksa, E Turunen, T Suhonen, T Varis, and S P Hannula. Optimization and characterization of high velocity oxy-fuel sprayed coatings: Techniques, Materials, and applications. Journal of Thermal Spray Coatings, 1(1): 17-52, 2011.

[9] J R Davis et al. Handbook of thermal spray technology. ASM international, 2004.

[10] JP Trelles, C Chazelas, A Vardelle, and JVR Heberlien. Arc plasma torch modelling. Journal of thermal spray technology, 18(5-6): 728-752, 2009.

[11] R B Heimann. Plasma spray coating: principles and applications. John Wiley & Sons, 2008.

[12] M Jadidi, S Moghtadernejad, and A Dolatabadi. A comprehensive review on fluid dynamics and transport of suspension/liquid droplets and particles in high velocity oxygen-fuel (HVOF) thermal spray. Coatings, 5(4): 576-645, 2015.

[13] V Sobolev, J Guilemany, J Nutting, and S Joshi. High velocity oxy-fuel spraying: theory, structure-property relationships and applications. Maney, 2004.

[14] S Grigoriev, A Okunkova, A Sova, P Bertrand, and I Smurov. Cold spraying: From process fundamentals towards advanced applications. Surface and coatings Technology, 268:77-84, 2015.

[15] L M Berger. Application of hardmetals as thermal spray coatings. International Journal of Refractory Metals and Hard Materials, 49:350-364, 2015.

[16] Available online: www.oerlikon.com/metco/en/. Last Accessed 09/2017

[17] G Bolilli, L-M Berger, T Borner, H Koivuluto, L Lusvarghi, C Lyphout, N Mrkocsan, V Matikainen, P Nylen, P Sassatelli , et al. Tribology of HVOF-and-HVAF-sprayed WC-10Co4Cr hardmetal coatings: A comparative assessment. Surface and Coatings Technology, 265:125-144, 2015.

[18] M Li and P D Christofides. Modelling and control of high-velocity oxygen-fuel (HVOF) thermal spray: A tutorial review. Journal of thermal spray technology, 18(5-6): 753-768, 2009.

[19] M Li and P D christofieds. Modelling and analysis of HVOF thermal spray process accounting for powder size distribution. Chemical Engineering Science, 58(3): 849-857, 2003.

[20] M Li, D Shi, and P D Christofiedes. Diamond jet hybrid HVOF thermal spray: gas-phase and particle behaviour modelling and feedback control design. Industrial & engineering

chemistry research, 43(14):3632-3652, 2004.

[21] Aerospaceweb.www.aerospaceweb.org/question/propulsion/q0224.shtml (Accessed 09/ 2017)

[22] H Tabbara. Numerical investigations of thermal spray coating processes: combustion, supersonic flow, droplet injection, and substrate impingement phenomena. PhD thesis, University of Southampton, 2012.

[23] W D Callister, and D G Rethwisch. Fundamentals of materials science and engineering: an integrated approach. John Wiley & Sons , 2012.

[24] M Bozorgtabar, M Salhi, M Rahimipour, and M Jafarpour. Influence of High Velocity Oxy-Fuel parameters on properties of nanostructured tio2 coatings. Bulletin of Materials Science, 33(6): 671-675, 2010.

[25] M Couto, S Dosta, and JM Guilemany. Comparison of the mechanical and electrochemical properties of WC-17 and 12Co coatings onto a17075-t6 obtained by High Velocity Oxy-Fuel and cold gas spraying. Surface and Coatings Technology, 268:180-189, 2015.

[26] R Vassen, D Hathiramani, J Metens, VAC Haanappel, and IC Vinke. Manufacturing of High performance solid oxide fuel cells (SOFC) with atmospheric plasma spraying (APS). Surface and Coating Technology, 202(3): 499-508, 2007.

[27] MP Planche, B Normand, H Liao, G Rannou, and C Coddet. Influence of HVOF spraying parameters on in-flight characteristics of inconel 718 particles and correlation with the electrochemical behaviour of the coating. Surface and Coatings Technology, 175(2): 247-256, 2002.

[28] M Jafari, MH Enayatai, M Salhi, SM Nahvi, and CG Park. Comparison between oxidation kinetics of HVOF sprayed WC-12Co and WC-10Co-4Cr coatings. International Journal of Refractory Metals and Hard Materials, 41:78-84, 2013.

[29] JA Picas, M Punset, MT Baile, E Martin, and A Forn. Effect of oxygen/fuel ratio on the in the flight particle parameters and properties of HVOF WC-CoCr coatings. Surface and Coatings Technology, 205:S364-S368, 2011.

[30] J Saaedi, TW Coyle, H Arabi, S Mirdamadi, and J Mostaghimi. Effects of HVOF process parameters on the properties of ni-cr coatings. Journal of thermal spray technology, 19(3):521-530, 2010.

[31] U Selvadurai, P Hollingsworth, I Baumann, B Hussong, W Tillmann, S Rausch, and D Biermann. Influence of the handling parameters on residual stresses of HVOF-sprayed wc-12co coatings. Surface and Coatings Technology, 268:30-35, 2015.

[32] M Goana, R S Lima, and B R Marple. Influence of particle temperature and velocity on the microstructure and mechanical behaviour of High Velocity Oxy-Fuel (HVOF) sprayed nanostructured titania coatings. Journal of materials processing technology, 198(1):426-435, 2008.

[33] M Watanabe, C Brauns, M Komatsu, S Kuroda, F Gartner, T Klassen, and H Katanoda. Effect of nitrogen flow rate on microstructures and mechanical properties of metallic coatings by warm spray deposition. Surface and Coatings Technology, 232:587-599, 2013.

[34] H Zhang, Y Hu, G Hou, Y An, and G Liu. The effect of High Velocity Oxy-Fuel spraying parameters on microstructure, corrosion and wear resistance of Fe-based metallic glass coatings. Journal of Non-Crystalline Solids, 406:37-44, 2014,

[35] M Gui, R Eybel, B Asselin, S Radhakrishnan, and J Cerps. Influence of processing parameters on residual stress of High Velocity Oxy-Fuel thermally sprayed WC-Co-Cr coatings. Journal of materials engineering and performance, 21(10): 2090-2098, 2012.

[36] N Cinca, A List, F Gartner, JM Guilemany and T klassen. Influence of spraying parameters on cold gas spraying of iron aluminide intermetallics. Surface and Coatings Technology, 268:99-107, 2015.

[37] Q Wang, J Xiang, G Chen, Y Cheng, X Zhao, and S Zhang. Propylene flow, microstructure and performance of WC-12Co coatings using a gas-fuel HVOF spray process. Journal of Materials Processing Technology, 213(10): 1653-1660, 2013.

[38] S Hong, Y Wu, Y Zheng, B Wang, W Gao, G Li, G Ying, and J Lin. Effect of spray parameters on the corrosion behaviour of HVOF sprayed WC-Co-Cr coatings. Journal

of Materials Engineering and Performance, 23(4):1434-1439, 2014.

[39] S Hassan, J Stokes. Design of experiment analysis of the Sulzer Metco DJ High Velocity Oxy-Fuel coating of hydroxyapatite for Orthopaedic applications. Journal of Thermal Spray Technology, 20(1-2): 186-194, 2011.

[40] A Scrivani, S Ianelli, A rossi, R Groppetti, F Casadei, and G Rizzi. A contribution to the surface analysis and characterization of HVOF coatings for petrochemical application. Wear, 250(1):93-100, 1999.

[41] B S Schorr, K J Stein, and A R Marder. Characterization of thermal spray coatings. Materials Characterization, 42(2):93-100, 1999.

[42] H-D Steffens and T Duda, Enthalpy measurements of direct current plasma jets used for ZrO_2. Y_2O_2 thermal barrier coatings. Journal of thermal spray technology, 9(2):235-240, 2000.

[43] JR Fincke, DC Haggard, and WD Swank. Particle temperature measurement in the thermal spray process. Journal of Thermal Spray Technology, 10(2):255-266, 2001.

[44] J Westerweel. Digital particle image velocimetry: theory and application. TU Delft, Delft University of Technology, 1993.

[45] J Holman. Experimental methods for engineers. McGraw-Hill, 1996.

[46] L Zhao, M Maurer, F Fischer, R Dicks, and E Lugscheider. Influence of spray parameters on the particle in-flight properties and the properties of HVOF coating of wc-cocr. Wear, 257(1):41-46, 2004.

[47] A Sova, A Okunkova, S Grigoriev, and I Smurov. Velocity of the particles accelerated by a cold spray micronozzle: experimental measurement and numerical simulation. Journal of thermal spray technology, 22(1):75-80, 2013.

[48] M Li and P Christofides. Computational study of particle in-flight behaviour in the HVOF thermal spray process. Chemical Engineering Science, 61(19):6540-6552, 2006.

[49] Available online:www.openfoam.com/. Last Accessed 9/2017.

[50] Available online:www.su2.com/. Last Accessed 09/2017.

[51] Available online:www.ansys.com/. Last Accessed 09/2017.

[52] S Turns. An introduction to Combustion, McGraw-Hill, 1996.

[53] Y Cengel, M Boles, M Kanoglu. Thermodynamics: an engineering approach. McGraw-Hill Education, 2015.

[54] M Moran, H Shapiro, Howard N and Boettner, Daisie D and Bailey, Margaret B Fundamentals of thermodynamics, 2010, John Wiley & Sons.

[55] Glassman, Irvin and Yetter, Rihcard A and Glumac, Nick G, Combustion, 2014, Academic press.

[56] C Law. Combustion physics. Cambridge university press, 2010.

[57] S Gu, DG McCartney, CN Eastwick, and K Simmons. Numerical modelling of in-flight characteristics of inconel 625 particles during High-Velocity Oxy-Fuel thermal spraying of nanocrystalline materials: an overview. Modelling and Simulation in Materials Science and Engineering, 11(1):R1, 2002.

[58] H Kobayashi, T Tamura, K Maruta, and T Niika. Turbulence measurements and observations of turbulent premixed flames at elevated pressures up to 3.0 mpa. Combustion and flame, 108(1):104-117, 1997.

[59] H Kobayashi, T Tamura, K Maruta, T Niioka, and F Williams. Burning velocity of turbulent premixed flames in a high-pressure environment. In Symposium (International) on Combustion, volume 26, pages 389-396. Elsevier, 1996.

[60] H Kobayashi, Y Kawabata, and K Maruta. Experimental study on general correlation of turbulent burning velocity at high pressure. In Symposium (International) on Combustion, volume 27, pages 941-948. Elsevier 1998.

[61] H Kobayashi, Experimental study of high-pressure turbulent premixed flames. Experimental Thermal and Fluid Science, 26(2):375-387, 2002.

[62] D Veynante and L Vervisch. Turbulent combustion modelling. Progress in energy and combustion science, 28(3):193-266, 2002.

[63] C Westbrook and F Dryer. Simplified reaction mechanisms for the oxidation of hydrocarbon fuels in flames. Combustion science and technology, 27(1-2):31-43, 1981.

[64] I Glassman, R Yetter, and N Glumac. Combustion. Academic Press, 2004. A book.

[65] B Hassan, WL Oberkampf, RA Neiser, and TJ Roemer. Computational fluid dynamics analysis of a High Velocity Oxy-Fuel (HVOF) thermal spray torch, thermal spray science and technology. ASM International Materials Park, OH, Pages 193-198, 1995.

[66] M Li, and D Christofides. Multi-scale modeling and analysis of an industrial HVOF thermal spray process, Chemical Engineering Science,60(13): 3649-3669, Elsevier, 2005.

[67] S Kamnis and S Gu. Numerical modelling of propane combustion in a High Velocity Oxy-Fuel thermal spray guun. Chemical Engineering and Processing: Process Intesification, 45(4):246-253, 2006.

[68] S Kamnis and S Gu. 3-D modelling of kerosene-fuelled HVOF thermal spray gun. Chemical Engineering Science, 61(16):5427-5439, 2006.

[69] H Tabbara and S Gu. Computational simulation of liquid-fuelled HVOF thermal spraying. Surface and Coatings Technology, 204(5):676-684, 2009.

[70] B Magnussen and B Hjertager. On mathematical modelling of turbulent combustion with special with emphasis on soot formation and combustion. In Symposium (International) on Combustion, Volume 16, Pages 719-729. Elsevier, 1997.

[71] F Jabbari, M Jadidi, R Wuthrich, and A Dolatabadi. A numerical study of suspension injection in plasma-spraying process. Journal of Thermal Spray Technology, 23(1-2):3-13, 2014.

[72] WL Oberkampf and M Talpallikar. Analysis of a High Velocity Oxy-Fuel (HVOF) thermal spray torch part 2: Computational results. Journal of Thermal Spray Technology, 5(1):62-68, 1996.

[73] S Hossainpour and AR Binesh. A CFD study of sensitive parameter effects on the combustion in a High Velocity Oxygen Fuel thermal spray gun. Proc. World Acad. Sci. Eng. Technol, 31:213-220, 2008.

[74] R Kamali and AR Binesh. The importance of sensitive parameters effect on the combustion in a High Velocity Oxygen-Fuel spray system. International Communications in Heat and Mass Transfer, 36(9):978-983, 2009.

[75] A Dolatabadi, J Mostaghimi, and V Pershin. Effect of a cylindrical shroud on particle conditions in High Velocity Oxy-Fuel spray process. Science and Technology of Advanced Materials, 3(3):245-255, 2002.

[76] VR Sirvatsan and A Dolatabadi. Simulation of particle-shock interaction in a High Velocity Oxygen Fuel process. Journal of thermal spray technology, 15(4):481-487, 2006.

[77] E Dongmo, M Wenzelburger, and R Gadow. Analysis and optimization of the HVOF process by combined experimental and numerical approaches. Surface and Coatings Technology, 202(18):4470-4478, 2008.

[78] X Wang, Q Song, and Z Yu. Numerical investigation of combustion and flow dynamics in a High Velocity Oxygen-Fuel thermal spray gun. Journal of Thermal Spray Technology, Pages 1-10,2016

[79] YR Sivathanu and Gerard M Faeth. Generalized state relationships for scalar properties in nonpremixed hydrocarbon/air flames. Combustion and Flame, 82(2):211-230, 1990.

[80] F White. Fluid Mechanics. McGraw-Hill, Boston, 1999. A book.

[81] J Anderson and J Wendt. Computational Fluid Dynamics, Volume 206. Springer, 1995. A book.

[82] J Anderson. Modern Compressible Flow: with historical perspective, Volume 12. McGraw-Hill New York, 1990. A book.

[83] H Versteeg and W Malalasekera. An introduction to computational fluid dynamics: the finite volume method. Pearson Education, 2007. A book.

[84] M Norman, K Winkler, L Smarr, and MD Smith. Structure and dynamics of supersonic jets. Astronomy and Astrophysics, 11(3):285-302, 1982.

[85] D Munday, E Gutmark, J Liu, and K Kailasanath. Flow structure and acoustics of supersonic jets from conical convergent-divergent nozzles. Physics of Fluids

(1994-present), 23(11):102-116, 2011.

[86] B Samareh, O Stier, V Luthen, and A Dolatabadi. Assessment of CFD modelling via flow visualization in cold spray process. Journal of thermal spray technology, 18(5-6):934-943, 2009.

[87] J Baik and Y Kim. Effect of nozzle shape on the performance of High Velocity Oxygen Fuel thermal spray system. Surface and Coatings Technology, 202(22):5457-5462, 2008.

[88] L Fan and C Zhu. Principles of gas-solid flows. Cambridge University, Press, 2005.

[89] G Rudinger. Relaxation in gas-particle flow. Technical report, DTIC Document, 1968.

[90] C Crowe, J Schwarzkopf, M Sommerfeld, and Y Tsuji. Multphase flows with droplets and particles. CRC press, 2011.

[91] R Berry. Ensemble Averaged Conservation Equations For Multiphase, Multi-Component, And Multi-Material Flows. Citeseer, 2003.

[92] B Kishiwa and R Rauenzahn. A multimaterial formalism. American Society of Mechanical Engineering, 1:19-23, 1994.

[93] S Elghobashi. On predicting particle-laden turbulent flows. Applied Scientific Research, 52(4):309-329, 1994.

[94] RS Sirvastava and JP Sharma. structure of normal shock waves in a gas-particle mixture.Zeitschrift fur angewandte Mathematik und Physik (ZAMP), 33(6):819-825, 1982.

[95] TD Varma and NK Chopra. Analysis of normal shock waves in a gas-particle mixture. Zeitschrift fur angewandte Mathematik und Physik (ZAMP), 33(6):819-825, 1982.

[96] S Morsi and AJ Alexander. An investigation of particles trajectories in two-phase flow systems. Journal of Fluid Mechanics, 55(02):193-208, 1972.

[97] C Crowe, J Schwarzkopf, M Sommerfeld, and Y Tsuji, Multiphase flows with droplets and particles. CRC press, 2001

[98] C Crowe. Drag coefficient of particles in a rocket nozzle. AIAA Journal, 5(5): 1021-1022, 1976.

[99] R Clip, J Grace, and M Weber. Bubbles, drops, and particles,Courier Corporation 2005.

[100] C Chang and R Moore. Numerical simulation of gas and particle flow in a High Velocity Oxygen Fuel (HVOF) torch. Journal of Thermal Spray Technology, 4(4):358-366, 1995.

[101] D Cheng, Q Xu, G Tapaga, and EJ Lavernia. A numerical study of High Velocity Oxygen Fuel thermal spraying process. Part 1: Gas dynamics. Metallurgical and Materials Transactions A, 32(7):1609-1620, 2001.

[102] Gu, S.; Eastwick, C.N.; Simmons, K.A.; McCartney, D.G. Computational fluid dynamic modelling of gas flow characteristics in a High-Velocity Oxy-Fuel thermal system. J. Therm. Spray Technol. 1996,5,175-184

[103] X Yang and S Eidelman. Numerical analysis of a High Velocity Oxygen Fuel thermal spraying system. Journal of Thermal Spray Technology, 5(2):175-184,1996.

[104] Cheng, D.; Xu, Q.; Trapaga, G.; Lavernia, E.J. The effect of particle size and morphology on the in-flight behaviour of particles during high-velocity oxyfuel thermal spraying. Metall. Mater. Trans. B 2001, 32B, 525-535.

[105] G Ganser. A rotational approach to drag prediction of spherical and nonspherical particles. Powder Technology, 77(2):143-152, 1993.

[106] S Gu and S Kamnis. Numerical modelling of in-flight particle dynamics of non-spherical powder. Surface and Coatings Technology, 203(22):3485-3490, 2009.

[107] S Kamnis and S Gu. Study of in-flight and impact dynamics of nonspherical particles from HVOF guns. Journal of thermal spray technology, 19(1-2):31-41, 2010.

[108] S.V Joshi; R Sivakumar. Particle behaviour during High Velocity Oxy-Fuel Spraying. J. Therm. Spray Technol. 1996, 5, 175-184.

[109] S.V Joshi. A prediction model to assist plasma and HVOF spraying. Mater. Lett. 1992, 14, 31-36.

[110] V.V Sobolov; J.M; Guilemany; J.C; J.A Carlo. Modelling of particle movement and thermal behaviour during high velocity oxy-fuel spraying. Surf.Coat. Technol. 1994, 63, 181-187.

[111] V.V Sobolov; J.M Guilemany; J.R Miguil; J.A Carlo. Influence of in-flight dissolution process on composite powder particle (WC−Ni) behaviour during high velocity oxy-fuel spraying. Surf. Coat. Technol. 1996, 81, 136-145.

[112] V.V Sobolov; J.M Guilemany; A.J Martin; J.A Carlo. Modelling of in-flight behaviour of the stainless steel powder particles in high velocity oxy-fuel spraying. J. Mater. Process. Technol. 1998, 79, 213-216.

[113] N Ait-Messaoudene; A El-hadj. Effect of the substrate and of themophoresis on the acceleration and heating of particles during HVOF spraying. Suf. Coat. Technol. 1998, 106, 140-144.

[114] N Zeoli; S Gu; S Kamnis. Numerical simulation of in-flight particle oxidation during thermal spraying. Comput. Chem. Eng. 2008, 32, 1661-1668.

[115] N Cabrera and NF Mott. Theory of the oxidation of metals, reports on progress in physics. IOP Publisher, 12;1, 169, 1949.

[116] S Kamnis; S Gu; N Zeoli. Mathematical modelling of Inconnel 718 particles in HVOF thermal spraying. Surf. Coat. Technol. 2008, 202, 2715-2724.

[117] C.M Hackett; G.S Settle. The influence of nozzle design on HVOF spray particle velocity and temperature. In Proceeding of 8th National Thermal Spray Conference, Houston, TX, USA, 11-15 September 1995.

[118] A.R Lopez; B. Hassan; W.L Oberkampf; R.A Neiser; T.J Roemer. Computational fluid dynamics analysis of a wire-feed high velocity oxygen fuel (HVOF) thermal spray torch. J. Therm. Spray Technol. 1998, 7, 374-382.

[119] S Gu; D.G McCartney; C.N Estwick; K.A Simmons. Numerical modelling of in-flight characteristics of Inconnel 625 particles during high-velocity oxy-fuel thermal spraying. J. Therm. Spray Technol. 2004, 13, 200-2013.

[120] H Katanoda; H Yamamoto; K Matsuo. Numerical simulation on supersonic flow in high-velocity oxy-fuel thermal spray gun. J. Therm. Sci. 2006, 15, 65-70.

[121] H katanoda. Quasi-one dimensional analysis of the effects of pipe friction, cooling and nozzle geometry on gas/particle flows in HVOF thermal spray gin. Mater. Trans. 2006, 47, 2791-2797.

[122] E Kadyrov; Y Evdokimenko; Y Kisel; V Kadyrov; F Worzala. Interaction of particles with carrier gas in HVOF spraying systems. J. Therm. Spray Technol. 1994, 3, 389-379.

[123] B Hassan; A.R Lopez; W.L Oberkampf. Computational analysis of a three-dimensional high velocity oxygen fuel (HVOF) thermal spray torch. J. Therm. Spray Technol. 1998, 7, 71-77.

[124] A Dolatabadi; J Mostaghimi; V Pershin. Effect of a Cylindrical shroud on particle conditions in high velocity oxy-fuel spray process. Sci. Technol. Adv. Mater. 2002, 3, 245-255.

[125] A Dolatabadi; J Mostaghimi; V Pershin. Effect of a Cylindrical shroud on particle conditions in high velocity oxy-fuel spray process. Sci. Technol. Adv. Mater. 2003, 137, 214-224.

[126] R.A Neiser; M.F Smith; R.C Dykhuizen. Oxidation in wire HVOF sprayed stell. J.Therm. Spray Technol. 1998, 7, 537-545.

[127] K Dobler; H Kreye; R Schwetzke. Oxidation of stainless steel in the high velocity oxy-fuel process. J. Therm. Spray Technol. 2000, 9, 407-413.

[128] K Sakaki; Y Shimizu. Effect of the increase in the entrance convergent section length of the gun nozzle on the high velocity oxygen fuel and cold spray process. J. Therm. Spray Technol. 2001, 10, 487-496.

[129] S.H Kim; Y.J Kim. Flow characteristics in compact thermal spray coating system with minimum length nozzle. Plasma Sci. Technol. 2009, 11, 550-554.

[130] S Eidelman; X Yang. Three dimensional simulation of HVOF spray deposition of nanoscale materials. Nanostruct. Mater. 1997, 9, 79-84.

[131] S Gordon; B.J McBride. 1994, Computer programme for calculation of complex chemical equilibrium compositions. NASA Reference Publication 13311, Lewis Research

Center, Cleveland, OH, USA.

[132] Robert, C Reid and John, M Prausnitz and Bruce, E Poling. The properties of gases and liquids, McGraw-Hill, New York, 1997. A book.

[133] Martinez, B and Mariaux, Gilles and Vardelle, Armelle and Barykin, G and Parco, M. Numerical Investigation of a hybrid HVOF-plasma spraying process,Journal of thermal spray technology, Springer, 18;(5-6),(909-920), 2009.

[134] J. Antony, Design of experiments for engineers and scientists, Elsevier, 2003.

[135] [ ] G. E. P. Box and K. B. Wilson, On the experimental attainment of optimum conditions, J. of the Royal Statistical Society B13, 1951, pp. 1- 45.

[136] D. C. Montgomery, Design and Analysis of Experiments. 2nd Edition, John Wiley & Sons, New York, 1984.

[137] A. I. Khuri and J. A. Cornell, Response Surfaces Design and Analysis. 2nd Edition, Marcel Dekker, New York, 1996.

[138] G. E. P. Box and D. W. Behnken, Some new three level designs for the study of quantitative variables, Technometrics, Vol. 2, n., 4, November 1960, pp. 455-475.

[139] M. J. Anderson and P. J. Whitcomb, RSM simplified: optimizing processes using response surface methods for design of experiments, Productivity Press, 2005.

[140] S. Chatterjee and B. Price, Regression analysis by example, 2nd Ed., Wiley and Sons, Inc., 1977, pp. 200-202.

[141] R. H. Hymers and D.C. Montogomery, Response surface methodology-process and product optimization using designed experiment, John Wiley & Sons, 1995.

[142] Available online: www.amt-ag.net. Last Accessed 09/2017